THE SOUTH ATLANTIC RADIATION ANOMALY.

A Thesis submitted for the
Degree of Master of Science of
Rhodes University.

by

H.O. VAN ROOYEN.

January. 1964.

Except where it is clear from the text that I am describing the work of others, or where it is obvious that I am making a survey of existing knowledge of the field concerned, the work described in this thesis is my own.

H.O. van Rooyen

drift perpendicular to $\bar{B}$ and $\bar{R}$ of the same type, though not for the same reason, as that shown in figure 2. We can easily calculate the drift velocity $\bar{v}_D$ if we define a new velocity, $\bar{v}'$, such that

$$\bar{v} = \bar{v}' + \bar{v}_D \qquad 1.22$$

Since we know that $\bar{v}_D$ is perpendicular to $\bar{B}$ and $\bar{R}$ we may write it as

$$\bar{v}_D = \frac{\frac{m v_{//}^2}{\bar{R} e} \times \bar{B}}{B^2} \qquad 1.23$$

[See reference (2)]. Notice that if the charge changes sign, the sense of rotation about the guiding centre changes, and the direction of $\bar{v}_D$ therefore reverses as we expect from 1.23. Provided that B and $\bar{R}$ are constant we can substitute from 2.23 and 2.22 into 2.21, taking $\bar{v}_D$ as constant, thus getting

$$m \frac{d \bar{v}'}{d t} = e \left[\frac{m v_{//}^2}{\bar{R} e} + \bar{v}' \times \bar{B} + \frac{m v_{//}^2}{e B^2} \left(\frac{1}{\bar{R}} \times B \right) \times \bar{B} \right]$$

and since the triple product is equal to $- B^2 \frac{1}{\bar{R}}$, this becomes

$$m \frac{d \bar{v}'}{d t} = e (\bar{v}' \times \bar{B}) \qquad 1.24$$

which describes, as does 1.1, gyration round a line of force. We have thus separated the velocity $\bar{v}$ into two components, $\bar{v}'$ and $\bar{v}_D$. $\bar{v}'$ Results in the type of motion with which we are familiar from section 1-3, and $\bar{v}_D$ in a drift of the guiding centre transverse to $\bar{B}$. Were the observer of such a trajectory to have velocity $\bar{v}_D$ the particle would appear to have only the force due to the magnetic field exerted on it. From 1.4 and 1.23 we may write

$$\bar{v}_D = \frac{m v_{//}^2}{\bar{R} e} = \frac{v_{//}^2}{\bar{R} w} \qquad 1.25$$

Figure 2 Schematic representation of the drift (in the equatorial plane and viewed from above the north pole) of a proton and an electron due to the inhomogeneity of the geomagnetic field. Note that we do not visualize the injection of charged particles into the magnetosphere as it is represented in this figure. Reproduced from reference (32)

CONTENTS.

ACKNOWLEDGEMENTS.

I wish to thank my research director, Professor J.A. Gledhill, for his expert guidance, and for his unfailing interest in this project. His sound advice and willingness to discuss my problems were very much appreciated.

I would like to thank the South African Council for Scientific and Industrial Research for a grant to cover the cost of computations connected with this research, and for their willingness to undertake this work at short notice, and Dr C.W. Cryer of the National Research Institute for Mathematical Sciences for arranging to have these computations done.

A sincere "thank you" too, to Mr Jos Nel who did the cover design, Mr G. Walters who did the photographic work for this thesis, Mrs J. Legrice and Miss L. Miles whose patience while typing the thesis from hand-written notes was little short of amazing, and Miss M. Stormont, who was kind enough to lend me a typewriter.

Finally, I wish to thank my friends in the Rhodes University Physics Department for their helpfulness at all times, and my father and mother, without whose help and encouragement this thesis might never even have been started.

INTRODUCTION.

THE PROJECT.

It has been recognized since the time of the Argus experiments that the relatively low values of the total magnetic intensity in the South Atlantic region must have a profound effect on the particles trapped in the Van Allen radiation belts. Observations of the counting-rates of charged particles at low altitudes over the South Atlantic Ocean have revealed the existence of two regions of anomalously high radiation intensity in this area. In this thesis, we focus our attention on the more southerly of these two "radiation anomalies" in an attempt to discover whether the energy deposited in the upper atmosphere, by the charged particles mentioned above, is sufficient to cause detectable geophysical phenomena.

PRESENTATION.

Since this is the first thesis, which deals with a topic so intimately connected with the Van Allen belts, to be presented at a South African University, a survey of the present status of our knowledge of the belts, together with an outline of the theory of the motion of charged particles in the geomagnetic field, has been presented in Part I. Also included in Part I is a chapter outlining the more important features of the radiation anomalies mentioned above.

In Part II, a new method is developed which enables us to estimate the energy deposited in the atmosphere, in a particular region, by charged particles. This method is applied to the radiation anomaly, and the results used to predict the geophysical effects which should be observable

there. The value of this new approach is assessed, and suggestions for further research are made.

EQUATIONS.

Equations are numbered independently in each chapter. Equation 1.4 is the fourth equation in Chapter 1, 5.2, the second equation in Chapter 5, and so on. Note that to avoid confusion, sections are referred to with a dash between the chapter number and the section number, e.g. 1-4, 5-2, and so on.

REFERENCES.

In selecting the references for this thesis we have used the criterion that they should be of general importance in the field in addition to being relevant to the topic under discussion. In other words, we have, in general, left out papers dealing with isolated observations. This was done in order to cut down the number of references, while at the same time ensuring that those included cover the subject completely. Articles are referred to by inserting a number, in brackets, in the appropriate place in the text.

UNITS.

Except where otherwise indicated, MKS units are used in this thesis. Earth radii are often used as units of length in this type of work. They will always refer to geocentric distance, and are abbreviated as E_R. Thus "$2E_R$" denotes a distance of two earth radii measured from the centre of the earth.

$$1E_R = 6378.3 \text{ km.}$$
$$\text{i.e.} \sim 6400 \text{ km.}$$

PART I.

THE VAN ALLEN RADIATION BELTS.

CHAPTER 1.

THE MOTION OF CHARGED PARTICLES IN A MAGNETIC FIELD.

1-1 Introduction.

Birkeland, in 1896, carried out a series of experiments designed to investigate the possibility that the aurora might be the result of the interaction with the atmosphere of cathode rays from the sun guided into the polar regions by the geomagnetic field. Stimulated by Birkeland's experiments, Störmer tackled the problem of calculating the trajectory of a single charged particle entering the geomagnetic field. Though he made the simplifying assumption that the geomagnetic field can be represented by that of a dipole, the task involved an immense amount of work, details of which are given in his book "The Polar Aurora" (1). In the course of his investigations he was able to show theoretically that particles moving in certain regions of the field must be 'trapped', i.e. confined to move only in these 'allowed' regions. He was unable to show how particles could enter these allowed regions (and thus be trapped). It has however been demonstrated that such trapping does in fact occur in the geomagnetic field. Observations carried out by the first artificial satellites and moon probes launched by the U.S.S.R. and the U.S. showed two zones of trapped radiation, the outermost of which extends out to a geocentric distance of four or five earth radii in the equatorial plane. These were named the Van Allen Belts after Prof. J. A. Van Allen of the State University of Iowa

whose pioneering work in this connection has made him famous the world over.

In any problem dealing with a large number of charged particles, as in the case of the trapped radiation, there are two complimentary treatments; first by analysis of the movement of single particles, and second by means of a fluid model. Either one of these two approaches when taken separately does not give a complete description of the system as a whole. In addition both approaches are necessarily complex in the case of the trapped radiation, one of the main complications being that no relatively simple model can be found which fits the geomagnetic field with the required accuracy. A rough idea of the behaviour of charged particles in the geomagnetic field can however be gained by considering the relatively simple and highly idealized cases presented in this chapter. The motion of a charged particle in a monopole field will be treated in some detail as it forms the basis of work presented in a later chapter of this thesis. In addition some cases will be treated which have no realistic bearing on the trapped radiation. This is done in order to illustrate thoroughly the basic ideas presented.

1-2 General Considerations (2)

Consider a particle of mass m and charge e moving with velocity $\bar{v}$ in a region in which there is a magnetic induction $\bar{B}$; then the force acting on the particle due to the magnetic field only is given by

$$m \frac{d \bar{v}}{d t} = e \ (\bar{v} \times \bar{B}) \qquad 1.1$$

which, though it produces a curvature of the path, does not produce a change in the scalar value of the velocity, v, since it is perpendicular to both $\bar{v}$ and $\bar{B}$. This is easily shown by taking the scalar product of both sides of equation 1.1 with $\bar{v}$, giving

$$m \frac{d \bar{v}}{d t} \cdot \bar{v} = e \ (\bar{v} \times \bar{B}) \cdot \bar{v} = 0$$

and then integrating, which gives

$$v^2 = \text{constant} \qquad 1.2$$

This is true for any magnetic field and implies that the kinetic energy of the particle is constant.

Consider now the case where the magnetic field is uniform in space and time and equation 1.1 gives the only force acting on the particle. If we resolve $\bar{v}$ into components perpendicular to, and parallel to the field direction, $v_\perp$ and $v_{//}$, then it is easily seen that $v_\perp$ will cause the particle to move in a circle round a line of force. Let the 'radius of gyration' be a. From 1.1 we get

$$\text{Acceleration} = \frac{e \, v_\perp \, B}{m} = \frac{v_\perp^2}{a} \qquad 1.3$$

since the centripetal force is that exerted by the magnetic field. The angular frequency of the circular motion will be

$$w = \frac{v_\perp}{a} \qquad 1.4$$

Thus from 1.3 we may write

$$a = \frac{m \, v_\perp}{e \, B} = \frac{v_\perp}{w} \qquad 1.5$$

w Is usually called the gyrofrequency of the particle. $v_{//}$ Will not be affected by the magnetic field and will not affect the motion perpendicular to the field direction. The combined effect of $v_{\perp}$ and $v_{//}$ will produce a helical path of constant pitch and radius about a line of force. $v_{//}$ Will remain constant, implying that the particle will traverse along the lines of force at constant speed.

1-3 Motion in the Field of a Monopole. (3)

The solution to this problem was first obtained by Poincaré in 1896 (4). The field of a monopole is given by an inverse square law, namely

$$\bar{B} = \frac{\mu_o M \bar{r}}{r^3}$$

where M is the pole strength, μ_o is the permeability of space, and $\bar{r}$ is the position vector with the monopole as origin. Substituting this value for $\bar{B}$ into equation 1.1 we get

$$\frac{d\bar{v}}{dt} = \frac{e M \mu_o}{m r^3} (\bar{v} \times \bar{r}) \qquad 1.6$$

A particle whose position vector is $\bar{r}$ will thus experience an acceleration given by 1.6. Splitting its velocity into components as in the previous section, and assuming that no other forces act on the particle, we can see that it will circle about a line of force and also move along it towards, or away from, the pole (provided that both components are non-zero).

Let d s be an element of path length along the trajectory of

the particle. Then $v = \frac{ds}{dt}$ and we may write

$$\frac{d\bar{v}}{dt} = \frac{d\bar{v}}{ds}\frac{ds}{dt} = v\frac{d\bar{v}}{ds} \qquad 1.7$$

If we now choose our unit of length as $\frac{e\,M\,\mu_o}{m\,v}$ metres we get from 1.6

$$\frac{d\bar{v}}{ds} = \frac{1}{r^3}(\bar{v} \times \bar{r}) \qquad 1.8$$

Since v is constant, the unit of length is constant for any one particle. In the same way we have

$$\bar{v} \equiv \frac{d\bar{r}}{dt} = v\frac{d\bar{r}}{ds} \qquad 1.9$$

and differentiating this with respect to s we get

$$\frac{d\bar{v}}{ds} = v\frac{d^2\bar{r}}{ds^2} \qquad 1.10$$

since the scalar v is constant. Substituting the value for $\frac{d\bar{v}}{ds}$ from equation 1.8 into 1.10 we get

$$\frac{d^2\bar{r}}{ds^2} = \frac{1}{v}\frac{d\bar{v}}{ds} = \frac{1}{v}\left[\frac{\bar{v} \times \bar{r}}{r^3}\right] \qquad 1.11$$

and using 1.9 we can write this as

$$\frac{d^2\bar{r}}{ds^2} = \frac{1}{r^3}\left[\frac{d\bar{r}}{ds} \times \bar{r}\right] \qquad 1.12$$

which is the final form of the equation of motion. If we now take the vector product of 1.12 with $\bar{r}$ and expand the resulting triple product we find that

$$\bar{r} \times \frac{d^2\bar{r}}{ds^2} = \bar{r} \times \frac{1}{r^3}\frac{d\bar{r}}{ds} \times \bar{r}$$

$$= \frac{1}{r^2}\left[r\frac{d\bar{r}}{ds} - \frac{dr}{ds}\bar{r}\right] \qquad 1.13$$

where we have used the fact that

$$\bar{r} \cdot \frac{d\bar{r}}{ds} = r\frac{dr}{ds}$$

We now note that

$$\frac{d}{ds}\left[\bar{r} \times \frac{d\bar{r}}{ds}\right] = \frac{d\bar{r}}{ds} \times \frac{d\bar{r}}{ds} + \bar{r} \times \frac{d^2\bar{r}}{ds^2}$$

$$= \bar{r} \times \frac{d^2\bar{r}}{ds^2} \qquad 1.14$$

so that we may write 1.13 as

$$\frac{d}{ds}\left[\bar{r} \times \frac{d\bar{r}}{ds}\right] = \frac{d}{ds}\left(\frac{\bar{r}}{r}\right) \qquad 1.15$$

since the right hand side of 1.13 is simply the expansion of the right hand side of 1.15. Equation 1.15 can be integrated directly to give

$$\bar{r} \times \frac{d\bar{r}}{ds} = \frac{\bar{r}}{r} - \bar{h} \qquad 1.16$$

where $\bar{h}$ is the constant of integration, and is a vector such that $\left[\frac{\bar{r}}{r} - \bar{h}\right]$ is perpendicular to both $\bar{r}$ and $\frac{d\bar{r}}{ds}$. To get the equation of the surface in which $\bar{r}$ and $\frac{d\bar{r}}{ds}$ lie we take the scalar product of $\bar{r}$ with both sides of equation 1.16 getting

$$0 = \frac{r^2}{r} - \bar{r} \cdot \bar{h}$$

i.e. $$r = \bar{r} \cdot \bar{h} = r\,h\cos\alpha$$

or $$h\cos\alpha = 1 \qquad 1.17$$

where α is the angle between $\bar{r}$ and $\bar{h}$. Since h is constant, α is constant, so that all the vectors $\bar{r}$ which are crossed by the trajectory make a constant angle α with the vector $\bar{h}$, that is, 1.17 is the equation of the surface of a cone with $\bar{h}$ along its axis. If we choose the z axis to be parallel with $\bar{h}$, with the pole at the origin, then the surface is that of a cone of half angle α, symmetric about the Z axis. (See Figure 1)

If we let χ be the angle between $-\bar{r}$ and the trajectory, $\frac{d\bar{r}}{ds}$, then from figure 1 and equation 1.16 we see that

$$r \sin \chi = \left| \frac{\bar{r}}{r} \right| \tan \alpha$$

i.e. $$r \sin \chi = \tan \alpha \quad (= h_{\perp}) \qquad \underline{1.18}$$

since $\frac{d\bar{r}}{ds}$ and $\frac{\bar{r}}{r}$ are unit vectors. $h_{\perp}$ Is the component of $\bar{h}$ perpendicular to the surface of the cone. χ Is usually called the 'pitch angle'.

If we imagine the conical surface opened out into a plane sheet the equation of the trajectory is r sin χ = constant, which is obviously the equation of a straight line in plane polar coordinates. Hence the trajectory is a geodesic in the surface of the cone. This can also be seen from 1.12 since it shows that the principal normal to the trajectory coincides with the normal to the surface in which $\bar{r}$ and $\frac{d\bar{r}}{ds}$ lie. (The acceleration given by the term on the left hand side of 1.12 must lie along the principal normal to the trajectory since v is constant).

Since the inverse square law holds and sin χ is inversely

Figure 1 Diagram showing part of the trajectory of a charged particle in a monopole field. The particle moves on the surface of a cone of semi-vertical angle α. Also labelled are the axis of the cone (z axis), the pitch angle χ at two points, and the vectors $\bar{r}/r$ and $-\bar{h}$ (see text).

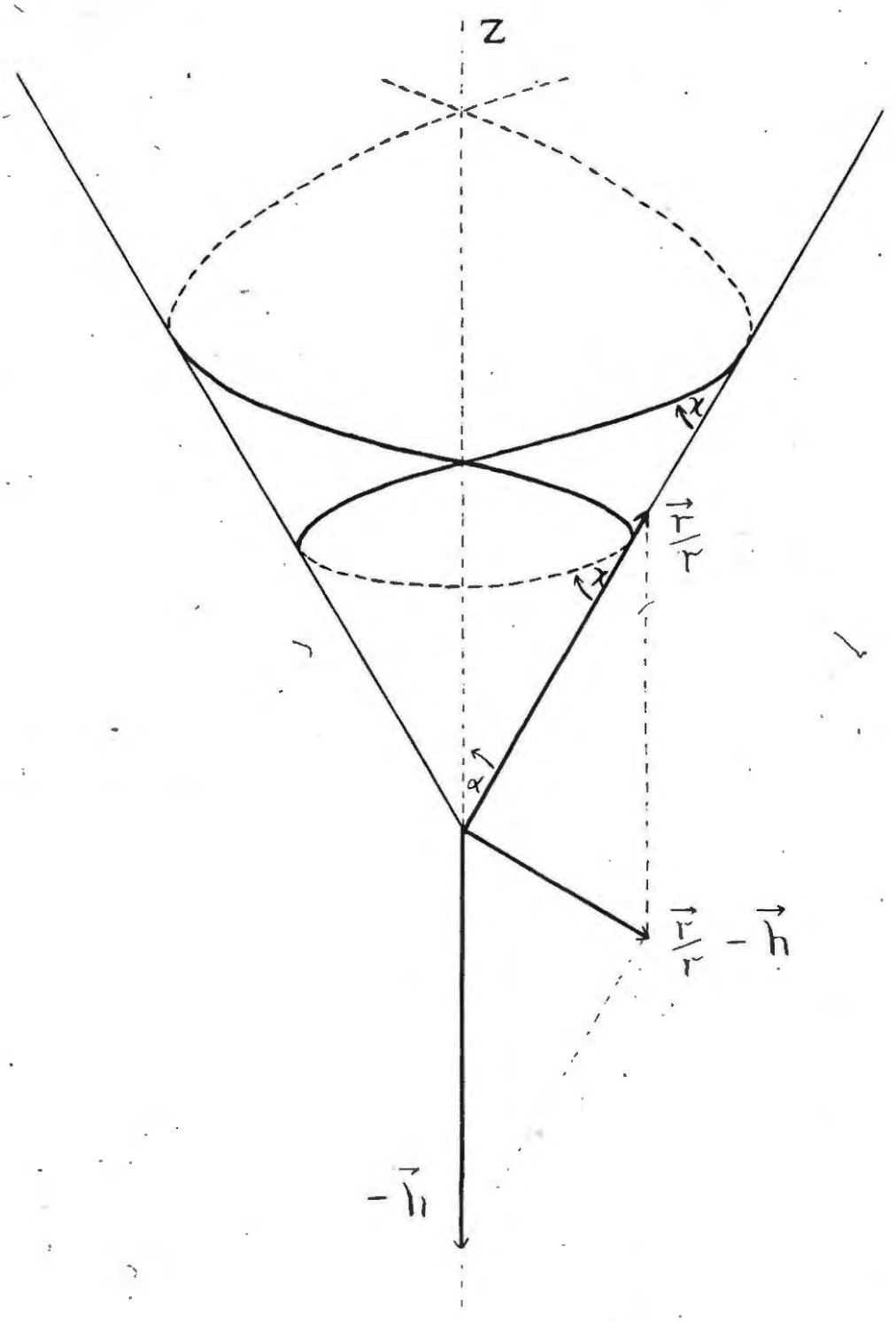
z
$\frac{\vec{r}}{2}$
$\frac{\vec{r}}{2} - \vec{h}$
$-\vec{h}$

proportional to r we can say that $\sin^2 \chi$ is proportional to B,

i.e. $\frac{\sin^2 \chi}{B}$ = constant.

If we let the values of χ and B be χ_o and B_o at some arbitary fixed distance from the monopole, then we may write

$$\frac{\sin^2 \chi}{B} = \frac{\sin^2 \chi_o}{B_o}$$

i.e. $$\sin^2 \chi = \frac{B}{B_o} \sin^2 \chi_o \qquad 1.19$$

As the particle approaches the monopole B increases which implies that χ increases. When $\frac{B}{B_o} = \frac{1}{\sin^2 \chi_o}$, $\sin \chi = 1$, that is $\chi = \frac{\pi}{2}$ and the particles' progress towards the pole is stopped. We label the value of B at this point B_m. It then moves out to infinity again as χ increases from $\frac{\pi}{2}$ to π.

This type of mirroring will occur in all cases where the field lines converge, that is where the field increases. The 'magnetic bottles' used in some thermonullear devices are an example of the application of this effect. Note the interesting point that the distance from the monopole at which the particle mirrors does not depend on the energy of the particle in any way.

1-4 Particle Drifts. (2)

Even to get a rough picture of the motion of particles in the geomagnetic field it will be necessary for us to take into account forces other than that due to the magnetic field. As idealized examples of such forces we will consider the effects of non-uniformity

of the magnetic field, the gravitational field, and the presence of an electric field. A very useful concept in dealing with such simple cases is that of the 'guiding centre' of the particle, which can be defined as its instantaneous centre of gyration. It can be shown that each of these extra forces causes a motion of the guiding centre transverse to $\bar{B}$. Such a motion is termed a 'drift' and we now proceed to demonstrate very briefly how these drifts arise.

1-4-1 The Drift due to Curvature of the lines of Force.

Let us imagine a magnetic field in which the lines of force have a constant radius of curvature $R >> a$. A particle moving along a field line with velocity $v_{//}$ will have acting on it, in addition to the force due to the magnetic field as given in 1-1, a centripetal force given by

$$\text{Centripetal force} = \frac{m v_{//}^2}{R e} \quad \text{per unit charge} \qquad 1.20$$

This force is directed inwards along the radius vector $\bar{R}$. From 1.1 and 1.20 the equation of motion of the particle is

$$m \frac{d \bar{v}}{d t} = \frac{m v_{//}^2}{\bar{R}} + e (\bar{v} \times \bar{B}) \qquad 1.21.$$

The centripetal force will accelerate the particle along the radius vector and as a result $v_\perp$ will be greater on the part of the trajectory nearest the centre of curvature of the field lines than on the part of the trajectory furthest from this centre of curvature. We see from 1.5 that the change in $v_\perp$ will cause the radius of gyration to change since m, e and B are constant, thus resulting in a

drift perpendicular to $\bar{B}$ and $\bar{R}$ of the same type, though not for the same reason, as that shown in figure 2. We can easily calculate the drift velocity $\bar{v}_D$ if we define a new velocity, $\bar{v}'$, such that

$$\bar{v} = \bar{v}' + \bar{v}_D \qquad 1.22$$

Since we know that $\bar{v}_D$ is perpendicular to $\bar{B}$ and $\bar{R}$ we may write it as

$$\bar{v}_D = \frac{\frac{m v_{//}^2}{\bar{R} e} \times \bar{B}}{B^2} \qquad 1.23$$

[See reference (2)]. Notice that if the charge changes sign, the sense of rotation about the guiding centre changes, and the direction of $\bar{v}_D$ therefore reverses as we expect from 1.23. Provided that B and $\bar{R}$ are constant we can substitute from 2.23 and 2.22 into 2.21, taking $\bar{v}_D$ as constant, thus getting

$$m \frac{d \bar{v}'}{d t} = e \left[\frac{m v_{//}^2}{\bar{R} e} + \bar{v}' \times \bar{B} + \frac{m v_{//}^2}{e B^2} \left(\frac{1}{\bar{R}} \times B \right) \times \bar{B} \right]$$

and since the triple product is equal to $- B^2 \frac{1}{\bar{R}}$, this becomes

$$m \frac{d \bar{v}'}{d t} = e (\bar{v}' \times \bar{B}) \qquad 1.24$$

which describes, as does 1.1, gyration round a line of force. We have thus separated the velocity $\bar{v}$ into two components, $\bar{v}'$ and $\bar{v}_D$. $\bar{v}'$ Results in the type of motion with which we are familiar from section 1-3, and $\bar{v}_D$ in a drift of the guiding centre transverse to $\bar{B}$. Were the observer of such a trajectory to have velocity $\bar{v}_D$ the particle would appear to have only the force due to the magnetic field exerted on it. From 1.4 and 1.23 we may write

$$\bar{v}_D = \frac{m v_{//}^2}{R e} = \frac{v_{//}^2}{R w} \qquad 1.25$$

Figure 2 Schematic representation of the drift (in the equatorial plane and viewed from above the north pole) of a proton and an electron due to the inhomogeneity of the geomagnetic field. Note that we do not visualize the injection of charged particles into the magnetosphere as it is represented in this figure. Reproduced from reference (32)

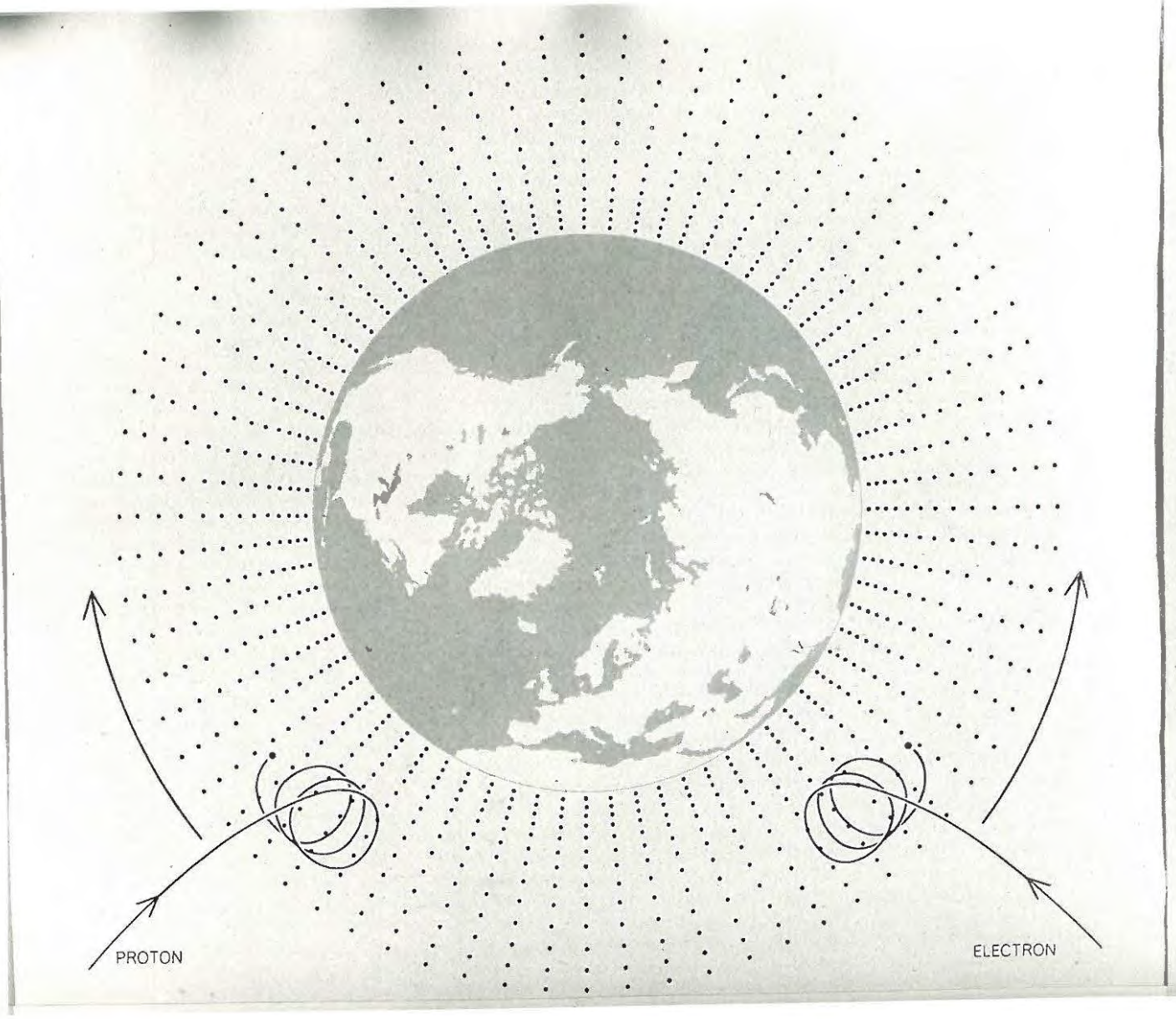
PROTON
ELECTRON

1-4-2 Drift in an inhomogeneous Magnetic Field.

We will deal here, in very brief form, with one simple case of inhomogeneity, namely the case where there is a gradient of the scalar value of the magnetic field, $\Delta_\perp B$, perpendicular to $\bar{B}$. We see from 1.4 that the radius of gyration depends inversely on B, so that again a drift will arise which is in opposite directions for oppositely charged particles, the direction being perpendicular to $\bar{B}$ and $\Delta_\perp B$, as shown in figure 2. In this case the theory is approximate and has been worked out by Alfvén (5) and others. If only terms of the first order in $\frac{v_D}{v_\perp}$ are considered, the result is

$$\frac{v_D}{v_\perp} = \frac{a \Delta_\perp B}{2 B} \qquad 1.26$$

Notice that the magnitudes of the drift velocities from both 1.25 and 1.26 depend on the energy of the particles.

1-4-3 Drift due to a Gravitational Field.

We can in general resolve the acceleration due to gravity into components perpendicular to and parallel to $\bar{B}$. Let us call these $g_\perp$ and $g_{/\!/}$. $g_{/\!/}$ Will increase $v_{/\!/}$. The force exerted by the gravitational field perpendicular to the magnetic field lines has magnitude $\frac{m g_\perp}{e}$ per unit charge, and will produce a drift in the same way as the centripetal force in section 1-4-1. Using the same analysis as in 1-4-1 and replacing $\frac{m v_{/\!/}^2}{R e}$ by $\frac{m g_\perp}{e}$ we find

$$v_D = \frac{m g_\perp}{e B} = \frac{g_\perp}{w} \qquad 1.27$$

Again $\bar{v}_D$ will have opposite directions for charges of opposite sign.

The comparatively small effect of the earth's gravitational field on the trapped radiation is usually ignored.

1-4-4 Drift due to the presence of an Electric Field.

An electric field $\bar{E}$ in the region in which the particle is moving will also produce a drift. If we assume $\bar{E}$ and $\bar{B}$ to be uniform in space and time, thus considering the simplest possible case, the drift velocity can again be found in the same manner as in section 1-4-1 by putting

$$\bar{v}_D = \frac{\bar{E} \times \bar{B}}{B^2} \qquad 1.28$$

since $\bar{E}$ is now the force per unit charge. This gives $v_D = \frac{E}{B}$ if $\bar{E}$ and $\bar{B}$ are perpendicular, or in the general case

$$v_D = \frac{E_\perp}{B} \qquad 1.29$$

where $E_\perp$ is the component of $\bar{E}$ perpendicular to $\bar{B}$. The component parallel to $\bar{B}$ will accelerate the particle along the magnetic field lines, which can have important effects on particles trapped in the geomagnetic field since the acceleration is not necessarily small as in the case of that due to the gravitational field. In this case the direction of the drift produced is obviously the same for all particles regardless of sign.

1-5 Motion of Charged Particles in the Geomagnetic Field. (6)

In this section we shall use the previous simple considerations to get a rough idea of the general motion of a charged particle in the geomagnetic field.

1-5-1 General Remarks.

It seems that we may expect charged particles in the geomagnetic field to spiral back and forth along the field lines, mirroring in the increasing field as they approach the poles. At the same time they will drift in longitude, mainly because of the inhomogeneous nature of the field, electrons drifting from west to east, and protons from east to west. Thus they may be expected to spread out round the earth giving rise to a radiation 'belt'. (See figure 3.) If we assume that the geomagnetic field possesses azimuthal symmetry and is constant in time, and that scattering is negligible, then each particle will return to its original field line after drifting round the earth, and will therefore not be lost from the trapping region once established in it. In fact all these conditions are violated by the geomagnetic field, which must result in marked radial drifts and subsequent loss of particles from the belts. However, provided that the variation of the geomagnetic field in space and time is fairly slow the concepts of guiding centre motion and adiabatic invariants can be used to predict the motion of a charged particle in it, and the continued existence of a radiation belt can readily be understood in terms of such an analysis. We now go on to examine briefly the treatment in terms of the adiabatic invariants.

1-5-2 The Adiabatic Invariants.

The time average magnetic field produced by a charged particle in rapid helical motion round a line of force is equivalent to that produced by a circular current i enclosing the same area. Thus the

Figure 3 Schematic representation of the motion of a proton and an electron in the geomagnetic field. (See note in caption of figure 2). Reproduced from reference (32)

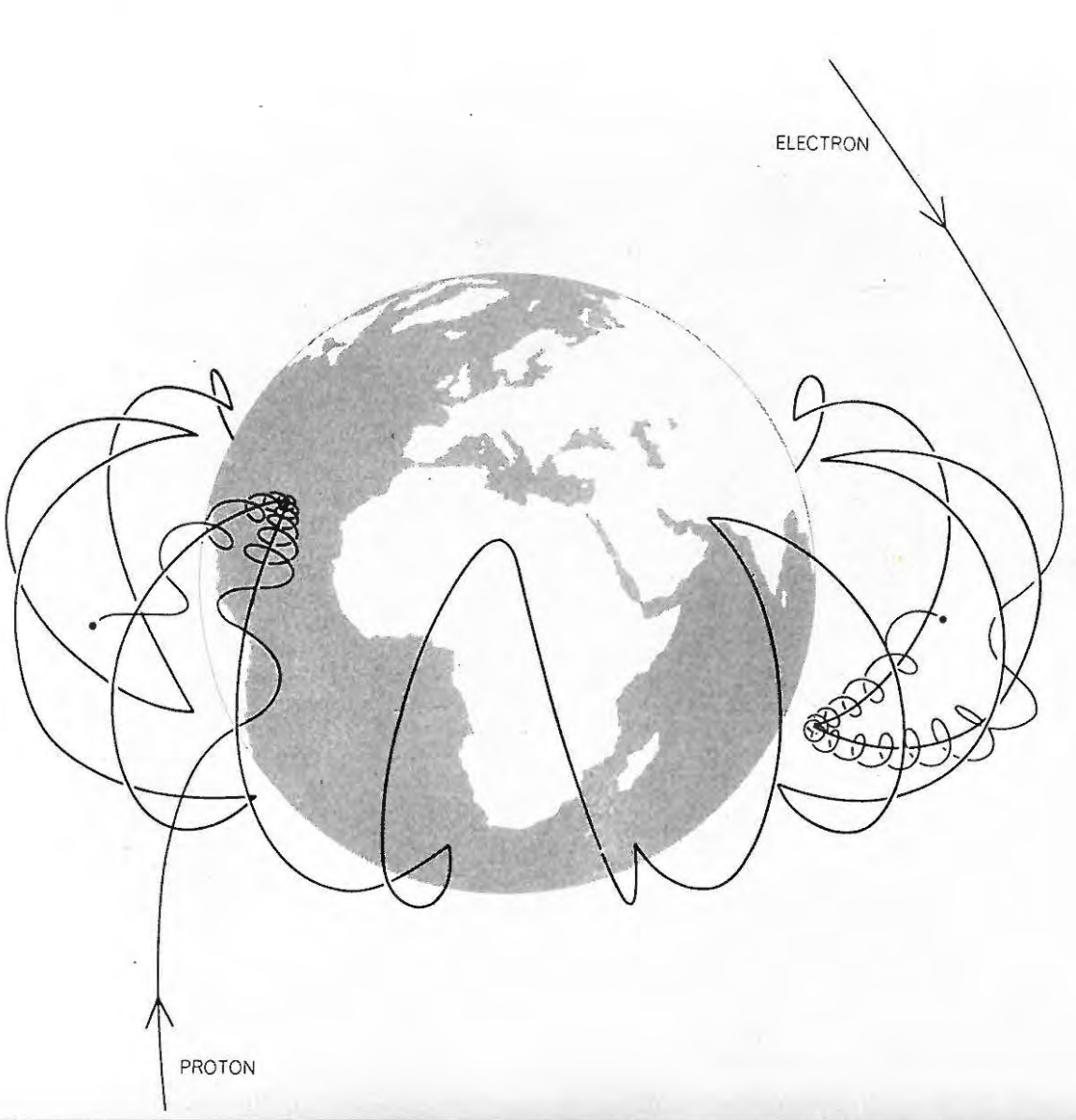
ELECTRON
PROTON

particle has a magnetic moment given by

$$\Gamma = \pi a^2 i = \pi a^2 \frac{e}{T} \qquad 1.30$$

where T is the period of gyration. Using 1.4 we get

$$\Gamma = \pi \left[\frac{m v_\perp}{e B} \right]^2 \frac{e}{T}$$

and since $w = \frac{2\pi}{T} = \frac{B e}{m}$,

$$\Gamma = \frac{w}{2 e} \left[\frac{m v_\perp}{B} \right]^2 = \frac{m v_\perp^2}{2 B} \qquad 1.31$$

Assuming that the magnetic field has only a small gradient parallel to the field lines, Γ will be an adiabatic invariant of the particles' motion provided that the magnetic field varies slowly compared with T. (6) This implies that $\frac{v_\perp^2}{B}$ is constant. If, then, the pitch angle is χ, we have

$$\frac{v^2 \sin^2 \chi}{B} = \text{constant}$$

which leads to the mirroring equation 2.19 again, namely

$$\sin^2 \chi = \frac{B}{B_o} \sin^2 \chi_o$$

where χ_o and B_o are the values of χ and B at some arbitrary fixed point on the trajectory. The above equation is Alfvén's mirror equation (5).

Since the geomagnetic field is not symmetric about any axis there will be field gradients and components of line curvature which produce drifts in a generally radial direction. However the particle will return to its original line of force if the 'longitudinal adiabatic invariant', J, is constant, that is

$$J \doteq \int_{B_m}^{B'_m} P_{//}\, d\,z = \text{constant} \qquad 1.32$$

Here $P_{//}$ is the component of the particles' momentum parallel to $\bar{B}$ and dz is an element of length along the field line. The integral is taken along the line of force between two consecutive mirror points B_m and B'_m (6). It has been shown that 1.32 holds if the effects of the drift and the time dependent variation of $\bar{B}$ are small during one period of oscillation, that is the time taken to move between consecutive mirror points. In a static field the particle thus sweeps out a 'longitudinal invariant surface', that is one on which 1.32 holds. These invariant surfaces form a three-parameter family, the three parameters being (for a static field) the magnetic moment, the longitudinal invariant, and the total energy of the particle. Thus if particles having different magnetic moments or total energies start on the same field line they will drift at different rates and on different invariant surfaces, but will all return to the original field line after drifting right round the earth.

To treat the time dependence of the field a third adiabatic invariant is required. This is the 'flux invariant' $\bar{\Phi}$, where $\bar{\Phi}$ is the flux enclosed by the invariant surface on which the particle moves. It has been shown that if the variation of the field is small during the time taken for the particle to move round the earth on the invariant surface, then $\frac{d\,\bar{\Phi}}{d\,t} = 0$. In a time dependent field the total energy of the particle is no longer constant, but if the variation of the field with time is slow enough the total

energy may be replaced by $\bar{\Phi}$, the three parameters then being , Γ the longitudinal invariant, and $\bar{\Phi}$. These then are sufficient to prescribe the motion of the particle. Notice that $\bar{\Phi}$ is a function of the magnetic moment, the longitudinal invariant, and the total energy of the particle.

Thus we see that if the time variation of the field is slow compared with the period of gyration but comparable with the period of oscillation, only Γ is retained as an invariant. If it is slow compared with the period of oscillation but comparable with the time taken to drift round the earth Γ is invariant and 1.32 holds. Lastly, if it is slow compared with the drift time round the earth, all three invariant conditions hold.

Detailed examinations of breakdown of these conditions have been presented by several authors but are beyond the scope of this chapter. [(7), (8), (9), (10)]. An approximate theory for movement of a charged particle in a dipole field has been presented by Alfvén (5), and in addition several authors have presented full treatments of motion in a perturbed dipole field (11) and in the geomagnetic field (12). An example of the fluid model treatment applied directly to the belts is the work of Walt and Mc Donald [(13), (14)].

In conclusion it must be pointed out that many of the trapped particles have relativistic energies and can not be treated using the theory as presented in this chapter. The equations for guiding centre motion and those for the adiabatic invariants can however be

written in a form which remains valid for relativistic particles (6).

1-6 Mc Ilwains Coordinates for Mapping the distribution of Trapped Particles.

As implied previously, dipole representations of the geomagnetic field have been found to have insufficient accuracy for the study of trapped particles. This prompted Mc Ilwain (15) to propose a co-ordinate system which not only takes account of the non-dipole character of the geomagnetic field but can also be used to order measurements along lines of force as is necessary in most theoretical studies and for clarity in the presentation of experimental data. This coordinate system has been widely used in the literature and will therefore be briefly described here.

For a static field, if we consider the case where there are no electric fields the system of invariant surfaces is degenerate and we may write

$$I = \frac{J}{P} = \int_{B_m}^{B'_m} \left[1 - \frac{B(z)}{B_m} \right]^{\frac{1}{2}} dz \qquad 1.33$$

where P is the total momentum of a particle which mirrors at B_m. [It should be noted here that Mc Ilwain is confused about the definition of I which he identifies with J. I is however an invariant in this case since P is constant here, and thus no error arises in his final result. Also his notation is confusing and we use in preference the notation of Stone (16)]. The way in which the

mirror equation is derived in section 1-5-2 makes it obvious that B_m is an invariant of the particles' motion, so that the two invariant parameters I and B_m are, in this case, sufficient to specify the invariant surface or 'shell' on which the particle moves. The points having the same value of B_m and I form a ring in each hemisphere and a particle mirroring at this B_m and I will remain in the shell described by the lines of force that connect these rings. In general of course two particles mirroring initially at different values of B along a particular line of force will not drift on the same shells. Mc Ilwain shows however that this effect is comparatively small in the geomagnetic field. An important consequence of this is that the omnidirectional intensity and also the directional intensity are approximately constant along the loci of constant B_m and I. This fact is the basis of an argument to be presented in Chapter 4 of this thesis since it implies that we may assume that the intensity at a point A in the Southern hemisphere is approximately the same as that at a point A' in the Northern hemisphere if the values of $B = B_m$ and I are the same for points A and A'.

A further consequence of the above is that equation 1-32 may be applied to all particles at a point in space, and not only to those mirroring at that point, without significant loss of accuracy. Mc Ilwain therefore chose to use I as a parameter which can be considered to be a scalar field that has a definite value at each point in space and <u>does not require explicit reference to the motion of trapped particles</u>. As pointed out by Stone (16), for strict

accuracy one must admit an implicit dependence on the motion of the trapped particles in as much as 1.33 really defines I in such a way that the value of the scalar field at a point applies only to the particles mirroring at that point. In other words we admit the fact that particles mirroring at different values of B on a particular line of force will drift in a different surface. Stone (16) shows that if we take this more accurate view, the coordinate system defined by Mc Ilwain may be redefined in such a way as to extend its usefulness considerably. Stone's article is however a fairly recent one (July 1963) and his ideas have not been used by the authors quoted in this thesis. We will therefore describe the coordinate system as originally defined by Mc Ilwain. We have seen that a coordinate system consisting of B and I may be used to bring order to measurements made at different geographic locations. Obviously it is desirable to find a method of labelling all points in space with a number which is unique for each invariant surface, and which, if possible, has some easily conceivable physical significance. Mc Ilwain has shown that a parameter $L = f(B, I)$ can be defined in such a way that it retains most of the desirable properties of I and has the additional property of coordinating measurements along lines of force. (Stone has defined the parameter by $L = f(B_m, I)$ and points out that it is an invariant when defined in this manner.)

In general L should be regarded as a parameter which retains most of the useful properties of I exactly and is also approximately

constant along the lines of force. It is defined in such a manner that for a pure dipole field an invariant surface (B, I) is labelled with an L numerically equal to the equatorial radius of the surface in units of earth radii. (Note that even in the geomagnetic field an invariant surface (B_m, I) has a characteristic radius L, which is equal to the radius of the same invariant surface in a dipole field if we use Stone's definition of L. (16)).

CHAPTER 2.

THE RADIATION BELTS.

2-1 Introductory Remarks.

In the previous chapter we have gained a rough idea of the motion of charged particles in the magnetosphere. The motion of each particle can be broken up into three components, (a) gyration round a line of force, (b) a 'bouncing' movement along the lines of force between mirror points in the northern and southern hemispheres, and (c), a drift in longitude. An idea of the time scale involved can be gained from the following. For a 1 MeV electron the gyrofrequency is of the order of 10^{-6} seconds, the 'bounce' period of the order of 10^{-1} seconds, and the time taken to drift once round the shell of the order of 10^{3} seconds.

In this chapter we shall discuss briefly, and in a very general manner, the distribution of radiation trapped in the geomagnetic field as revealed by experimental data from rocket and satellite observations. Before doing so however, it is necessary to define two terms which will be used frequently throughout this thesis, and say a few words about them. Firstly, we shall refer to the region (above the ionosphere) in which the geomagnetic field has a dominant control over the motions of fast charged particles as the '*Magnetosphere*'. [This is the way in which the term was originally defined by Gold. (17)] . Secondly, we shall refer to that region, in the magnetosphere, in which particles can

remain trapped for relatively long times, as the 'Trapping Region'. We now discuss briefly the shape and extent of the magnetosphere and the trapping region.

The diversity and variability of conditions in the magnetosphere and the trapping region are such that we have only the sketchiest of pictures of their outlines from the data available to date. From such observations as are at present available [(18), (19), (20), (21), (22), (23)] and from theoretical work in this connection [(12), (24), (25), (26), (27), (28), (29), (30), (31)], we may draw the following conclusions.

Plasma from the sun's corona is streaming radially outward from the sun in the vicinity of the earth. This 'solar wind', the density and velocity of which apparently depends on the level of solar activity to a certain degree, confines the geomagnetic field to the vicinity of the earth. (Recent satellite magnetometer data have shown that the geomagnetic field has a definite, but highly turbulent and distorted boundary.) The solar wind thus distorts the magnetosphere with the result that it measures some tens of thousands of kilometres perpendicular to the direction of the solar wind [i.e. perpendicular to the earth-sun line (18)], and perhaps 200,000 kilometres or more parallel to the direction of the solar wind. Conditions on the sunward side are at present much better known than those on the night side. On the sunward side the distance, in the equatorial plane, to the boundary of the magnetosphere can vary between about 40,000 kilometres and about

70,000 kilometres, depending on the 'strength' of the solar wind. This is of course the distance to the boundary of the trapping region as well, since this boundary is determined roughly by the degree of distortion of the field lines. (Trapped radiation can only move along relatively undistorted field lines.) Again referring to the sunward side, the most distant lines of force which can guide a charged particle down to the surface of the earth meet it at about 75° north and south magnetic latitude. The corresponding lines of force on the night side meet the surface of the earth at about 70° north and south magnetic latitude. Thus there are 'holes' in the trapping region in the north and south polar regions. The lower boundary of the trapping region is determined by the height at which trapped particles encounter an atmospheric density great enough to absorb them or at least to scatter them out of the trapping region. We must therefore visualize a toroidal trapping region inside an 'egg-shaped' magnetosphere.

The complexity and variability of the phenomena we are about to describe are such that we can give only the broad outline in the following sections. This outline has been extracted from the most quoted and significant articles in the field, and a reasonably complete set of references is given. Detailed results will be presented, where required, in the later chapters of this thesis.

2-2 The Discovery of the Radiation Belts.

The existence of an unexpectedly high intensity of energetic

charged particles trapped in the magnetosphere was discovered by Van Allen and his colleagues at the State University of Iowa in 1958, and represents the most spectacular achievement of the I.G.Y. Some of the principal accounts of early observations are to be found in references (33), (34), (35), (36), (37), (38), (39), (40), (41), (42), (43), (44). The first U.S. satellite, Explorer I, went into orbit on the 31st January, 1958, and was equipped with a Geiger tube for the purpose of detecting cosmic-rays. At low altitude the counting rate increased with height as expected, but at great height the count rate dropped and sometimes even fell to zero, particularly in the equatorial regions. It was suspected at the time that the violence of the launching had damaged the Geiger tube. A similar Geiger tube, carried into orbit in Explorer III on March 26th, 1958, behaved in the same manner. When the satellite went out to between 650 and 800 kilometres altitude, the apparent counting rate rose rapidly and then dropped almost to zero. It was then realized that the low apparent counting rate might be the result of saturation and jamming of the counters by an unexpectedly high flux of radiation.

This was soon confirmed, and information about the radiation was greatly extended by readings taken by U.S. satellite Explorer IV, U.S. moon probes Pioneer I, Pioneer III and Pioneer IV, and by the Soviet satellites Sputnik I and Sputnik II, and moon probe Lunik I (when the Russian data was published). Explorer IV was equipped with high radiation intensities in mind and was launched into an orbit having a larger inclination (51°) than its predecessors in

order to cover a larger area of the earth. It was launched on July 26th, 1958, and during the following two months sent back readings covering a range of latitude of more than 50° on either side of the equator up to an altitude of 2,200 kilometres. This altitude however corresponds only to the lower reaches of the Van Allen belts as they were revealed by Pioneer III, launched on December 6th, 1958. Though this rocket failed to reach the vicinity of the moon as was originally intended, detectors mounted by Van Allen and his colleages gave excellent readings of radiation intensities to a radial distance of 107,400 kilometres from the centre of the earth both on the outward and return journey. These revealed clearly the existence of two belts of high energy particles round the earth, separated by a distinct 'slot'. The inner belt had a peak intensity at approximately 10,000 kilometres from the centre of the earth, while the outer belt had a peak intensity at approximately 23,000 kilometres from the centre of the earth, both these distances being measured in the equatorial plane. Pioneer IV, launched on March 3rd, 1959, after a period of intense auroral and magnetic activity, showed the outer belt expanded and greatly enhanced in intensity. Results obtained from Sputnik III and Mechta by Soviet observers were in general agreement with those from Explorer IV and Pioneer III.

By March, 1959 Prof. Van Allen was able to present the tentative picture of the radiation belts shown in Figure 4. (35)

Figure 4 The Van Allen radiation zones as pictured in March, 1959. Lines of equal radiation intensity are shown, and the horizontal scale shows the distance, in earth radii, from the centre of the earth. Reproduced from reference (32).

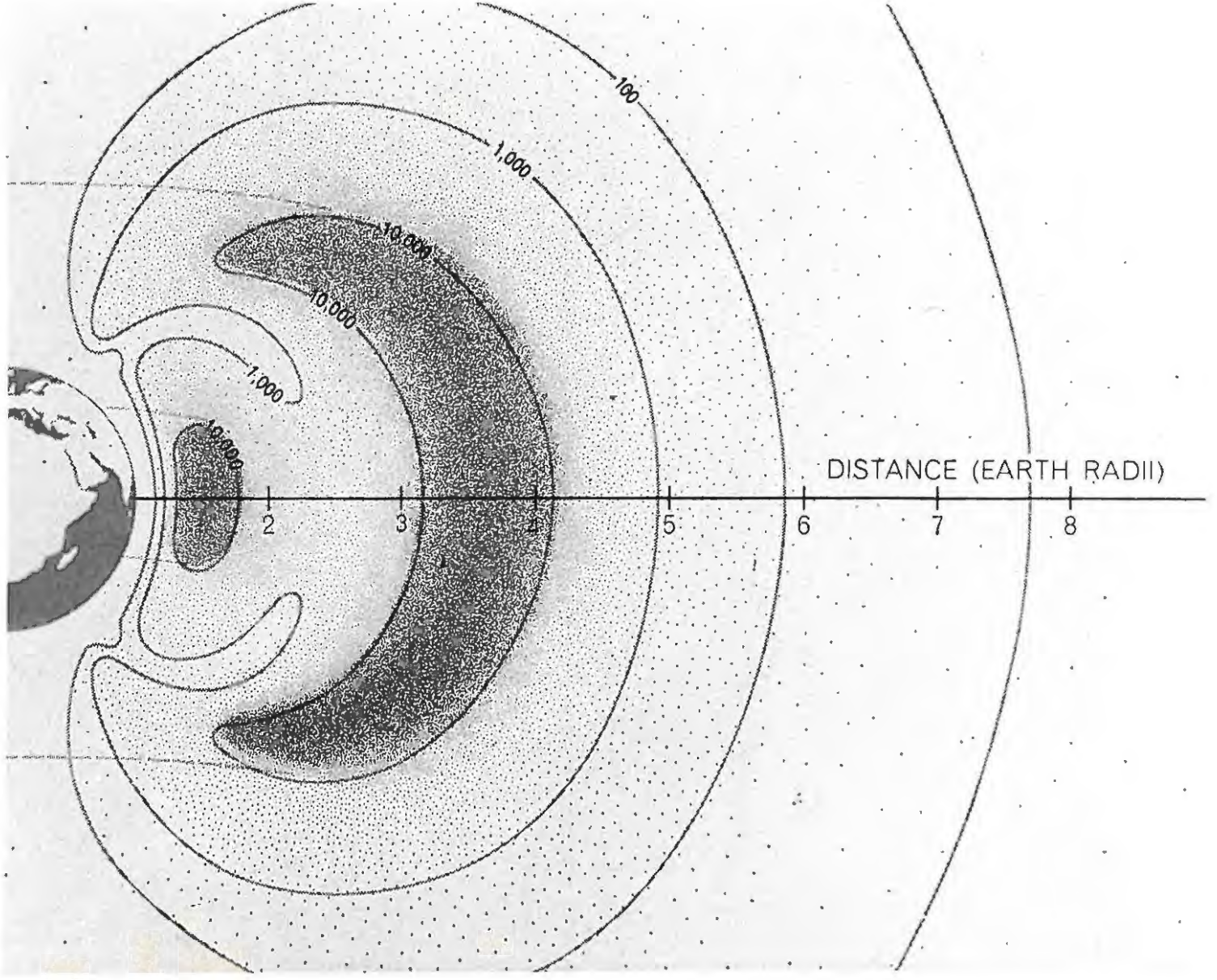
100
1,000
10,000
10,000
1,000
10,000
DISTANCE (EARTH RADII)
2
3
4
5
6
7
8

2-3 The Distribution and Characteristics of the Trapped Radiation.

The variability of conditions in the trapping region, particularly at distances beyond about 3 E_R, is such that the figures given in this section should be treated with reserve. In addition the difficulty of arriving at representative figures from readings taken at various times and positions in the trapping region should be borne in mind. One of the most important things we must realize here is that for a particular satellite or rocket the observed distribution depends critically on the range of energies observed, and hence on the instrumentation. The early observations described in the previous section were, except in the case of the Soviet space vehicles, confined to high energies, and it is only in such cases that it becomes necessary to distinguish clearly two separate radiation belts. These, then, are the Van Allen Belts.

The first conclusion we may draw from the earliest satellite observations is that the radiation observed consists of charged particles since the counting rate at an altitude of 700 kilometres is considerably less than that at an altitude of 1000 kilometres. Then because the path between 1000 kilometres and 700 kilometres in the atmosphere is very much less than the path through the detector shielding we may conclude that a large part of the radiation observed at 1000 kilometre altitude is mirroring before it gets to 700 kilometres (in the region of these measurements) and must therefore consist of charged particles (34). The rockets Pioneer I, Pioneer III and Mechta showed that the inner belt extends from about 1.25 E_R

to about 1.75 E_R and the outer belt from about 3.1 E_R to about 4.2 E_R for high energy particles (figure 4). (These are geocentric distances measured in the equatorial plane.) We propose in the following outline to divide the trapping region rather arbitarily into two zones. We consider first radiation which crosses the equatorial plane at geocentric distances of less than 2.2 E_R, and then radiation crossing the equatorial plane beyond this distance. In the following sections and subsections the word 'distance' should be taken to mean radial geocentric distance in the equatorial plane unless otherwise stated. 'Altitude' should be taken to mean altitude at the particular location of the observations unless otherwise stated. In addition, the following points will prove helpful.
(1) The words 'intensity' or 'flux' will be used to denote the number of particles crossing unit area per unit time. (c.g.s. Units are used in the literature and we will therefore use them in our discussion.) In a realistic case the alignment of a detector with respect to the direction of the magnetic field lines in its vicinity is found, its aperture determined, and the count rate recorded interpreted in terms of the number of particles crossing unit area per unit time per unit solid angle in a specified direction. This is called the 'unidirectional intensity'. (From what we know of the movement of charged particles in the geomagnetic field it is clear that we need, in general, specify only the angle between the vector $\bar{B}$ and the axis of the detector, since rotating the detector round a field line will not produce changes in the counting rate in the

idealistic case.) We then integrate the unidirectional intensity over the whole of space to get the 'omnidirectional intensity'. What is often done in order of magnitude calculations is to make the assumption that the flux is isotropic, in which case $J_o = 4\pi J_u \sim 10 J_u$, where

$J_u \equiv$ unidirectional intensity and

$J_o \equiv$ omnidirectional intensity. (2) The energy spectrum of the particles is usually given in exponential form. Thus the statement that 'the energy spectrum has the form $E^{1.6}$, indicates that we find that

$$\frac{d N}{d E} = E^{1.6}$$

where N is the number of particles per unit range of energy per unit area per unit time. A number of different conventions are in use however, and in general the units given will show how the mathematical form of the spectrum is expressed. The spectrum is said to be 'hard' if a lot of high energy particles are present, and 'soft' if a lot of low energy particles are present.

The attention of the reader is drawn to the fact that many of the earlier figures derived for intensities (particularly in connection with the outer belt) were too high by a factor of approximately 10^3 since they were derived from the observed response of detectors with a minimum wall thickness of approximately 1 gm/cm^2 of intermediate Z material on the assumption that this response was due mainly to bremsstrahlung from non-penetrating electrons (i.e. with energy

$E_e < \sim 2$ MeV) with an effective energy of approximately 50 keV. It was only in January, 1962 that O'Brien et al. were able to demonstrate conclusively that this assumption was wrong (58). They showed that the response of this type of detector was in fact mainly due to penetrating particles. This led to a large scale revision of the interpretation of the counting rates.

The following outline has been drawn up using references (33) to (82).

2-3-1 Trapped Radiation out to $2.2E_R$ ($L \sim 2.2$)

A. Protons. Of the radiation penetrating 140 mg/cm^2 approximately 1% penetrates several gms/cm^2. The more penetrating radiation has been identified as protons of approximately 20 to 40 MeV. The energy flux due to these protons is only about 0.05 of the total energy flux. At approximately 1000 kilometers altitude over the central Atlantic only 3% to 7% of the particles having range greater than that of a 160 keV electron are protons. At a given altitude the spectrum and intensity of protons is found to vary with latitude. Some of the proton energies, measured by means of nuclear emulsions mounted in rockets, are as large as 600 or 700 MeV. It is these energetic protons which account for the large intensities recorded by early experiments in the inner belt. The energy spectrum has been investigated by the same means and for energies $E_p > 30$ MeV has the form $E_p^{1.65}$ at about 28°

geomagnetic latitude in the northern hemisphere, generally becomming softer with increasing L. The dependence of the spectrum on L has been given in the form

$$\frac{d N}{d E} = I_o e^{- E/E_o}$$

where $E_o = (306 \pm 28) L^{- (5.2 \pm 0.2)}$ MeV (80).

B. Electrons: As implied previously electrons form the major component, though they are less penetrating than the proton component, their maximum energy being about 1 MeV. Peak intensities occur at a distance of about 10,000 kilometres. The position of the peak intensity follows this line of force to a magnetic latitude of about 25^o and then turns outward from the earth. At the position of peak intensity in the equatorial plane the flux is of the order of 10^8 electrons/cm^2sec for $E_e >$ 200 keV. Some sample figures for the unidirectional flux perpendicular to $\bar{B}$, which we call J'_u, are as follows. On the geomagnetic equator at L = 1.22,

J'_u (E_e 40 keV) = 5 x 10^6 electrons/cm^2sec ster.

At altitude 1,600 kilometres and for

L = 1.3, J'_u ($E_e \geq$ 0.6 MeV) = 4.5 x 10^5 /cm^2sec ster

L = 1.6, J'_u ($E_e \geq$ 0.6 MeV) = 1.8 x 10^5 /cm^2sec ster

L = 1.8, J'_u ($E_e \geq$ 0.6 MeV) = 5 x 10^4 /cm^2sec ster

L = 2.2, J'_u ($E_e \geq$ 0.6 MeV) = 3 x 10^3 /cm^2sec ster.

In general we may say that the maximum value of J_u ($E_e \geq$ 40 keV) is of the order of 10^6 and falls off less rapidly with L at constant altitude than the proton intensity does.

The electron energy spectrum rises rapidly towards low energies and becomes slightly softer with increasing L.

2-3-2 Trapped Radiation beyond 2.2 E_R ($L \sim 2.2$)

A. Protons: Protons permeate the entire region out to about 70,000 kilometres, becomming less and less dense as the distance increases. (This is not surprising as their gyroradius increases with distance for a given energy and they therefore have an increasing tendency to escape from the trapping region.) Low energy protons become increasingly important for distances less than about 27,000 kilometers. Rocket measurements taken at altitudes between 1200 and 5600 kilometres (42°N to 30°N geomagnetic latitude) show that the unidirectional flux averaged over pitch angles between 90° and 58° of the order of 10^5 protons/cm^2 sec ster. There is a tendency for this to increase with increasing altitude and decreasing latitude. We quote some results from Explorer XII for a pass on October 5th 1962 (78) which seem to be the best figures to date. Distances given here are in the plane of the satellite orbit which is inclined at 71° to the earth-sun line.

Between 103,000 and 75,000 kilometres:-

$$J_o\ (E_p \geqslant 50\ \text{keV}) \leqslant 500\ /\text{cm}^2\ \text{sec.}$$

At 65,000 kilometres:-

$$J_o\ (E_p \geqslant 500\ \text{keV}) \leqslant 1.5 \times 10^4\ /\text{cm}^2\ \text{sec.}$$

At 55,000 kilometres:-

$$J_o\ (E_p \geqslant 500\ \text{keV}) \leqslant 5 \times 10^4\ /\text{cm}^2\ \text{sec.}$$

(In the region between 72,000 and 52,000 kilometres rapid time variations, and/or irregular spacial distributions, of the intensity are observed. These fluctuations disappear at approximately 48,000 kilometres.) The intensity remains fairly constant to about 27,000 kilometres where low energy protons become a very important component of the flux.

At 20,000 kilometres:-

$$J_o\ (E_p \geqslant 500\ \text{keV}) = 4 \pm 2 \times 10^6\ /\text{cm}^2\ \text{sec.}$$

$$J_o\ (E_p \geqslant 4.5\ \text{MeV}) \leqslant 1.5 \times 10^4\ /\text{cm}^2\ \text{sec.}$$

The proton spectrum changes markedly between 20,000 and 10,000 kilometres. Beyond 20,000 kilometres it softens, as we may expect.

B. Electrons: It seems that a clear cut outer belt structure is only observed when considering electrons with $E_e \geqslant 1.6$ MeV. In this case we find a peak intensity at 32,000 kilometres and the slot at 18,000 kilometres. (Distances in the plane of Explorer XIV orbit - see A.) On a number of occasions bifurcation of the outer zone

has been observed with one peak in intensity at 17,000 kilometres and another at a distance varying between 23,000 and 28,000 kilometres. Data from Explorer VI (67) over a period of two months shows bifurcation in only 12% of the analysed passes however, and time averaged data from U.S. satellite Injun I indicates no clear cut bifurcation. This phenomenon has not been clearly explained yet. The position of the peaks seems to be dependant on other factors besides the energy range of the detector.

Soviet results with Lunik II (60) for low energy electrons with $E_e > 200$ eV show that these permeate the entire region. For altitudes $< 22,000$ kilometres they get $J_o (E_e > 200 \text{ eV}) < 2 \times 10^7 /\text{cm}^2$ sec. Low energy electrons appear to dominate the regions between altitudes of 50,000 and 70,000 kilometres where $J_o (E_e > 200 \text{ eV}) \sim 10^8 /\text{cm}^2$ sec. These results are in general agreement with those from Injun I (62) which show that the time averaged value of $J (E_e > 40 \text{ keV})$ $\sim 10^5$ to $10^6 /\text{cm}^2$ sec ster between $L \sim 2$ and $L \sim 10$. The intensity falls off very rapidly between $L \sim 10$ and $L \sim 15$ and is extremely variable in this region.

Results from Explorer XII [(58), (70)], the first satellite to provide conclusive measurements of the intensities of electrons of approximately 50 keV,

indicate the following for a typical pass. Between 25,000 and 55,000 kilometres J_o (E_e; 40 to 55 keV) $\sim$ 10^7 /cm^2 sec and is constant within a factor 2 or 3. It then diminishes rapidly near the boundary of the geomagnetic field which is typically at about 65,000 kilometres. $J_o(E_e$; 80 to 110 keV) shows similar radial dependence and has a similar value, but drops towards zero at a smaller distance.

Again we quote Explorer XIV results for the pass of 5th October, 1962 (78). (Distances in the plane of the orbit - see A.)

Between 103,000 and 75,000 kilometres:-

$$J_o\ (E_e \geq 40 \text{ keV}) \leq 500 \text{ /cm}^2\text{sec.}$$

This increases sharply at 72,000 kilometres. Between 72,000 kilometres and 52,000 kilometres there are rapid time variations and/or irregular spacial distributions of intensity. Typical intensities in this region are as follows.

At 65,000 kilometres:-

$$J_o\ (E_e \geq 40 \text{ keV}) = 1 \times 10^6 \text{ /cm}^2\text{sec.}$$
$$J_o\ (E_e \geq 230 \text{ keV}) \leq 6 \times 10^3 \text{ /cm}^2 \text{ sec.}$$
$$J_o\ (E_e \geq 1.6 \text{ meV}) \leq 2 \times 10^2 \text{ /cm}^2 \text{ sec.}$$

At 55,000 kilometres:-

$$J_o\ (E_e \geq 40 \text{ keV}) = 2 \times 10^7 \text{ /cm}^2\text{sec}$$
$$J_o\ (E_e \geq 230 \text{ keV}) \leq 3 \times 10^4 \text{ /cm}^2 \text{ sec.}$$
$$J_o\ (E_e \geq 1.6 \text{ meV}) \leq 1.5 \times 10^3 \text{ /cm}^2 \text{ sec.}$$

At approximately 48,000 kilometres the fluctuations disappear, and the energy spectrum becomes flatter. Peak intensities are reached at the following distances.

For $E_e \geqslant 230$ keV and $E_e \geqslant 1.6$ MeV - $\sim 32,000$ kms.

For E_e ; 40 to 200 keV - $\sim 38,000$ kms.

Typical intensities in the heartof the zone are.

At 39,000 kilometres:-

$$J_o\ (E_e \geqslant 40\ \text{keV}) = 1.5 \times 10^8\ /\text{cm}^2\ \text{sec.}$$

$$J_o\ (E_e \geqslant 230\ \text{keV}) \leqslant 1.5 \times 10^6\ /\text{cm}^2\ \text{sec.}$$

$$J_o\ (E_e \geqslant 1.6\ \text{MeV}) = 2 \times 10^5\ /\text{cm}^2\ \text{sec.},$$

and at 31,000 kilometres:-

$$J_o\ (E_e \geqslant 40\ \text{keV}) = 1 \times 10^8\ /\text{cm}^2\ \text{sec.}$$

$$J_o\ (E_e \geqslant 230\ \text{keV}) \leqslant 5 \times 10^6\ /\text{cm}^2\ \text{sec.}$$

$$J_o\ (E_e \geqslant 1.6\ \text{MeV}) = 1 \times 10^6\ /\text{cm}^2\ \text{sec.}$$

A marked change in the characteristics of the radiation occurs at approximately 27,000 kilometres as mentioned in A.

At 20,000 kilometres:-

$$J_o\ (E_e \geqslant 230\ \text{keV}) \leqslant 4 \times 10^4\ /\text{cm}^2\ \text{sec.}$$

The electron spectrum and pitch angle distribution up to an altitude of 1045 kilometres along a line of force ($L = 2.4$) has been measured by Cladis et al. (55). Some of their results are shown in figures 5 and 6. No change in the shape of the spectrum was observed above an altitude of 600 kilometres, but the

Figure 5 Reproduction of figure 8 Cladis et al (55) showing the electron energy spectrum at 980 km.

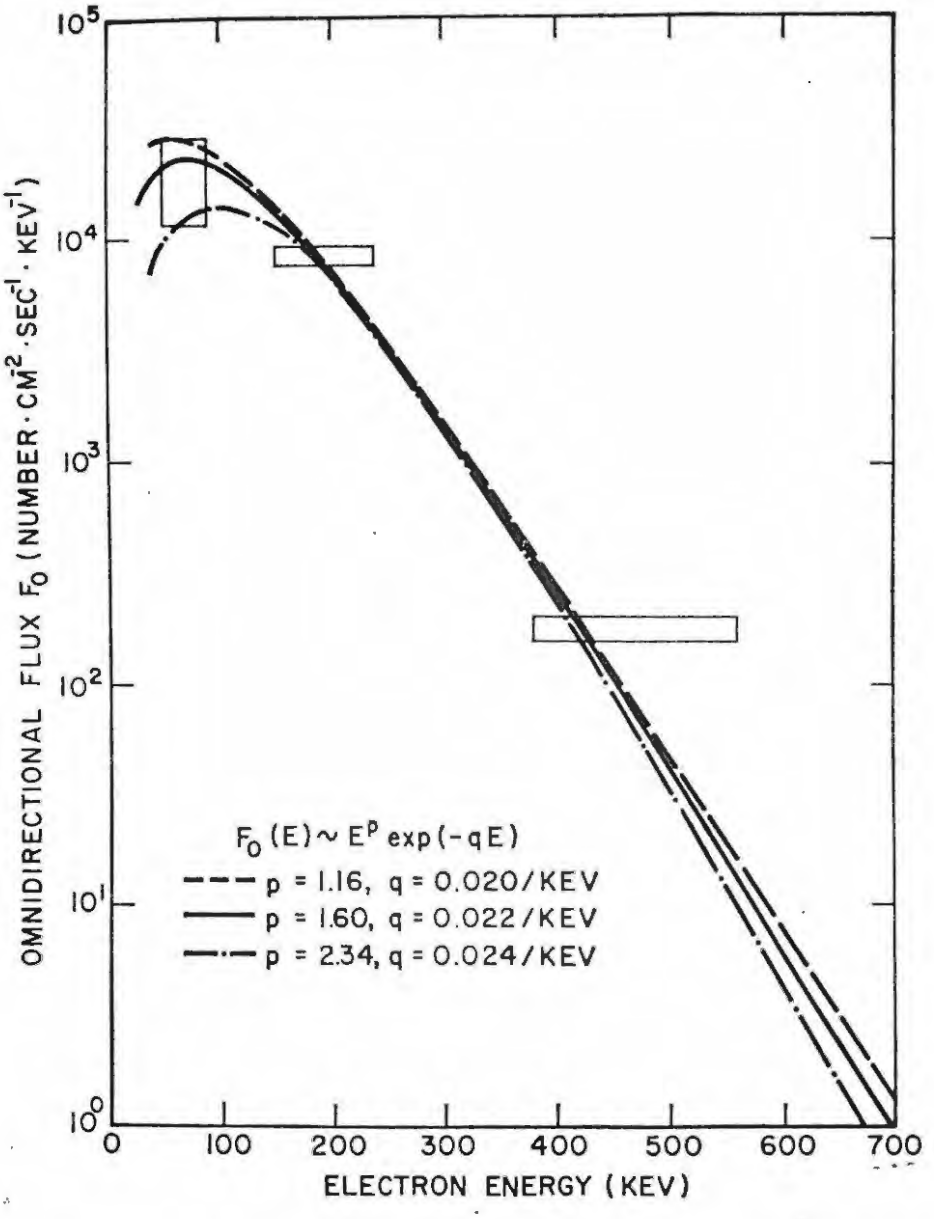

Fig. 8. Omnidirectional electron flux at 920 km. The rectangles give the first approximation to the spectrum; the heights of the rectangles designate probable errors of the measurements; and the horizontal extents of the rectangles represent the energy-sensitive regions of the Geiger tubes (half-height values of response functions). The solid-line curve gives the best fit of the mathematical form $E^p \exp(-qE)$ to the data. This best-fit curve was obtained for $p = 1.60$, $q = 0.022$/kev. The dashed lines give the extreme spectrum shapes that fit the data with a probability of $1/e$ that of the best fit.

Figure 6 Reproduction of figure 5 from Cladis et al (55) showing the pitch-angle distribution of electrons at 750 km.

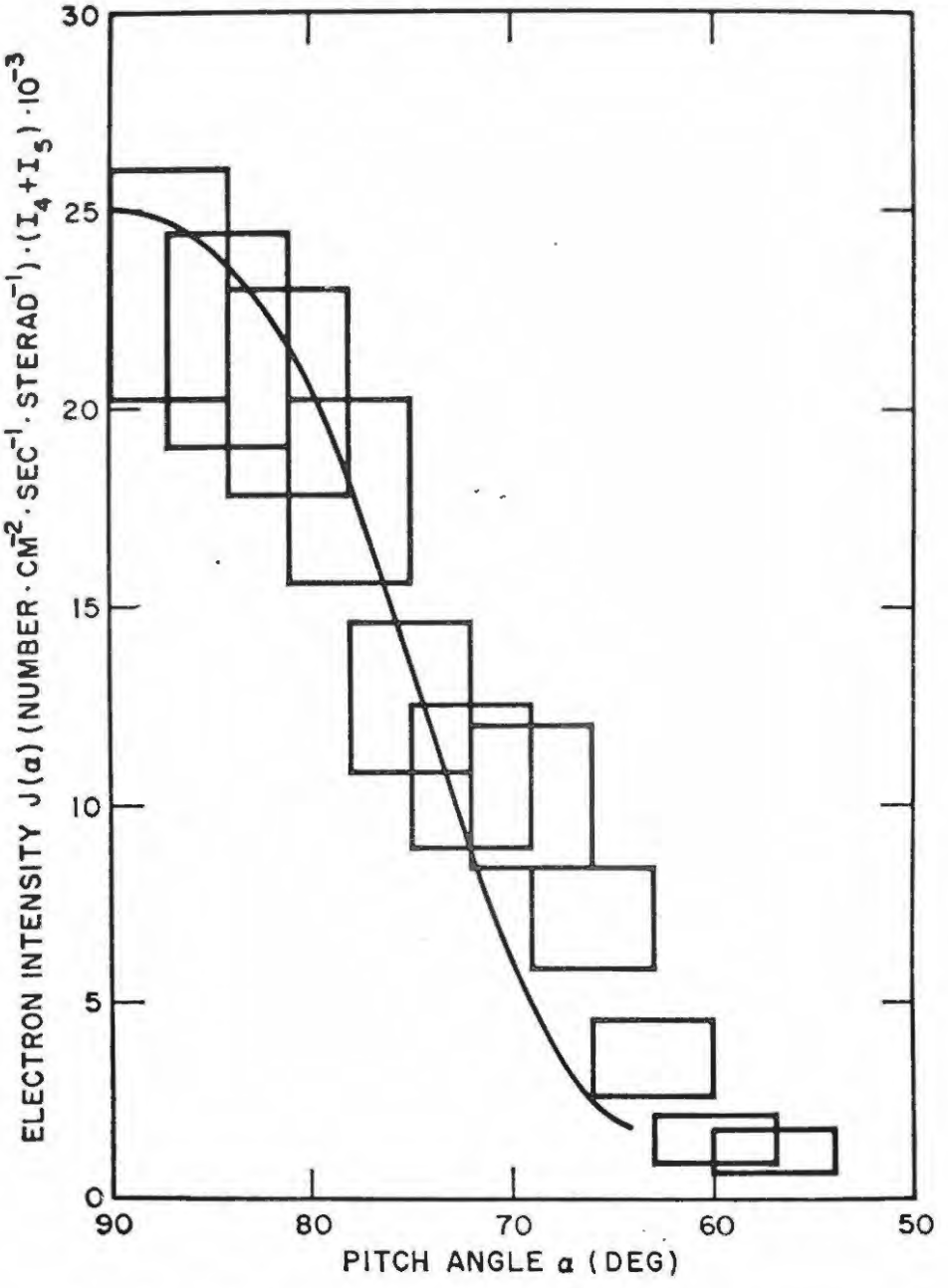

Fig. 5. Pitch-angle distribution of electrons at 750 km. The rectangles represent the direct measurements of the distribution obtained by correlating the counting rates of the Geiger tubes with the angle the collimator made with the local geomagnetic field vector. The curve in the figure is the distribution computed from the measurements of the mirror-point values of the flux along the geomagnetic field line at lower altitudes.

pitch angle distribution gets wider as the altitude increases, as we would expect from trapped particles. The width of the distribution increases from 31.2° to 41.6° as the altitude increases from 750 to 900 kilometres. Injun I measurements (62) indicate that the spectrum depends strongly on distance and that it is subject to important time variations, but is consistent with that of Cladis et al. where comparison is possible. Further indications (70) are that the outer fringe of the outer zone at approximately 64,000 kilometres has a much steeper spectrum than the inner part, but that the radiation is softer. In general the radiation softens as the radial distance increases.

2-4 Variability of the Trapped Radiation.

From our discussion in the previous section we see that the quiet time situation in the trapping region, as far as we know it at present, may be represented schematically as in figure 7. The following brief outline of variations in the trapping region has been compiled mainly from references (40), (48), (50), (51), (53), (56), (57), (63), (67), (68), (71).

Analysis of Explorer VII data, pertaining to the inner belt, over the period October 13th, 1959 to December 31st, 1960 shows that the intensity increased by a factor 2 or 3 (for high energy particles) but that the geometric form remained the same even during periods of

Figure 7 Schematic representation of the quiet time situation in the trapping region. Lines of force of the geomagnetic field are shown as white lines. The grey line represents the boundary of the magnetosphere, and the white arrows represent the solar wind. Reproduced from reference (32)

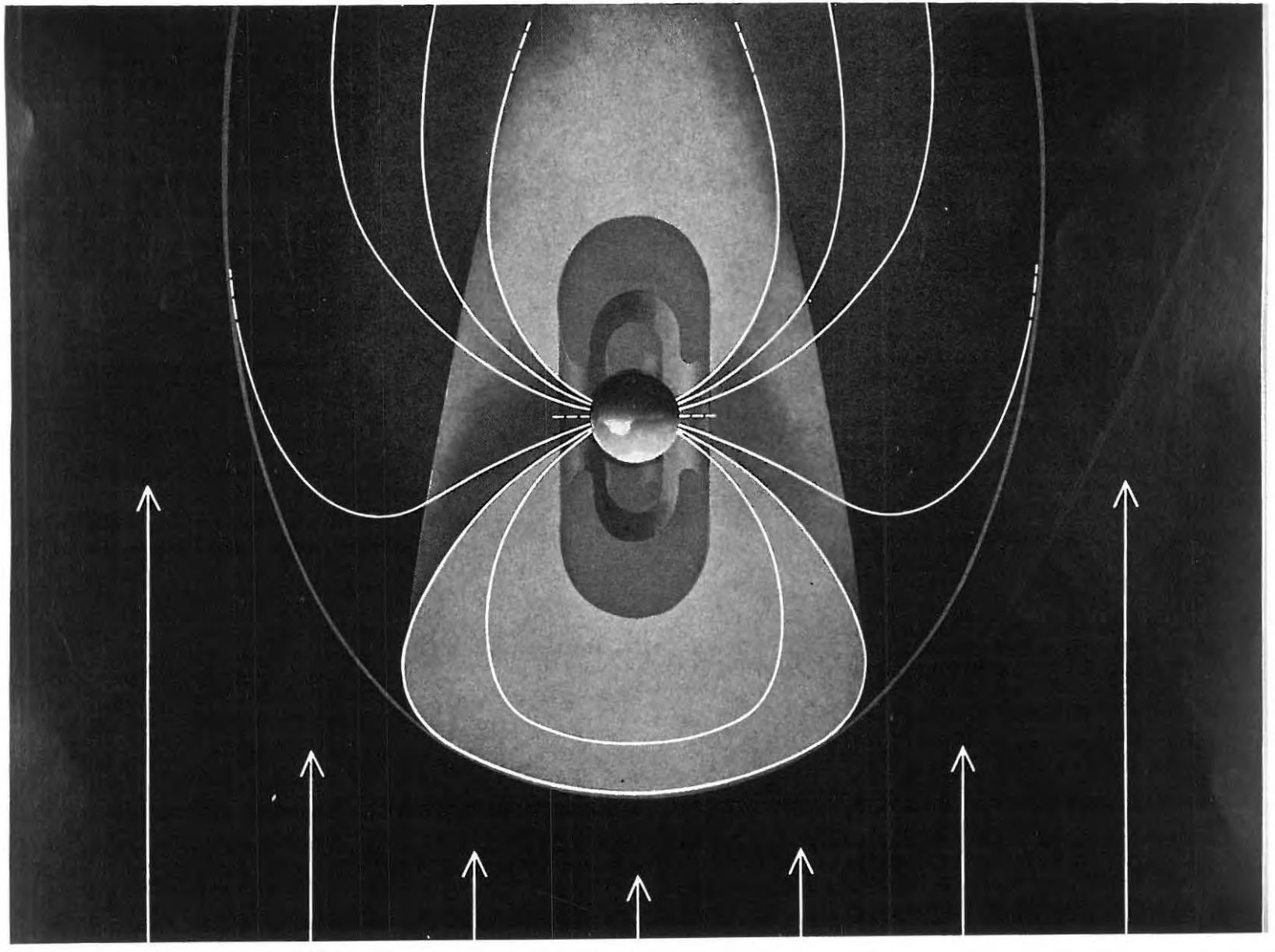

relatively rapid increase of intensity (63). The overall increase in intensity did not occur in a uniform manner but appears to have been the result of a series of discrete increases, the times of occurrence of which were correlated with solar proton events and/or magnetic storms. In general the inner zone appears to be stable and many investigators find results consistent with no variation at all.

Though the overall picture of the outer belt as it has emerged over the past four or five years seems to indicate a fairly definite average configuration when considered over such a period of time, this fact can only be termed remarkable when the large fluctuations in intensity and geometric configuration over short periods of time are considered. Observations with Explorer IV record a marked decrease in intensity of high energy particles at altitudes of 1,000 kilometres over North America and Australia during magnetic storms (40). At lower altitudes where the intensity was low in quiet times, the counting rates increased markedly, indicating a broadening of the pitch - angle distribution. After the great magnetic storm of September 4th and 5th, 1958, a significant increase in the average energy of trapped high energy particles was recorded. Explorer VI recorded a large decrease in intensity following the sudden commencement of a geomagnetic storm (48). Later in the storm intensities increased to values much in excess of the prestorm level. During the first 24 hours of the storm approximately two-thirds of the detectable radiation was lost, the remaining radiation being considerably harder

than the prestorm radiation. Similar variations were observed by Explorer VII (50) during a magnetic storm. Comparison of data from Explorer VII and Pioneer V, which monitored particles with energy greater than a 30 keV electron in the solar wind, apparently shows that over the two-day period following the magnetic storm of March 31st, 1960, intensities of high energy particles in the outer zone increased to several thousand times those recorded in the original solar plasma before its arrival at the boundary of the geomagnetic field. Evidence of substantial day to day variations of intensity in the same positions in space has been found, and intensities measured at high latitudes by Injun I have been found to change by an order of magnitude in times of a few seconds (or distances of a few tens of kilometres) (62). A study of data from Explorer VII (monitoring protons with $E_p > 30$ MeV and $E_p > 18$ MeV and electrons with $E_e > 2.5$ MeV and $E_e > 1.1$ MeV), covering the period October 26th to December 9th, 1959 during which four magnetic storms occurred, indicates the following. The intensity decreases to a minimum value one day after the onset of the storm, and then recovers gradually from the second day after onset. At the same time the position of the intensity maximum moves to lower L values and then gradually recovers. Large changes of intensity occur at high L values, and for a fixed L value these changes may be negatively correlated with geomagnetic activity (56). When bifurcation of the outer zone was observed, the outermost peak was seen to undergo rapid inward movement over a large distance, and showed a large increase in intensity during magnetic storms [(53), (57)].

Recently more comprehensive analyses of Explorer VI and Explorer VII data have been published. The results of an investigation of time variations of intensity in the 'horn' of the outer belt using Explorer VII measurements from October 1959 to December 1960 (for electrons with $E_e > 1.1$ MeV) lead to the following conclusions (67). The L value corresponding to the peak intensity showed a marked tendency to decrease as the 'southward equatorial geomagnetic field of the ring current' increased [see (67)] . Also this L value decreased during the main phase of magnetic storms. For $L > \sim 3.5$ the intensity decreased during magnetic storms, while for $L < 3.5$ the intensity increased. Thus there is apparently a redistribution of particles among the shells during magnetic storms. The variations of the five day averages of intensities were found to be similar at $L = 4.7$ and $L = 4.1$, though quite distinct from those at $L = 2.9$ and $L = 2.5$, which were also similar. For the two larger values the intensities varied by a factor of 10 or so within two or three weeks, this type of variation not being evident at the two smaller values. The two smaller values are characterised by monotonic decreases lasting months, and sudden increases. For example, there was a hundredfold increase in April 1960, followed by a gradual decline over the next two or three months. Also discovered from Explorer VII data were order of magnitude variation in a matter of hours for $L > \sim 2$ (for electrons with $E_e > \sim 1.5$ MeV) and, from Explorer XII data, order of magnitude variations in less than one day (for electrons with $E_e \sim 50$ keV) during magnetic storms. (68)

Finally an analysis of Explorer VI data covering four magnetic storms and the August 29th to September 1st, 1959, quiet period (71) has yielded the following information about the associated time variations of the intensity of electrons with $E_e \sim 5$ MeV. (a) The major intensity changes always correlate with solar activity, the time delay involved (~ 40 hours) indicating coupling by means of solar plasma streams. (b) The larger the radial distance considered the larger are the variations, and the less the correlation with earth surface magnetic field changes. The lower side of the belt, at 17,000 kilometres, is the most stable, and variations are reasonably well correlated with earth surface field changes. The counting rate at the equator on this line of force always recovers to its prestorm value, though small changes in pitch-angle distribution may remain. (An interesting discussion of pitch-angle distributions and their variations is given in the paper (71) and is generously illustrated.) (c) Counting rate decreases:- Counting rates near the equator decrease for all lines of force if a magnetic storm having a main phase occurs. This decrease may occur before, or after, the main phase is observed at the surface of the earth. If the decrease is not large or rapid at the equator, the counting rate increases for points nearer the atmosphere, implying that the mirror points of particles in this region are moved down the lines of force. The percentage decrease is usually larger for larger radial distances. Decreases may occur when the magnetic field at the surface of the earth is quite stable. It is significant that when large decreases occur on all

lines, auroras appear at subauroral-zone latitudes. (d) Counting rate increases:- Increases occur during the recovery phase of magnetic storms and are apparently due to a local acceleration mechanism. The 'new' particles have larger pitch angles and therefore higher mirror points than prestorm particles, but a spectrum similar to the prestorm spectrum.

2-5 Artificial Radiation Belts.

It is immediately evident that the deliberate injection of charged particles into the trapping region, with a known source strength and at a known time could be helpful in determining such little known variables as the drift time, and also in identifying the geophysical effects definitely correlated with trapped particles. In addition such experiments should in theory give vital hints as to the source strength required to maintain the observed intensities in the natural radiation zones. In the cases in which such experiments have been carried out to date, the predominant considerations have however been of a political and military nature. In some of these cases confusion has arisen due to a lack of exact data on the yield of the nuclear bombs used as sources. The scientific uses of such spectacular experiments were first realized by Christofilos who proposed such an experiment a few weeks after the launching of Sputnik I. A direct result of his proposals was Project Argus (96) in which three small atom bombs were exploded above the South Atlantic, injecting particles into shells with L values 1.715, 2.115 and 2.16 (15).

These explosions created easily observable radiation belts which were detected by Explorer IV for several weeks. Many interesting geophysical effects were observed, but one of these being that clearly visible aurorae occur both on the site of the explosions and at their conjugate points. A large number of papers has been published dealing with this and subsequent high altitude explosions and some of the results reported will be mentioned in chapter 5.

2-6 The Origin of the trapped radiation.

At the present stage no definite conclusion can be reached as to the origin of the radiation in the trapping region, but several factors have been brought to light by rocket and satellite data which make it clear that we must accept the existence of at least two sources for the radiation. The two most important suggestions will be discussed very briefly here.

For the inner belt, where a comparatively weak and stable source appears to meet the requirements, the decay of neutrons, produced in the upper atmosphere by cosmic rays and subsequently diffusing to greater radial distances, was suggested as a source by Singer in 1958 [(83), (84)] and was later enthusiastically supported by Hess, Lenchek, and others. Extensive theoretical work has been done in this connection by the proponents of the theory [(85), (86), (87), (88), (89), (90), (91), (92), (93)] whose tenacity in the face of some unfavourable indications from experimental results from time to time has been rewarded with a fair measure of confirmatory

experimental data [(47), (52), (54), (64), (81), (95) . For a review see Lenchik and Singer (94)]. It does however appear that the theory is at this stage unable to account for the low energy particles in the inner zone adequately, and it is possible that an additional source must be sought for these. [See (91)] .

In the case of the outer belt a very strong and highly variable source is required. [See O'Brien (65) for a summary of the evidence justifying this conclusion]. It seems certain that solar plasma streams provide the only source strong enought to fit the requirements of observational data in this connection, but the particles in this plasma are dominantly in the eV range. It is obvious then that some local acceleration mechanism exists (and there may be more than one type of mechanism operating) which accelerates these particles from the order of eV to the order of keV or MeV. The various proposals for such a mechanism will not be discussed here. None of them has succeeded in gaining general acceptance. Two general qualitative models of the outer belt have been proposed. It will however be more appropriate for us to discuss these in Chapter 5, since they deal mainly with the connection between the outer belt and the aurorae.

CHAPTER 3.

THE SOUTH ATLANTIC RADIATION ANOMALY.

3-1 The Geomagnetic Field in the South Atlantic Region.

Figure 8 shows lines of equal total magnetic intensity for the South Atlantic region, a region on which we will shortly focus our attention for the main part of this thesis. The simplest model of the geomagnetic field which gives results which are in reasonable agreement with observational data is the so-called 'eccentric dipole' model. This is obtained from the 'centred dipole' model, in which we imagine a pure dipole situated at the geometric centre of the earth, by shifting the dipole to the 'magnetic centre' of the earth (97) without changing the direction of its axis. Since the magnetic centre lies only about 10 kilometres south of the equatorial plane of the centred dipole [though it is 0.0536 E_R from the geometric centre of the earth (97)] , the dipole is shifted in a direction practically perpendicular to its axis. It is therefore relatively easy to visualize the field of the eccentric dipole. Figure 9 shows lines of equal total magnetic intensity calculated from the eccentric dipole model (97). These agree reasonably well with the broad outline of the observational data, but comparison with figure 8 reveals that an 'anomalous' region exists around the south western tip of Africa. Particularly noticeable when comparing these figures is the relatively low value of the total magnetic intensity over South Africa. In the context of our discussion here this region must be regarded as anomalous, and it is

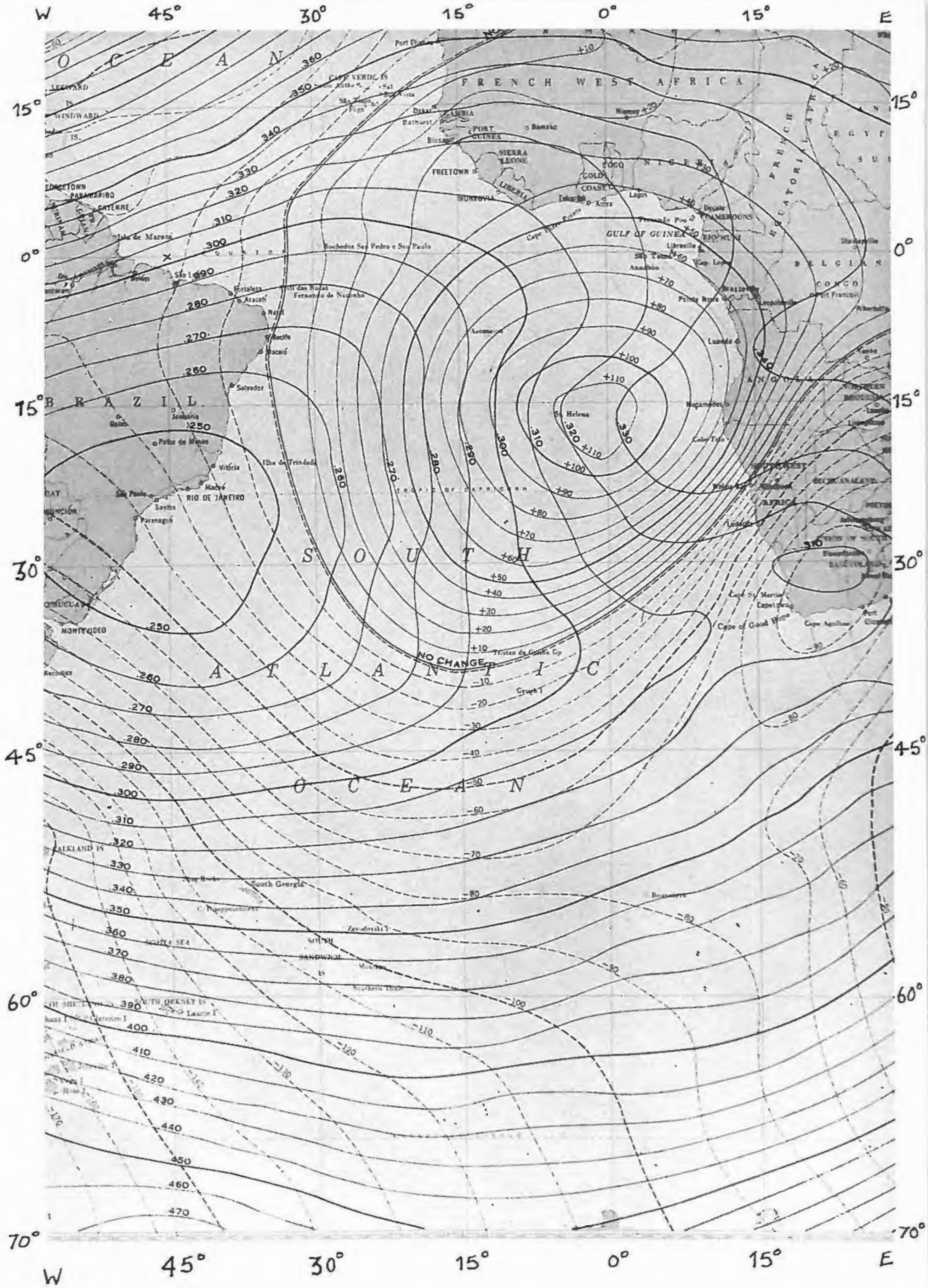

W
45°
30°
15°
0°
15°
E
O C E A N
FRENCH WEST AFRICA
CAPE VERDE IS
GAMBIA
PORT GUINEA
SIERRA LEONE
LIBERIA
GOLD COAST
TOGO
NIGERIA
GULF OF GUINEA
CAMEROONS
RIO MUNI
BELGIAN CONGO
ANGOLA
BECHUANALAND
B R A Z I L
RIO DE JANEIRO
MONTEVIDEO
S O U T H
A T L A N T I C
O C E A N
NO CHANGE
St. Helena
Ascension
Tristan da Cunha Gp
Ilha da Trindade
Cape of Good Hope
South Georgia
SCOTIA SEA
SOUTH SANDWICH IS
FALKLAND IS
TROPIC OF CAPRICORN
15°
0°
15°
30°
45°
60°
70°
250
260
270
280
290
300
310
320
330
340
350
360
370
380
390
400
410
420
430
440
450
460
470
+10
+20
+30
+40
+50
+60
+70
+80
+90
+100
+110
-10
-20
-30
-40
-50
-60
-70
-80
-100
-110
-120
-130

Figure 9 Lines of total magnetic intensity calculated from the eccentric dipole model. Reproduced from reference (116)

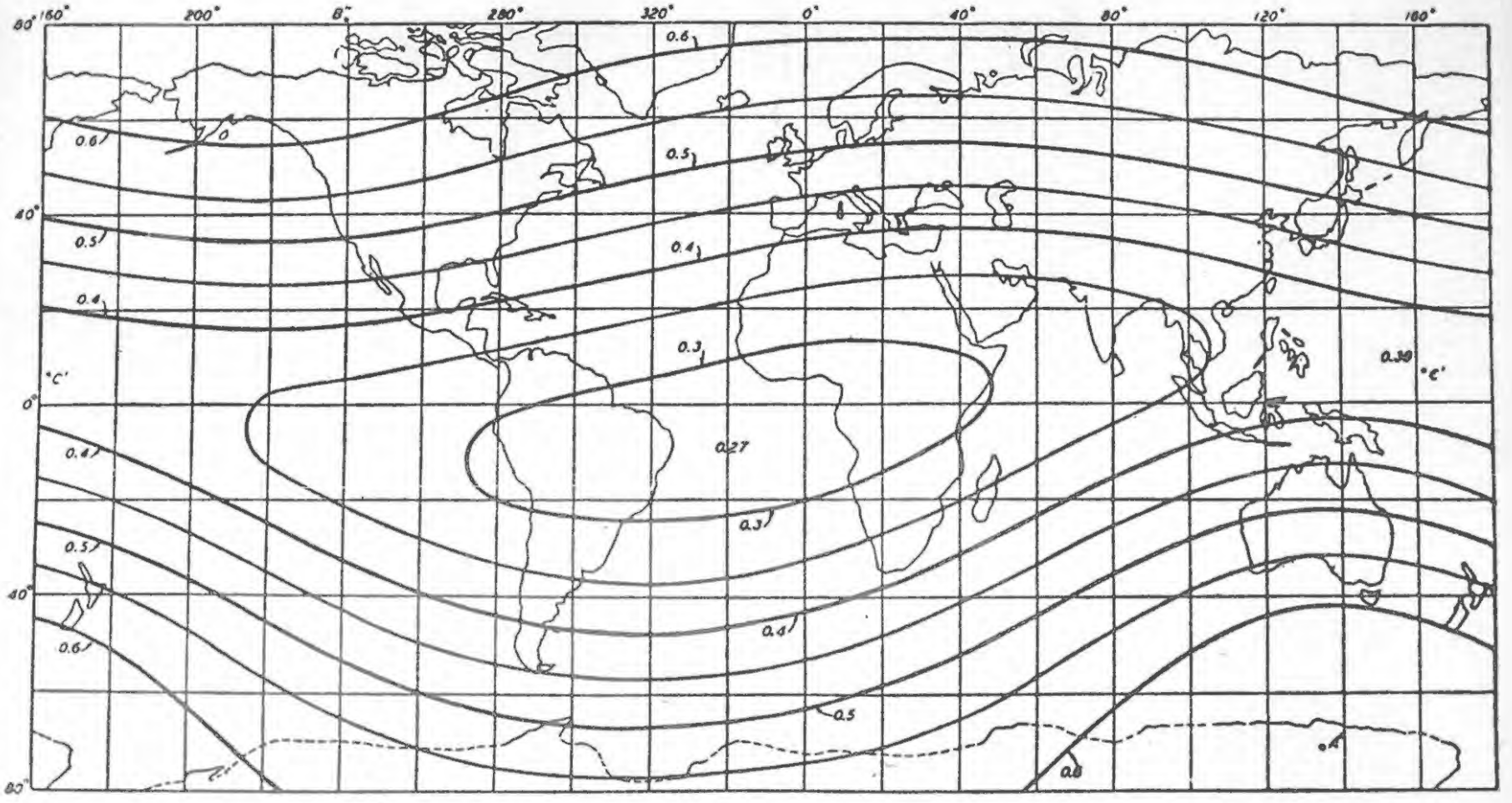

Lines of equal total magnetic intensity corresponding to the eccentric dipole field

this anomaly which has been named the 'Cape Town Magnetic Anomaly' (sometimes shortened to Cape Magnetic Anomaly). Another noticeable feature of figure 8 is the region of very low total magnetic intensity centred approximately on Sao Paulo in Brazil. As pointed out by Dessler (98) it is incorrect to refer to this as a magnetic anomaly in this context, as has been done from time to time in the literature, since it is merely the region furthest from the eccentric dipole.

It is interesting to note in passing that it was at one time thought that the Cape Town magnetic anomaly might be responsible for the slot in the radiation zones [(99), (100)] since a lot of the trapped radiation in the region of a magnetic anomaly would penetrate deep into the atmosphere due to the lowering of the mirror points there. It was however pointed out by Hoffman (101) that the value of I in the Cape magnetic anomaly does not correspond with the value of I in the slot. It is, in any case, evident from our discussion of the trapped radiation in Chapter 2, that reference to the slot is only meaningful when high energy particles are considered.

3-2 Radiation Anomalies in the South Atlantic Region.

Two regions of anomalously high charged particle intensity have been observed at altitudes between 150 and 500 kilometres over the South Atlantic ocean with the second and third Soviet space-ships [Sputnik 5 and Sputnik 6 respectively, (61), (102), (103), (104), (105), (106), (107), (108), (109)], and with U.S. satellites in

the Discoverer series (110). Maps of counting rates over the earth prepared by Ginzburg et al. (105) are shown in figure 10 (for Sputnik 5 at an altitude of ~ 310 kilometres) and figure 11 (for Sputnik 6 at an altitude of ~ 230 kilometres). Similar maps, for the Southern Hemisphere only, were prepared by the American group (110) and are shown in figure 12 (for $E_p > 15$ MeV and $E_e > 2$ MeV) and figure 13 (for $E_p > 2$ MeV and $E_e > 100$ keV). Unfortunately absolute intensities cannot be reliably deduced from the Russian data (105).

Except in the case of figure 11, the radiation anomaly off the coast of Brazil seems to coincide reasonably well with the region of low total magnetic intensity there (see figure 8). We will refer to this radiation anomaly as the 'Brazil Radiation Anomaly'. The radiation anomaly lying at higher latitudes will be referred to as the 'South Atlantic Radiation Anomaly'. (Our terminology differs from that used by the Russian groups in regard to these anomalies.) We will now discuss these anomalies very briefly. In doing so we must take into account the shells on which the charged particles observed in the anomalies move round the earth. Figure 14 shows some contours of constant L at 1000 kilometre altitude published by Lin et al. (111). These can be used as a rough guide to the drift paths of the charged particles in question.

3-2-1 The Brazil Radiation Anomaly.

The particles concerned here have L values between ~ 1.20 and ~ 1.75 at the altitude of the observations, and thus belong to the inner radiation belt. Electrons drifting from west to east across

Figure 10 Reproduction of figure 4 from Ginzburg et al (105), showing lines of equal counting rate measured with Sputnik 5.

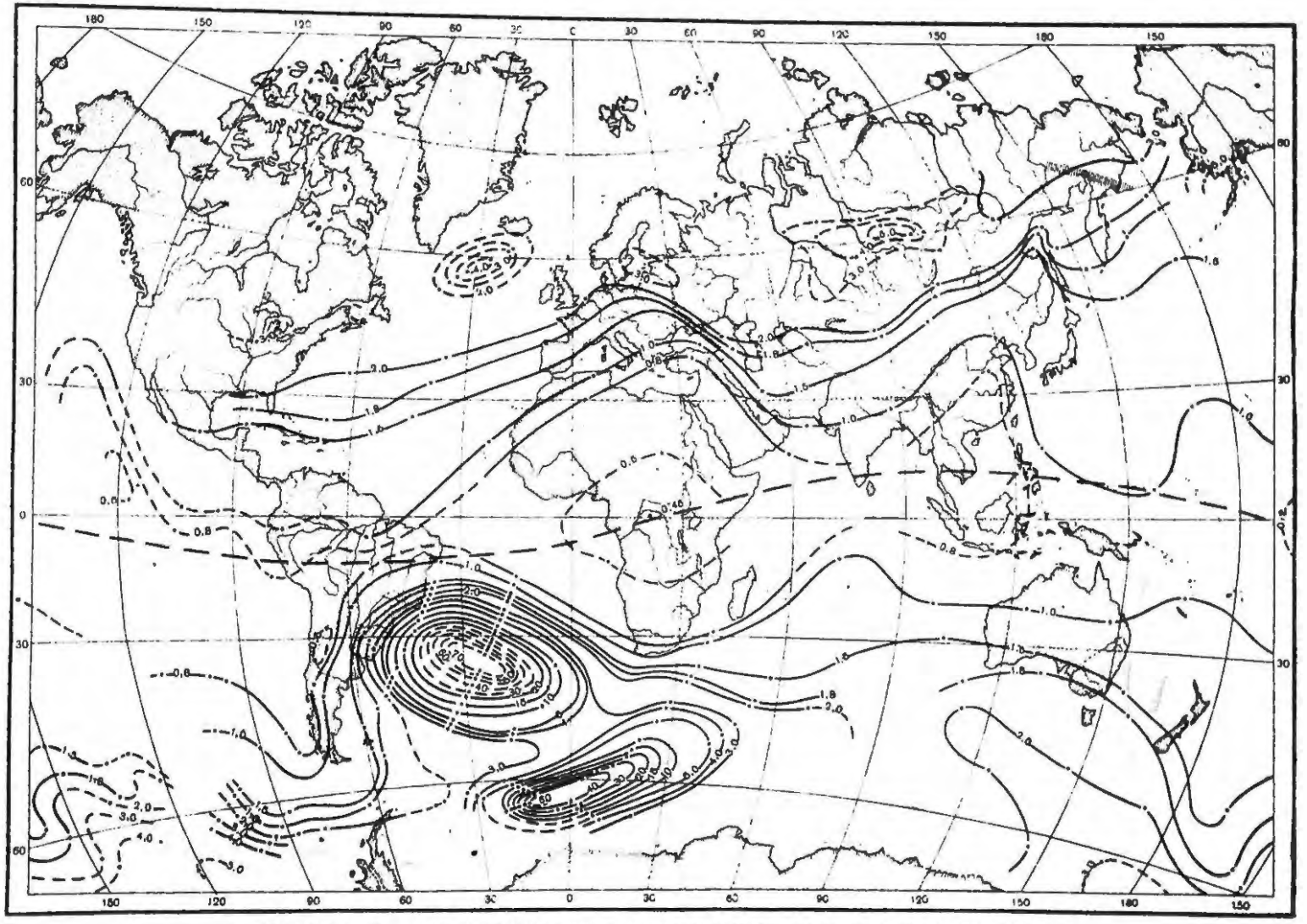

FIG. 4. DISTRIBUTION OVER THE TERRESTRIAL GLOBE OF LINES OF EQUAL TELESCOPE COUNTING RATE ON THE SECOND SPACE-SHIP.

Lines of equal intensity constructed from a small number of points or from points determined with less reliability are shown dotted; the dash-line represents the geomagnetic equator; the hatching shows the zone where a large intensity increase of a temporary nature was observed ("northern anomaly")

Figure 11 Reproduction of figure 5 from Ginzburg et al (105), showing lines of equal counting rate measured with Sputnik 6.

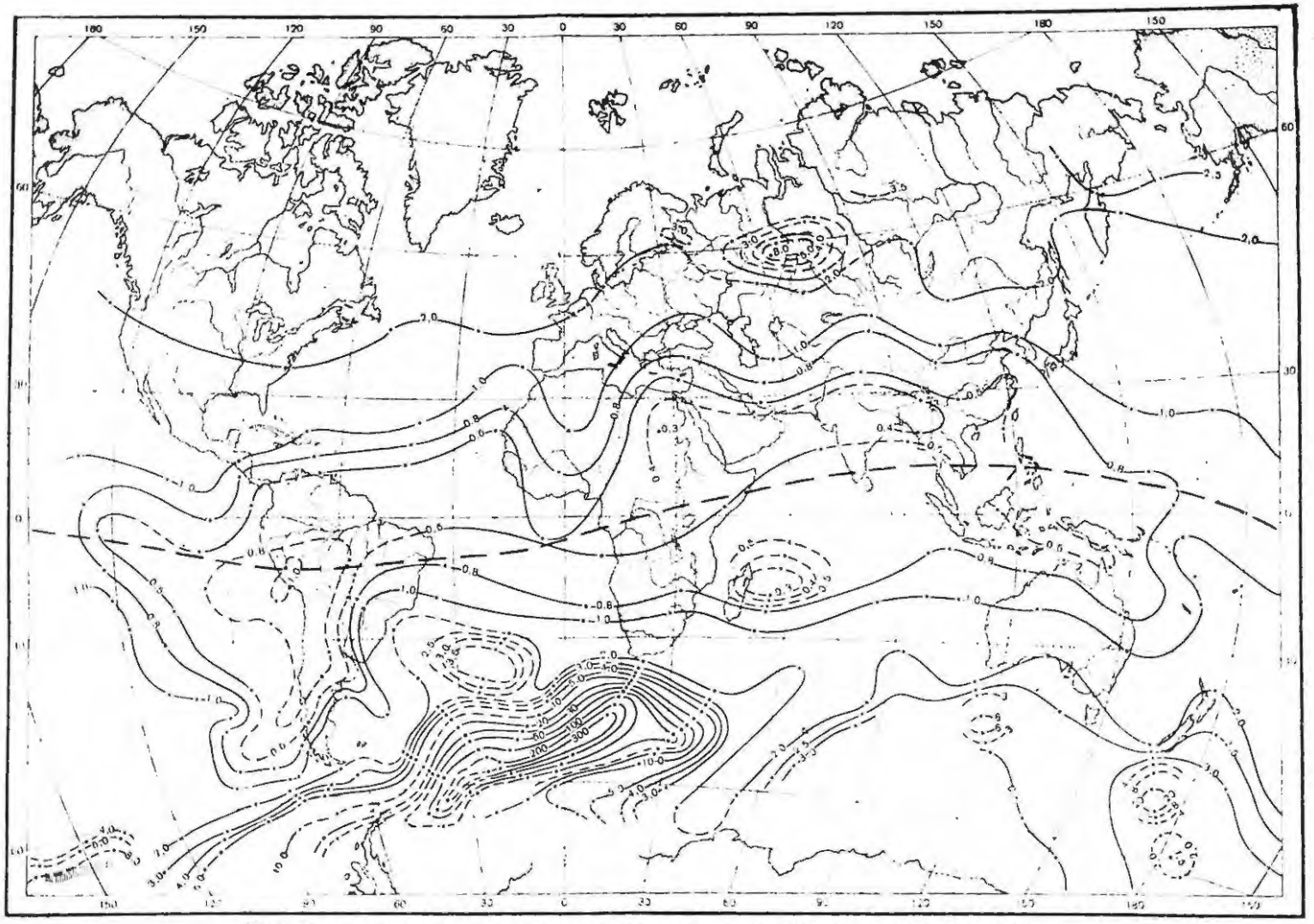

FIG. 5. DISTRIBUTION OVER THE TERRESTRIAL SPHERE OF LINES OF EQUAL TELESCOPE COUNTING RATE ON THE THIRD SPACE-SHIP.

Lines of equal intensity constructed from a small number of points, determined with poor reliability, are shown dotted; the dash-line shows the geomagnetic equator, the hatching shows the region in the southern sector of the Pacific Ocean where an intensity rise of a temporary nature was observed.

Figure 12 Map showing lines of equal counting rate for the South Atlantic region measured with U.S. satellites in the Discoverer series. $E_p > 15$ MeV, $E_e > 2$ MeV. Map made available to us by Prof. F.D. Seward.

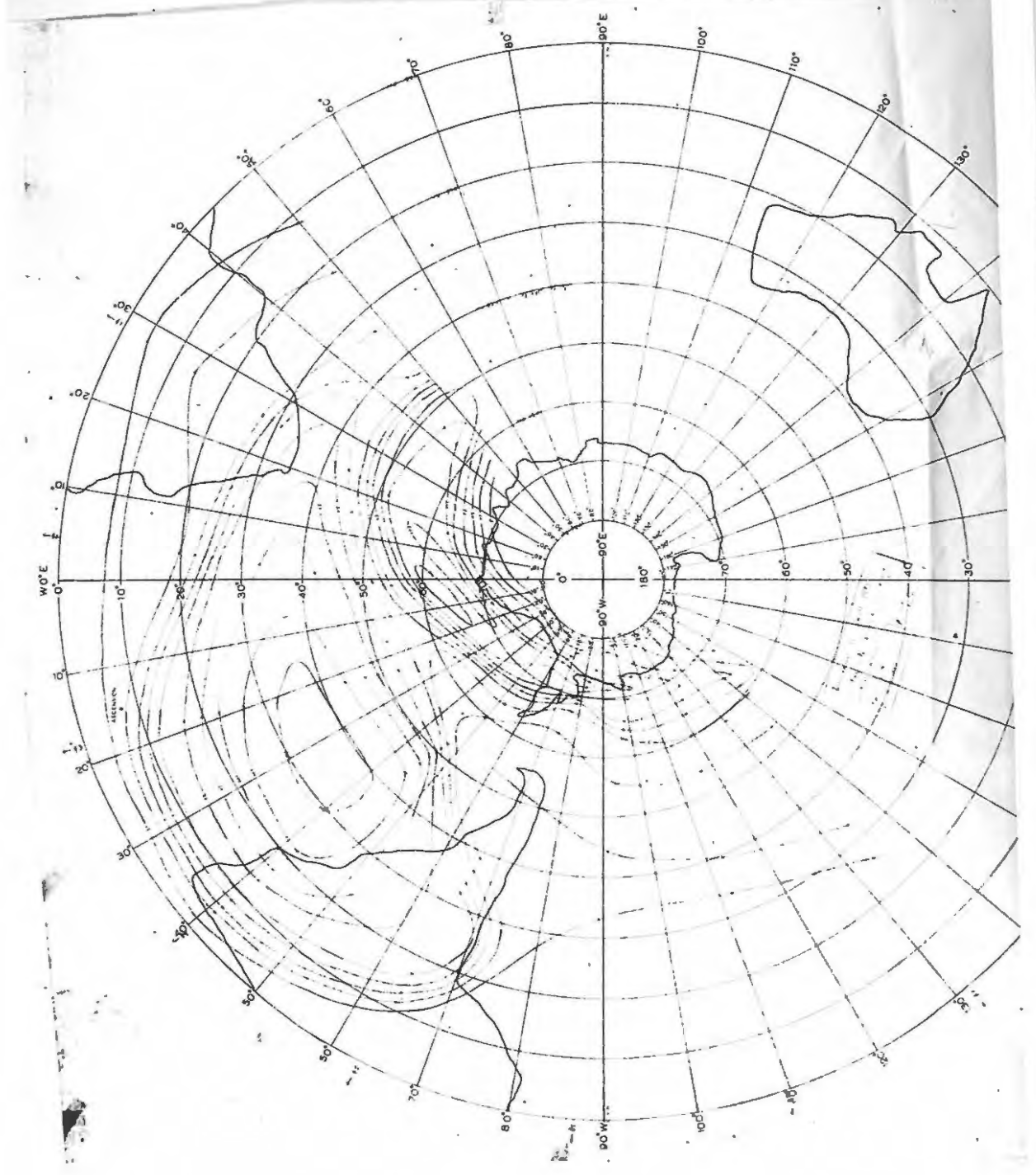
90°E
90°W
0°
180°
W0°E

Figure 13 Map showing lines of equal counting rate for the South Atlantic region measured with U.S. satellites in the Discoverer series. $E_p > 2$ MeV, $E_e > 100$ keV
Map made available to us by Prof. F.D. Seward.

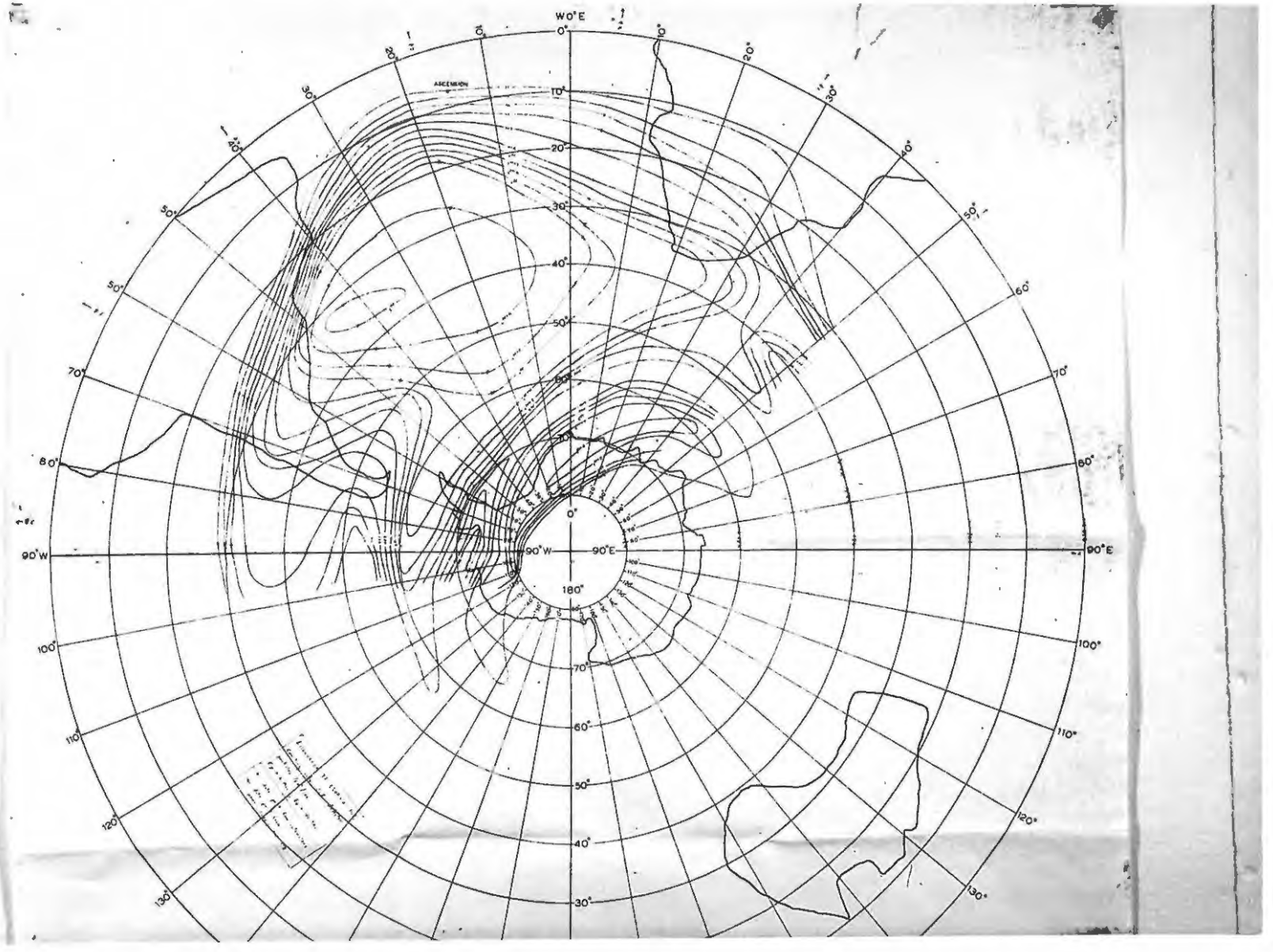
W0°E
90°W
90°E
180°
ASCENSION

Figure 14 Map showing some contours of constant L at 1000 km altitude. Reproduced from reference (111).

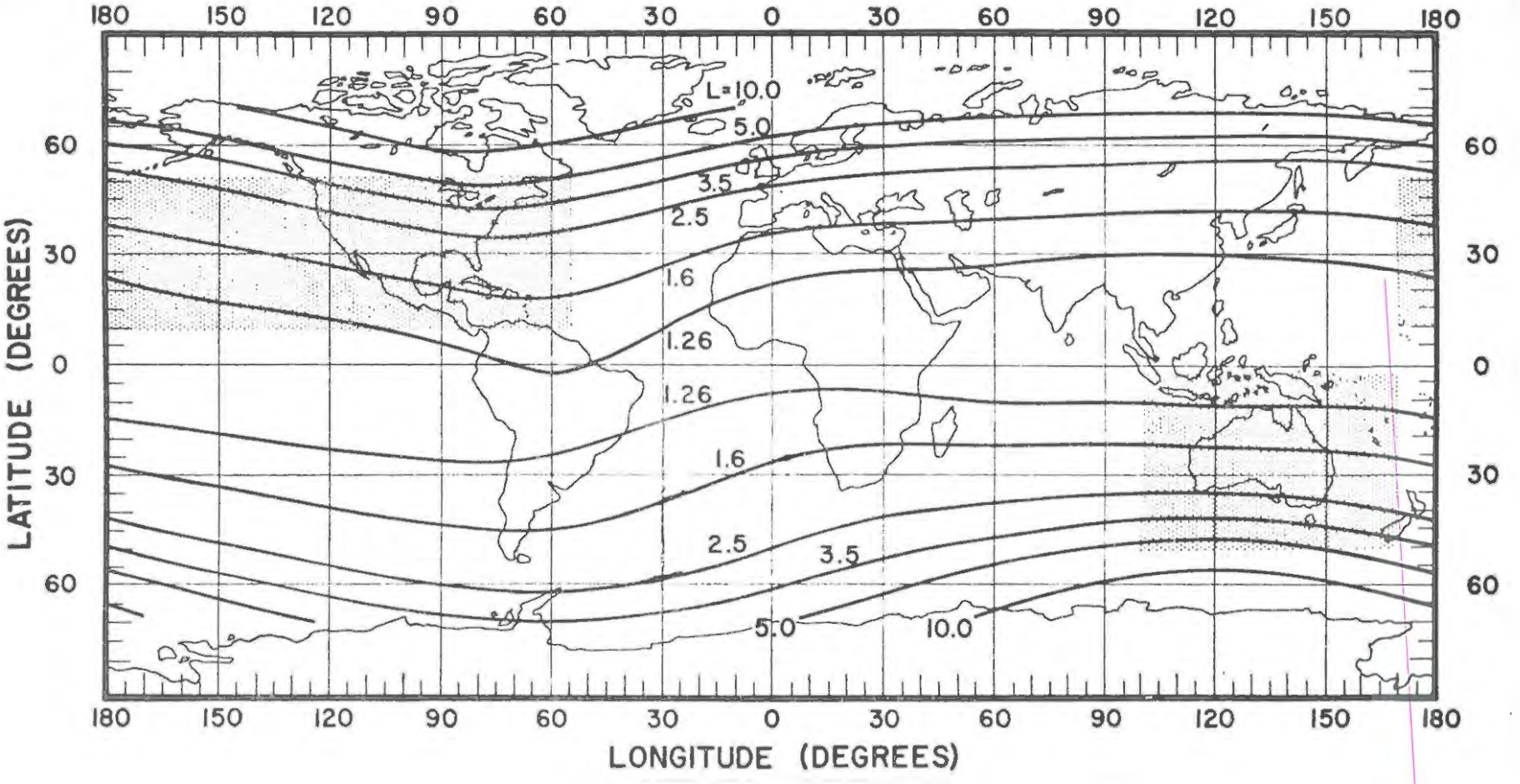
180 150 120 90 60 30 0 30 60 90 120 150 180
L=10.0
5.0
3.5
2.5
1.6
1.26
1.26
1.6
2.5
3.5
5.0
10.0
60
30
0
30
60
LATITUDE (DEGREES)
LONGITUDE (DEGREES)

Brazil will mirror at lower and lower altitudes as the total magnetic intensity at the earth's surface decreases along their drift path. As they move out of the region of low total magnetic intensity, drifting towards the African coast, their mirror points will rise again. Recourse to figures 8 and 14, and the maps of the radiation intensity, shows that the Brazil radiation anomaly is precisely where we might expect it to be, i.e. in the region where the shells, in which the relevant particles move, meet the surface of the earth at points of low total magnetic intensity. Comparison of figures 10 and 11 indicates that most of the radiation observed at 310 kilometres altitude mirrors above 230 kilometres altitude. The southward shift of the anomaly in figure 11 seems to indicate that for the energy range observed by Sputnik 5 and Sputnik 6, the pitch-angle distribution broadens with increasing L.

3-2-2 The Cape Magnetic Anomaly.

It is clear from the maps that there is no region of anomalously high counting rate coincident with the Cape magnetic anomaly. At the altitude of the observations, the particles drifting through the Cape magnetic anomaly will be those with L between ~ 1.75 and ~ 2.2. This means that they drift between the radiation anomalies as they appear in figures 10 and 12. Since the counting rate is low in this region we conclude that these particles mirror above about 400 kilometres in the region between the anomalies. Further, since electrons are the major component, and since these drift towards the South African coast and through the Cape magnetic anomaly over regions where

the total magnetic intensity is essentially constant (see figures 8 and 14) we do not expect them to be observed at low altitude over the Cape magnetic anomaly. The reason for the relatively low count rate over the Cape magnetic anomaly in the case of figures 11 and 13 is not immediately apparent. More exact information about the L values and pitch-angle distribution of the relevant particles over the South Atlantic and Cape Town regions is required for interpretation of these figures. We suggest however that radiation described as 'lost over South Africa' in the literature is in fact precipitated from the belts over the South Atlantic.

3-2-3 The South Atlantic Radiation Anomaly.

Considering L values greater than ~ 2.2, and reasoning as in 3-2-1, we find that the South Atlantic radiation anomaly is situated approximately where we expect it to be. This is clear from figure 15, taken from reference (112), which shows the South Atlantic radiation anomaly as observed by Sputnik 5 and the approximate traces on the earth's surface of the mirror points of particles entering the zone. These traces were estimated with the aid of the curves of constant I and B_m published by Vestine and Sibley (113) [their diagram for the Southern Hemisphere is shown in figure 16 as an example], and the diagram of conjugate points [i.e. points in opposite hemispheres which are joined by lines of force of the geomagnetic field] published by Vestine and Sibley in reference (113). [This diagram is shown in figure 17.] The cross-hatching on the northern trace of figure 15 is the conjugate position of the anomaly.

Figure 15 Reproduction of figure 1 from Gledhill and van Rooyen (112). Notice that the region marked "A" was incorrectly called a magnetic anomaly. The cross hatching on the northern mirror point trace marks the conjugate region of the South Atlantic radiation anomaly, (labelled B). Some lines of equal total magnetic intensity (in oersteds) are also shown.

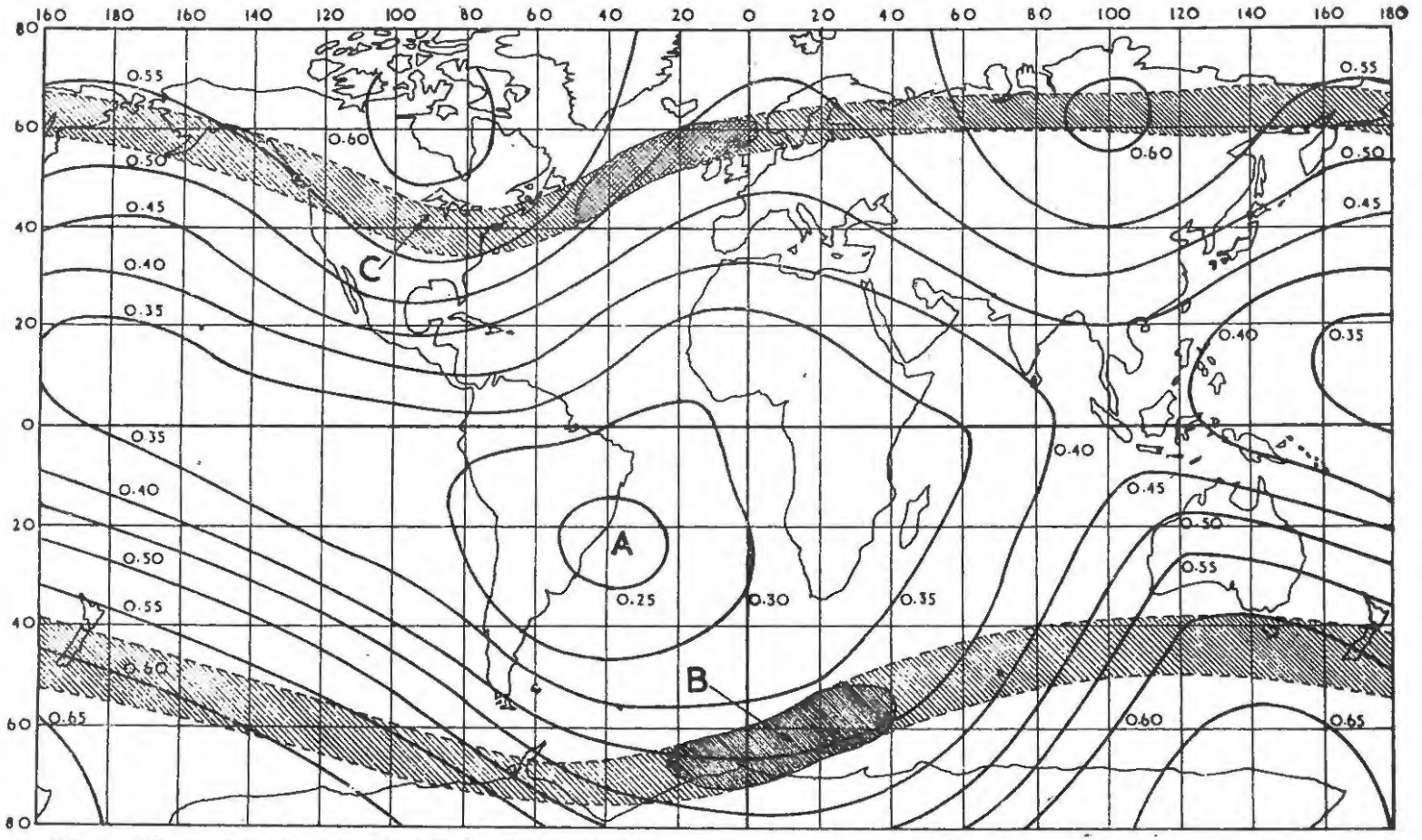

Fig. 1. The geomagnetic anomaly (*A*), the south radiation anomaly (*B*) and traces of the mirror points of electrons falling into the latter. *C* indicates the position of Iowa City

Figure 16 Reproduction of figure 4 from Vestine and Silbey (113) showing curves of equal I and B_m (labelled F in this figure) for the Southern Hemisphere.

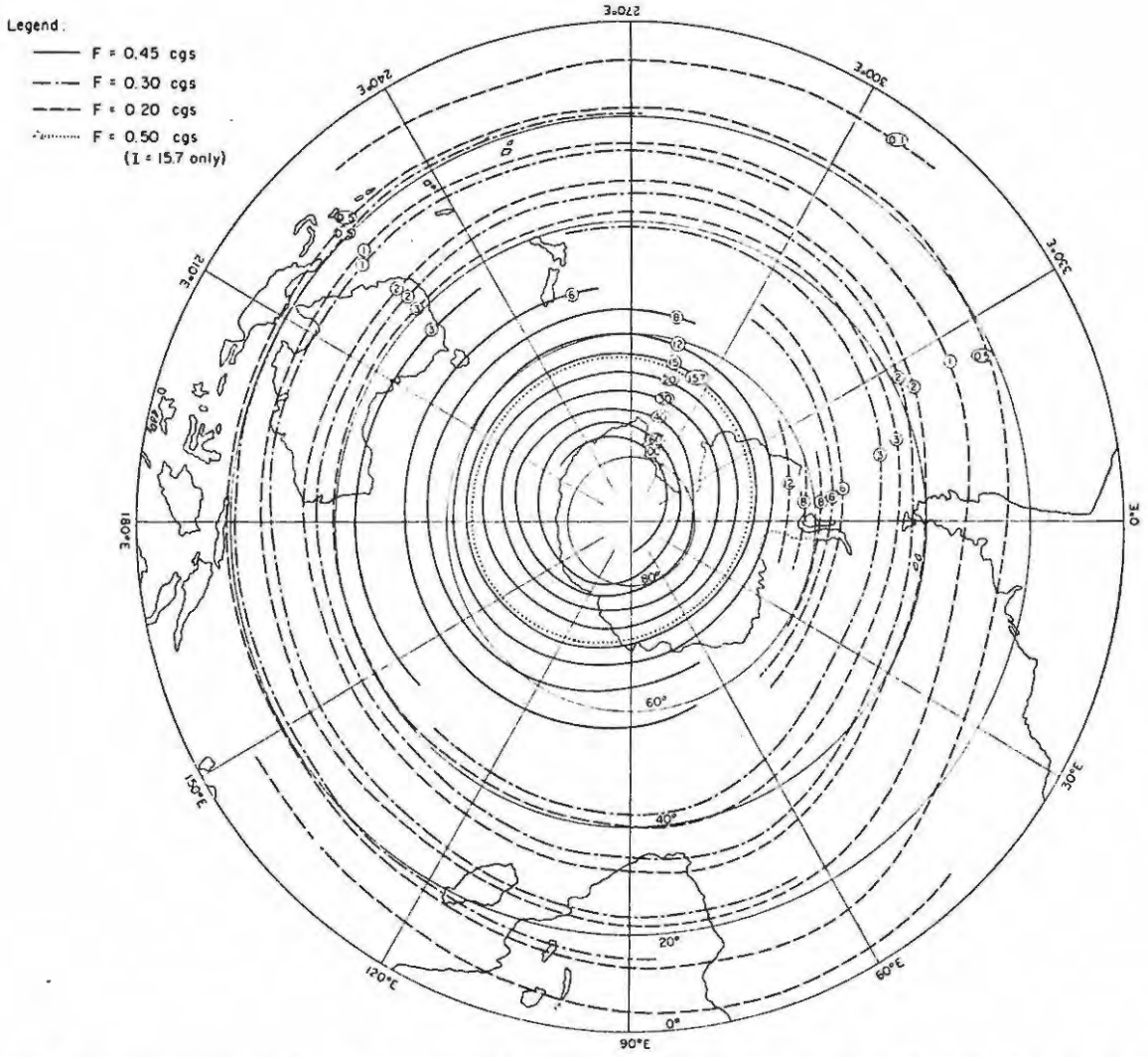

Fig. 4. Contour lines corresponding to equal integral values I, southern hemisphere, geomagnetic coordinates.

Figure 17 Reproduction of figure 9 from Vestine and Silbey (113) showing the conjugate points of selected positions in the Northern Hemisphere.

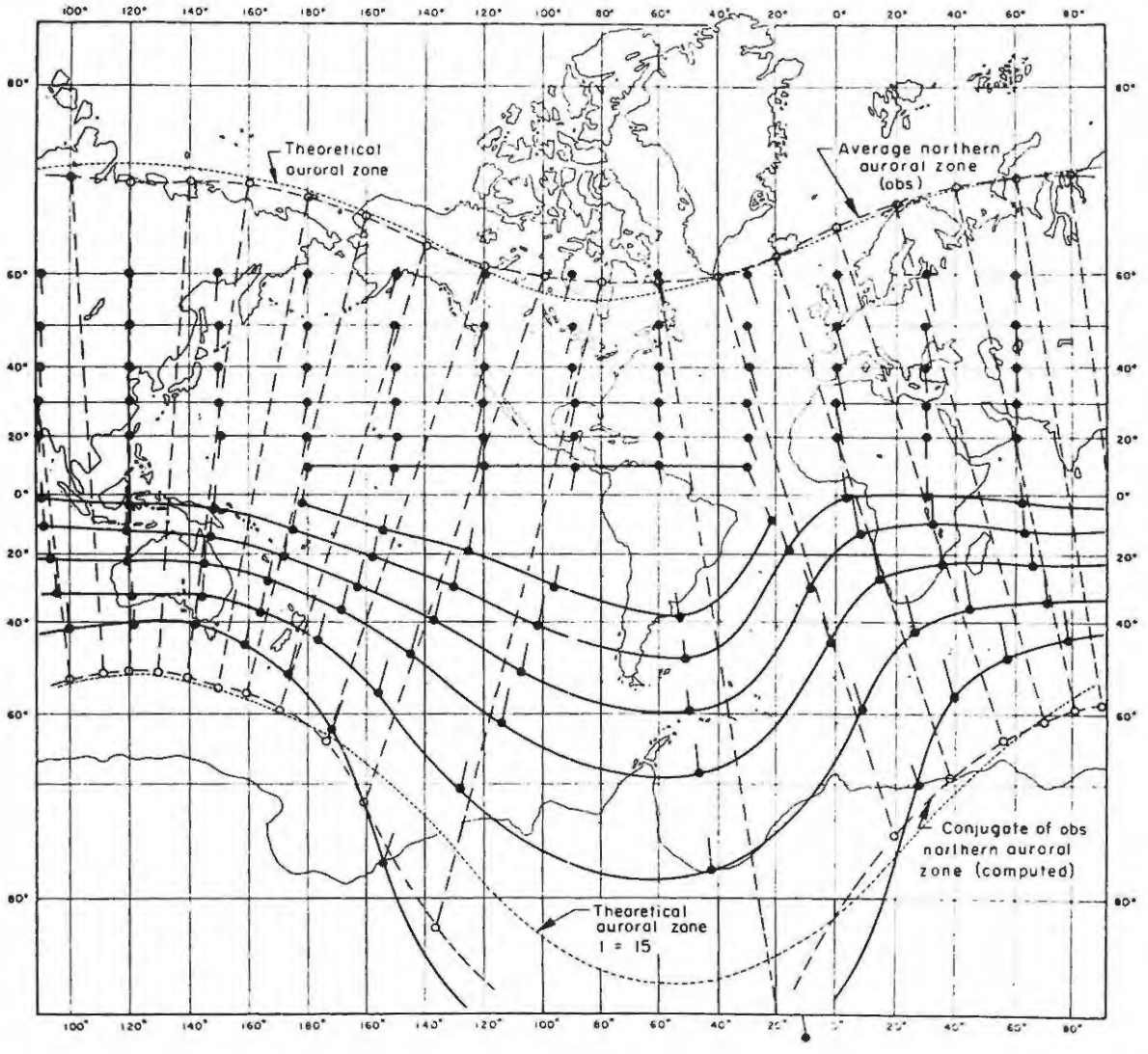

Fig. 9. Approximate intersections of lines of force of the geomagnetic field with the earth's surface, northern and southern hemispheres, based on first 48 Gauss coefficients.

Also shown in figure 15 are approximate curves of constant total magnetic intensity.

Also to be expected, from what we know of the outer zone radiation, is (a), that the anomaly should exhibit variability of counting rate and/or pitch angle distribution (see figures 10 and 11), and (b), that the peak intensity for low energy particles should be at higher latitudes (i.e. higher L values) than that for high energy particles (see figures 12 and 13). One important feature of all four maps is that the eastern boundary is about where we expect it to be from consideration of the value of total magnetic intensity along the drift path of the electrons. Since the counting rates at low altitude are large throughout the expected region, and since it is likely that a reasonably high percentage of the particles counted have mirror points so close to the earth that they are absorbed in the atmosphere, we may conclude that particles lost in the anomaly are replaced almost immediately. Of course this does not necessarily imply the continuous injection of new particles into the outer belt. It is in fact more likely that particles originally mirroring at fairly high altitudes are scattered down to lower altitudes [(114), (13), (14)], thus taking the place of those which have been lost. [Hess (115) suggests that the boundary is in fact further east than one would expect it to be, and accounts for this by saying that scattering of particles to lower altitudes at the expected eastern edge of the anomaly, and eastward from it, broadens the anomaly significantly]. To back up this argument, we reproduce from reference (112), a

Figure 18 Diagrams showing the approximate variation of mirror height with longitude along the traces shown in figure 15 for a particle mirroring at 1000 km. altitude of Iowa. In preparing this figure an inverse cube field was assumed, and the values of the magnetic field at the earth's surface were taken from figure 15. Reproduced from reference (112).

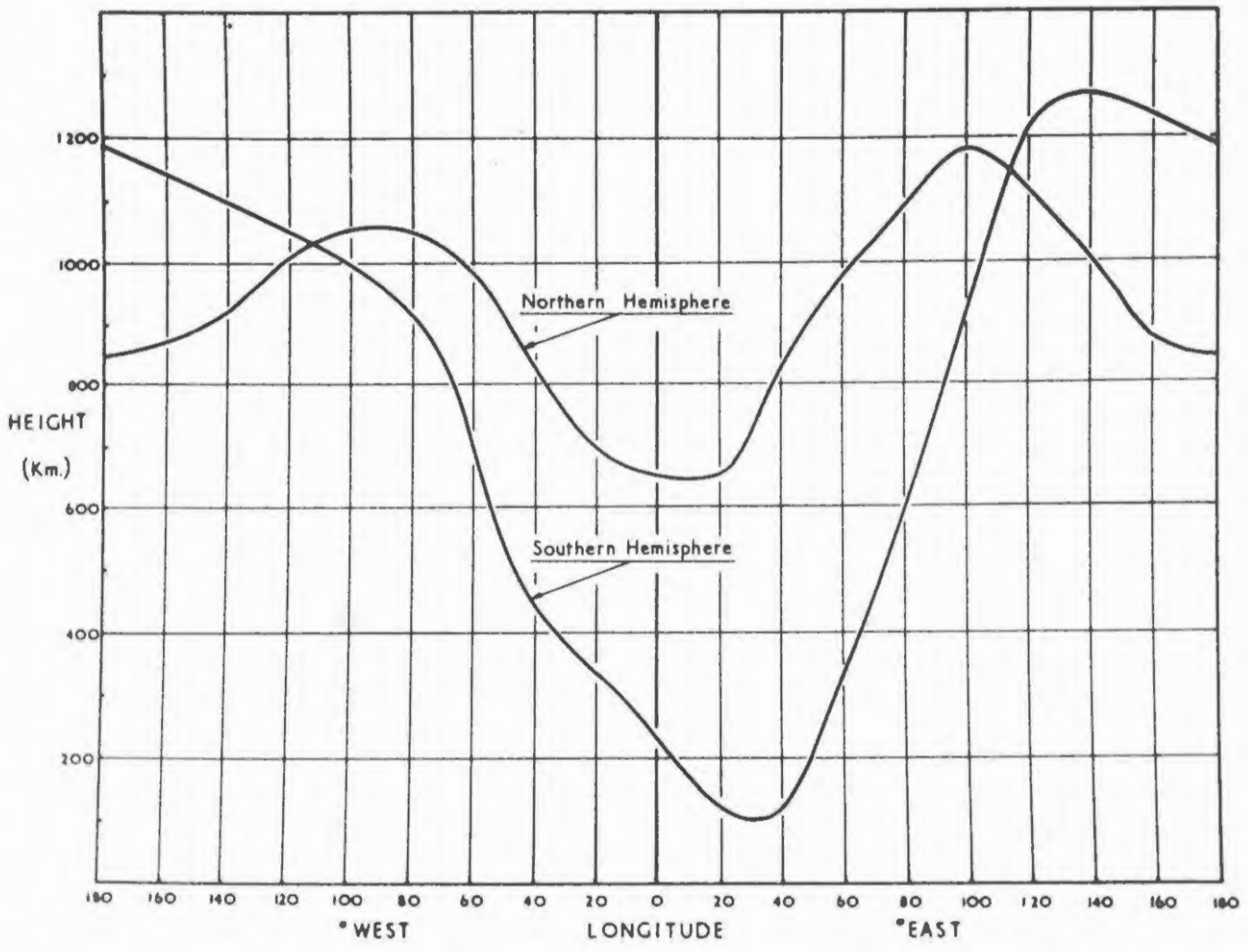
1200
1000
800
600
400
200
HEIGHT
(Km.)
Northern Hemisphere
Southern Hemisphere
180 160 140 120 100 80 60 40 20 0 20 40 60 80 100 120 140 160 180
°WEST
LONGITUDE
°EAST

diagram showing the approximate variation of mirror height with longitude along the traces shown in figure 15 for a particle mirroring at 1000 kilometres altitude over Iowa city (figure 18). The reason for choosing such a particle will become clear in Chapter 4. Figure 18 shows very clearly the pronounced effect of the relatively low value of total magnetic intensity in the South Atlantic radiation anomaly in lowering the mirror points, and demonstrates that all electrons observed at 1000 kilometres over Iowa will penetrate to altitudes below 150 kilometres in the heart of the South Atlantic radiation anomaly.

Part II of this thesis will be devoted to an investigation of the precipitation of electrons into the upper atmosphere in the heart of the South Atlantic radiation anomaly, and a discussion of the associated geophysical effects.

PART II.

ELECTRON PRECIPITATION IN THE SOUTH ATLANTIC RADIATION ANOMALY.

"Learning without thought brings ensnarement.
Thought without learning totters".

Sayings of Confucius - II, 15.

CHAPTER 4.

ELECTRON PRECIPITATION.

4-1 Introduction.

In this chapter we develop a simple theory which enables us to estimate, with the help of experimental data, the energy absorbed from trapped electrons as they spiral down into the atmosphere. We confine our attention mainly to the South Atlantic radiation anomaly. The theory of the motion of charged particles in a dipole field in the atmosphere was discussed by Störmer (1). He pointed out that for motion over relatively short distances, the dipole field may be replaced by that of a monopole of suitable strength and placed in an appropriate position. The relatively simple theory of Poincaré, which we discussed in 1-3, can then be employed. By taking the observed total magnetic intensity at the ground as datum, and using the inverse cube law to find its value at a suitable reference height, the distance of the monopole which would produce the same field is easily found from the equation

$$\frac{B}{B_s} = \frac{Z_s^2}{Z^2} \qquad 4.1$$

where B_s and B are the magnetic induction at the earth's surface and the reference point respectively, and Z_s and Z are the distances of the earth's surface and the reference point from the monopole measured along the field line, i.e. along the axis of the cone (see figure 1). In finding Z and Z_s we use 4.1 and the approximate relation

$$Z - Z_s = \frac{h}{\sin \phi} \qquad 4.2$$

where h is the reference height above the earth's surface (measured along an earth radius) and ϕ is the angle of dip at the position of interest. 4.2 Is obviously only a good approximation at high latitudes. It is of course not necessary to specify the strength of the monopole since we have described it completely by fixing the magnetic induction at two distances from it.

We now choose another reference level in the upper atmosphere at such a height that an electron mirroring at this level will lose only a very small part of its energy through interaction with the atmosphere. Let this reference level be at a distance Z, from the monopole, and consider the path of an electron which passes through this level with a given energy E_o and pitch angle χ. We have seen in 1-3 that if we neglect energy losses, its path lies on the surface of a cone whose base is the circle of gyration at the reference level and at whose apex lies the monopole. In the atmosphere however, the energy of the electron will be progressively reduced. This implies that the radius of gyration of the electron, and with it the semi-vertical angle of the cone, will be progressively reduced. We will show that this effect may be neglected in the cases which we consider.

In order to avoid the complications of our basic equations which would be introduced by the use of a mathematical expression for the variation of density with height in the atmosphere, we divide the atmosphere into laminations and assume that the density in each

lamination is constant. These laminations are labelled 1, 2, 3, ... etc. from the reference level down. Thus the first lamination lies between Z_1 and Z_2, the second between Z_2 and Z_3, and so on. (Note that in general the Z axis is not perpendicular to the lamination.) We will then derive an equation for the path length (in kgm/m^2) in the n'th lamination, of an electron whose energy and pitch angle at Z_1 are known. Having found this, we may employ a range-energy relation to find the energy absorbed in each lamination. Though the last step will involve us in further approximations it is justified by the fact that it enables us to avoid consideration of the constitution of the atmosphere at great heights i.e. it is yet another 'simplifying assumption'.

4-2 Path Length in the n'th Lamination.

Consider a section of the path of an electron (with energy E_o and pitch angle χ at Z_1) lying between Z_n and Z_{n+1}, i.e. in the n'th lamination. Let the semi-vertical angle of the cone on which it moves be α, and the position vector of the particle (with the monopole as origin) be $\bar{r}$ at some point on this section of path. Let the corresponding coordinate (i.e. the distance from the monopole measured along the Z axis) be Z. Then, since α is the angle between the Z axis and the surface of the cone, and $\bar{r}$ lies in that surface,

$$dZ = dr \cos\alpha$$

where we regard α as a constant for the moment. Now let the

electron move from the point where its position vector is $\bar{r}$ to an adjacent point where its position vector is $\bar{r} - d\bar{r}$, and let the element of path length traversed be d s. Then

$$d r = d s \cos \chi_Z$$

where χ_Z is the pitch angle when the coordinate is Z. Thus we have that

$$d s = \frac{d Z}{\cos \chi_Z \cos \alpha} \qquad 4.3$$

Now we know from Alfvén's mirror equation (1.19) that

$$\sin^2 \chi_Z = \frac{B_Z}{B_1} \sin^2 \chi \qquad 4.4$$

where B_1 is the magnetic induction at Z_1. But, since we are dealing with a monopole field,

$$\frac{B_Z}{B_1} = \frac{Z_1^2}{Z^2}$$

so that 4.4 can be written

$$\sin^2 \chi_Z = \frac{Z_1^2}{Z^2} \sin^2 \chi \qquad 4.5$$

from which we get

$$\cos \chi_Z = \left[1 - \frac{Z_1^2}{Z^2} \sin^2 \chi \right]^{\frac{1}{2}} \qquad 4.6$$

At the mirror point χ_Z is 90° which implies that cos χ_Z is zero. Thus at the mirror point,

$$\frac{Z_1^2}{Z_\chi^2} \sin^2 \chi = 1$$

or

$$Z_\chi^2 = Z_1^2 \sin^2 \chi \qquad 4.7$$

where Z_χ is the coordinate, at its mirror point, of an electron which has initial pitch angle χ at Z_1. Substituting 4.6 into 4.3, and using 4.7, we get

$$d s = \frac{d Z}{\left[1 - \frac{Z^2_\chi}{Z^2}\right]^{\frac{1}{2}} \cos \alpha}$$

$$= \frac{Z \, d Z}{\left[Z^2 - Z^2_\chi\right]^{\frac{1}{2}} \cos \alpha} \qquad 4.8$$

It is clear from 4.8 that d s is indeterminate at the mirror point, and imaginary below it. Above the mirror point d s may be either positive or negative, which simply means that the electron may move either towards or away from the monopole. It follows immediately from 4.8 that the path length (in kgms/m^2) through the n'th lamination for an electron with initial pitch angle χ , $X_{n,\chi}$, is given by

$$X_{n,\chi} = \frac{\rho_n}{\cos \alpha} \int_{Z_{n+1}}^{Z_n} \frac{Z \, d Z}{\left[Z^2 - Z^2_\chi\right]^{\frac{1}{2}}}$$

$$= \frac{\rho_n}{\cos \alpha} \left[\left(Z_n^2 - Z^2_\chi\right)^{\frac{1}{2}} - \left(Z^2_{n+1} - Z^2_\chi\right)^{\frac{1}{2}} \right] \qquad 4.9$$

Where ρ_n is the average density in the n'th lamination. We see that for particles mirroring in the n'th lamination only the first square root term in 4.9 need be considered.

4-3 An Intuitive derivation of equation 4.9.

Let us visualize the path of an electron which spirals down towards the monopole on a cone of constant semi-vertical angle α, and reaches its mirror point in lamination number $n + 1$. Now imagine the conical surface cut down one of the position vectors, and opened out into a plane sheet. We know from 1-3 that the path will now appear as a straight line. Thus we have the picture shown in figure 19, where W_n and W_{n+1} are the distances from the monopole to the boundaries of the n'th lamination and W_χ is distance from the monopole to the mirror point, these distances being measured in the plane surface. It follows immediately from this figure that the path length through the n'th lamination is given by

$$X_{n,\chi} = \rho_n \left[\left(W^2_n - W^2_\chi \right)^{\frac{1}{2}} - \left(W^2_{n+1} - W^2_\chi \right)^{\frac{1}{2}} \right]$$

and thus, for a cone of semi-vertical angle α, we have

$$X_{n,\chi} = \frac{\rho_n}{\cos \alpha} \left[\left(z^2_n - z^2_\chi \right)^{\frac{1}{2}} - \left(z^2_{n+1} - z^2_\chi \right)^{\frac{1}{2}} \right]$$

which is equation 4.9.

4-4 Numerical Computation.

In this section we describe, step by step, some numerical computations based on equation 4.9, and give a brief discussion of the results obtained. The limit on time and funds available did not allow extensive computations, but we are able to present enough data here to allow an assessment of the value of our approach to

Figure 19 Diagram showing the part of the surface of the cone opened out into a plane sheet. A few laminations, and the section of the electron's trajectory just preceding the mirror point, are shown.

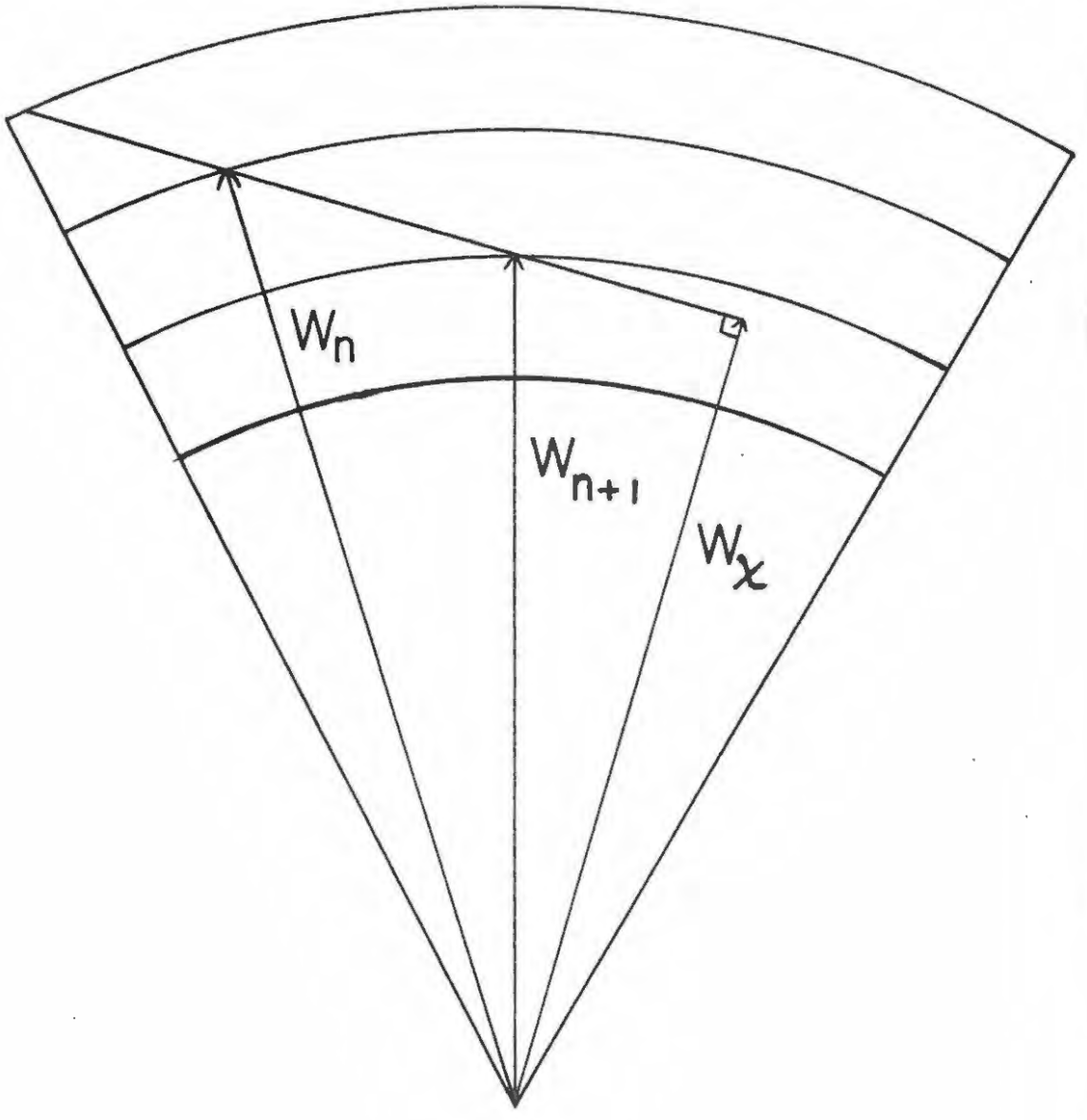
W_n
W_{n+1}
W_x

be made. We will do this, and discuss possible extensions of the work, in Chapter 6.

4-4-1 Locations.

Computations were made for three geographic locations, with appropriate choice of the monopole field in each case. Details of these three cases are as follows.

Case I

Initial conditions at a height of 200 km.:

E_o = 100 keV,

χ = 1, 2, 3, .. by one .., 90^o

Location: 6^o E, 63^o S ... Geographic coordinates

Significance: This point is in the heart of the South Atlantic radiation anomaly (see figure 16).

At this location: $\phi \sim 65^o$ [see reference (116)]

B_s = 0.40 gauss (see figure 8)

The required monopole has

Z_s = 4653.2 x 10^3 metres.

Case II

Initial conditions at a height of 200 km.:

E_o = 20 keV,

χ = 1, 2, 3, .. by one .., 90^o

Location: 20^o W, 46^o S ... Geographic coordinates

Significance: This point is near the Argus shells (96), and approximately between the Brazil radiation anomaly and the South Atlantic radiation anomaly.

At this location: $\phi \sim 50^{\circ}$ [see reference (116)]

B_s = 0.30 gauss (see figure 8)

The required monopole has

Z_s = 5520.3 x 10^3 metres.

Case III

Initial conditions at a height of 1000 km.:

E_o = 100 keV,

χ = 1, 2, 3, .. by one .., 90°

Location: 95° W, 40° N ... Geographic coordinates.

Significance: This point is near Iowa City, i.e. in the northern trace shown in figure 15. Electrons observed at this point will thus drift through the South Atlantic radiation anomaly, as was pointed out in 3-2-3.

At this location: $\phi \sim 70^{\circ}$ [see reference (116)]

B_s = 0.57 gauss (see figure 20)

The required monopole has

Z_s = 4500.4 x 10^3 metres.

4-4-2 Atmospheric Densities.

We assume, for all cases, an atmospheric model in which the air densities given by Cook (117) from satellite data are combined with those calculated by Nicolet (118). A curve of density versus altitude was prepared from these figures, and laminations each 2.5 kilometres

Figure 20 Map showing lines of equal total magnetic intensity (in oersteds) for the Iowa region. Also shown are lines which indicate annual change in total intensity expressed in gammas, full lines denoting increasing intensity, and dotted lines decreasing intensity. Reproduced from map for epoch 1955 published by the United States Hydrographic Office.

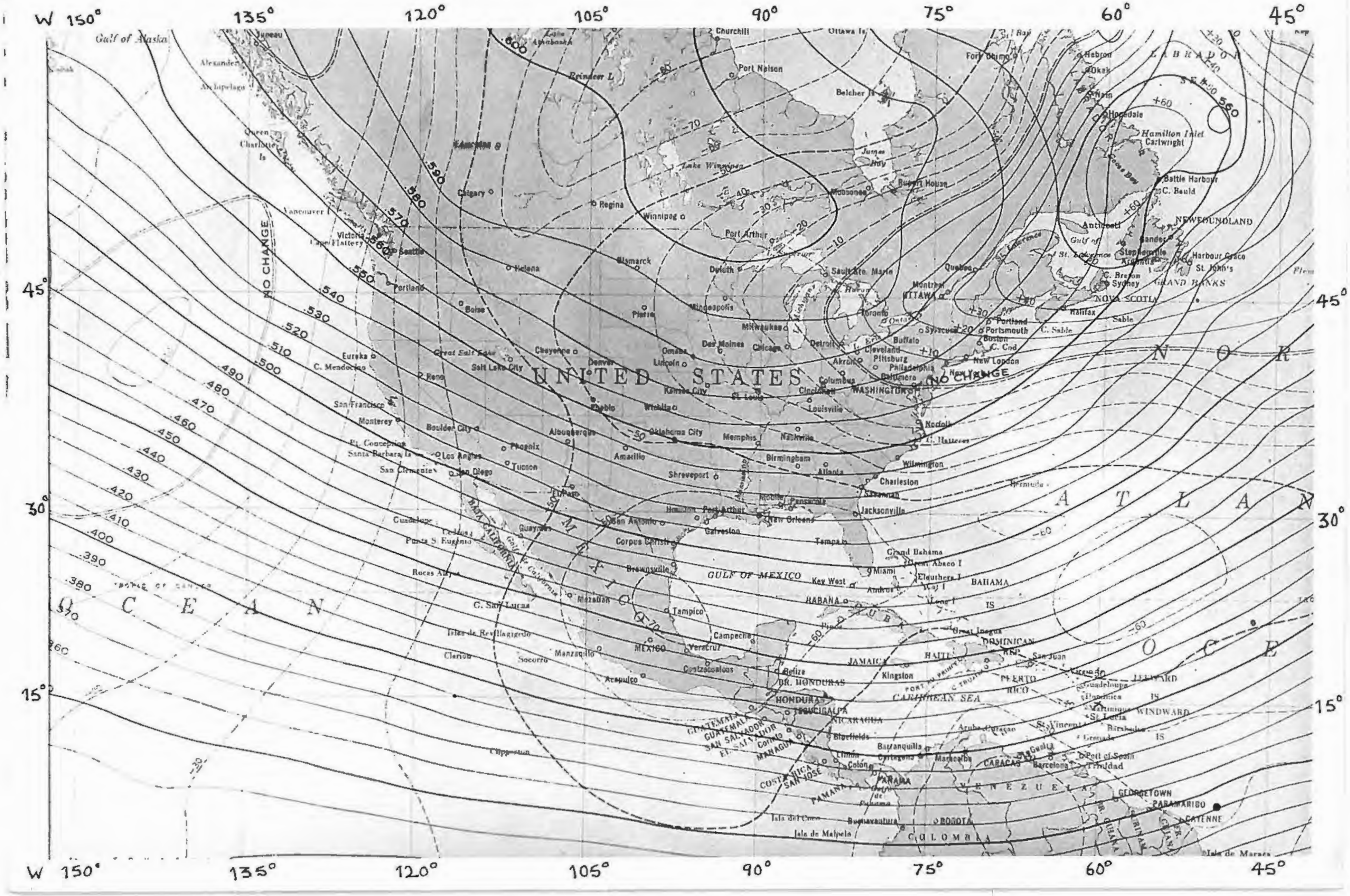

W 150°
135°
120°
105°
90°
75°
60°
45°
45°
30°
15°
UNITED STATES
NO CHANGE
NO CHANGE
GULF OF MEXICO
CARIBBEAN SEA
N O R
A T L A N
O C E
O C E A N
MEXICO
Gulf of Alaska
Alexander Archipelago
Queen Charlotte Is
Vancouver I
Churchill
Port Nelson
Belcher Is
James Bay
Reindeer L
Lake Winnipeg
Hudson Bay
Hebron
Okak
Hopedale
Hamilton Inlet
Cartwright
Battle Harbour
C. Bauld
NEWFOUNDLAND
Gander
St. John's
Harbour Grace
GRAND BANKS
NOVA SCOTIA
Halifax
Sable
C. Sable
Anticosti
Gulf of St. Lawrence
Quebec
Montreal
OTTAWA
Toronto
Portland
Portsmouth
Boston
C. Cod
New London
New York
Philadelphia
Baltimore
WASHINGTON
Norfolk
C. Hatteras
Wilmington
Charleston
Savannah
Jacksonville
Tampa
Key West
Miami
Grand Bahama
Great Abaco I
Eleuthera I
Andros
BAHAMA IS
HABANA
CUBA
JAMAICA
Kingston
HAITI
DOMINICAN REP
San Juan
PUERTO RICO
Great Inagua
LEEWARD IS
WINDWARD IS
Guadeloupe
Dominica
Martinique
St. Lucia
St. Vincent
Barbados
Grenada
Trinidad
Port of Spain
Barcelona
CARACAS
Maracaibo
Aruba
Curaçao
Barranquilla
Cartagena
VENEZUELA
GEORGETOWN
PARAMARIBO
CAYENNE
COLOMBIA
BOGOTA
Buenaventura
Isla de Malpelo
Isla del Coco
PANAMA
Colón
Limón
COSTA RICA
SAN JOSÉ
MANAGUA
NICARAGUA
Bluefields
HONDURAS
TEGUCIGALPA
Belize
BR. HONDURAS
GUATEMALA
SAN SALVADOR
EL SALVADOR
Campeche
Veracruz
Coatzacoalcos
Tampico
MEXICO
Acapulco
Manzanillo
Mazatlan
Guaymas
C. San Lucas
Islas de Revillagigedo
Clarion
Socorro
Clipperton
Guadalupe
Punta S. Eugenio
Roca Alijos
BAJA CALIFORNIA
Gulf of California
San Diego
Los Angeles
Santa Barbara Is
San Clemente
Pt. Conception
Monterey
San Francisco
Reno
Eureka
C. Mendocino
Portland
Seattle
Victoria
Cape Flattery
Boise
Helena
Calgary
Edmonton
Regina
Winnipeg
Port Arthur
Duluth
Bismarck
Pierre
Minneapolis
Milwaukee
Chicago
Des Moines
Omaha
Lincoln
Kansas City
St. Louis
Denver
Cheyenne
Salt Lake City
Great Salt Lake
Pueblo
Wichita
Oklahoma City
Amarillo
Albuquerque
Phoenix
Tucson
Boulder City
El Paso
San Antonio
Corpus Christi
Brownsville
Houston
Galveston
Port Arthur
New Orleans
Mobile
Pensacola
Shreveport
Memphis
Nashville
Birmingham
Atlanta
Louisville
Cincinnati
Columbus
Akron
Cleveland
Pittsburg
Detroit
Buffalo
Syracuse
Sault Ste. Marie
Moosonee
Rupert House
Fort Chimo
Lake Superior
Lake Michigan
Lake Huron
Lake Ontario
Bermuda
600
590
580
570
560
550
540
530
520
510
500
490
480
470
460
450
440
430
420
410
400
390
380
370
360
560
+60
+60
+40
+30
+20
+10
-10
-20
-30
-40
-60
-70
-80
-50
-60
-60
-60
-70

thick below 100 kilometres, and 5 kilometres thick above 100 kilometres were considered. The average density of each of these laminations was found. Rough estimates showed that electrons mirroring above 200 kilometres in this model atmosphere would lose a negligible proportion of their energy. The reference height was therefore taken as 200 kilometres, and Z_1, Z_2, etc. were calculated for each case from

$$Z_n - Z_s = \frac{h_n}{\sin \phi}$$

where h_n is the height of the top of the n'th lamination (measured along an earth radius). Note that for Case III E_o and χ are given at an altitude of 1000 kilometres. Nevertheless we consider absorption of energy in the atmosphere below 200 kilometres only. The reason for this will be made clear in section 4-6. Table 1, in the Appendix to this thesis, gives the values of h_n and ρ_n, and the values of $Z_n - Z_s$ for cases I, II and III, for values of n from 1 to 40. Table 2 gives the values of Z_n^2 for cases I, II and III for values of n from 1 to 40. (It was found to be unnecessary to consider n greater than 40, i.e. h_n less 50 kilometres, since all electrons considered here either mirror, or are absorbed, before reaching this level.)

4-4-3 Mirror Point Coordinates.

The value of Z^2_χ for each $\chi = 1, 2, 3, \ldots$ by one ..., 90^o for each case was calculated from equation 4.7, i.e.

$$Z^2_\chi = Z_1^2 \sin^2 \chi,$$

using the values of Z_1^2 from Table 2. These values are listed in Table 3 in the Appendix.

4-4-4 Range-Energy Relation.

The range-energy relation employed was that given for soft β-rays by Katz and Penfold (119), namely

$$R = 412\, E_o^{1.265 - 0.0954 \ln E_o} \qquad 4.11$$

where R is the range in mg/cm^2 and E_o is the initial energy in MeV. To find $E_{1,\chi}$ the energy of an electron (with initial pitch angle χ) at the bottom of the first lamination, we first calculate R and $X_{1,\chi}$. The residual range of the particle is then taken as $R - X_{1,\chi}$ (using the appropriate units of course), and $E_{1,\chi}$ found by solving the equation

$$\left(R - X_{1,\chi}\right) = 412\, E_{1,\chi}^{1.265 - 0.0954 \ln E_{1,\chi}}$$

In general, to find $E_{n,\chi}$, we would thus solve the equation

$$\left(R - \sum_{1}^{n} X_{n,\chi} \right) = 412\, E_{n,\chi}^{1.265 - 0.0954 \ln E_{n,\chi}} \qquad 4.12$$

In the lamination in which the particle mirrors only the contribution of the first square root term in equation 4.9 is considered for the summation. If the particle subsequently moves up out of this lamination, we add this contribution twice, and then add the value of $X_{n,\chi}$ for each lamination on the way up as well. We stop the calculation only when the L H S of equation 4.12 becomes zero or the particle moves up through the reference level.

4-4-5 Variation of α.

We have pointed out in section 4-1 that α should strictly be

regarded as a variable whose value decreases as the energy of the electron decreases. Thus the term cos α which appears in equation 4.9 should be regarded as a variable. Now, we have also pointed out that the radius of the cone at the reference level is simply the gyroradius of the electron at this level. This is given by equation 1.5 as

$$a = \frac{m v_{\perp}}{e B}$$

It is obvious from this that the radius of the cone at the reference level is in fact a function of $v_{\perp}$ and B at this level, i.e. a function of E_o, χ, and the value of B at the reference level. These embarrassing complications are however removed by the following considerations. If we take the value of E_o = 100 keV, that of $\chi = 90^o$ (so that $v_{\perp} = v$), and that of B = 0.1 gauss = 10^{-5} webers/m^2 (which is less than the least value encountered in the cases we consider), we find that a is of the order of 15 metres. This represents the maximum value of a with which we will have to deal, and since it is insignificant when compared with the values of Z, which we use, these being of the order of 5,000 kilometres, we are justified in assuming that we may put cos α = 1 for all $E_o \leqslant$ 100 keV, B $\geqslant$ 0.1 gauss, and for all χ. Thus equation 4.9 becomes

$$X_{n,\chi} = \rho_n \left[\left(z_n^2 - z^2 \chi \right)^{\frac{1}{2}} - \left(z_{n+1}^2 - z^2 \chi \right)^{\frac{1}{2}} \right] \qquad \underline{4.13}$$

4-4-6 Programming.

The computer was programmed from a set of notes and instructions similar to those listed below. The appropriate conversion factors have been included so that the final values of the energy are in joules.

(1) Variables are n and χ

(2) For each case we find first the constant A_o, given by

$$A_o = E_o^{1.265} - 0.0954 \ln E_o \qquad 4.14$$

where E_o (given in MeV) is a constant for each case.

(3) We find, for all n, for a given χ,

$$X_{n,\chi} = \rho_n \left[\left(Z_n^2 - Z^2\chi \right)^{\frac{1}{2}} - \left(Z_{n+1}^2 - Z^2\chi \right)^{\frac{1}{2}} \right] \qquad 4.15$$

(4) We calculate

$$\frac{1}{4.12} \sum_{1}^{n} X_{n,\chi} = F_{n,\chi} \qquad 4.16$$

where we have multiplied by 100 to convert from kgm/m^2 to mg/cm^2.

(5) We then calculate $1.602 \times 10^{-13} \times E_{n,\chi}$ (joules) from the equation

$$E_{n,\chi}^{1.265 - 0.0954 \ln E_{n,\chi}} = A_o - F_{n,\chi}$$

or

$$0 = 0.0954 \left(\ln E_{n,\chi}\right)^2 - 1.265 \left(\ln E_{n,\chi}\right) + \ln \left(A_o - F_{n,\chi}\right) \qquad 4.17$$

taking the + ve root.

(6) Tabulate $X_{n,\chi}$ and $1.602 \times 10^{-13} \times E_{n,\chi}$ versus n.

(7) We repeat steps (3), (4), (5) and (6) for each χ = 1, 2, 3, .. by one .., 90, and list the value of χ with each table.

(8) We contine computation until $E_{n,\chi} = 0$ and then stop.

(9) If Z^2_{n+1} falls below Z^2_{χ}, we ignore the second term in 4.15 and contine the calculation with the first term only. In this case Z^2_n will fall below Z^2_{χ} on the next step. We then continue the computation by adding $X_{n,\chi}$ again with 4.16 and then decreasing n by one unit per step. in place of increasing by one. We note in this connection, (a) that the values of $X_{n,\chi}$ required have already been calculated from 4.15, and (b), that in the event of there being two values of $1.602 \times 10^{-13} \times E_{n,\chi}$ corresponding to a particular value of n for a particular value of χ, they are tabulated separately against that n for that χ.

(10) If n goes > 40 we stop the calculation.

(11) If n goes < 1 we stop the calculation.

(12) The values of $1.602 \times 10^{-13} \times E_{n,\chi}$ were worked correct to five significant figures so that the energy loss of the electron in each lamination could be followed in some detail.

We wish to thank the C.S.I.R. for a grant to cover the cost of computations on its I.B.M. 704 computer, and Dr Cryer of the N.R.I.M.S. for arranging to have the computations done.

4-4-7 Presentation of results.

Figures 21, 22 and 23, for cases I, II and III respectively, were prepared from the results of these computations. In each case

we have plotted, for selected values of χ, the total energy absorbed from the electron in each lamination (where this is significant) against the median altitude of this lamination. In other words, for the n'th lamination, we plot $E_{n-1} - E_n$ (plus any contribution on the way up) against $\frac{1}{2}(h_n + h_{n+1})$. For cases where the electron's energy goes to zero before it mirrors, we have estimated the height at which this occurs, and plotted $E_{n,\chi} = 0$ against this height in the lamination in which the energy becomes zero. It must be pointed out that the maximum energy for each curve is in general not well defined merely by plotting the points as described above. For cases where the electron's energy goes to zero before it mirrors, we have used the obvious condition that the area enclosed by each curve should be the same. (In fact, the area is of course numerically equal to E_o in each case.)

4-5 Discussion of Results.

Let us consider each of the cases in turn. In figure 21 (Case I) it is apparent that energy loss is negligible at heights above 120 kilometres. For small χ the electrons penetrate deep into the atmosphere and lose most of their energy between $\sim$ 65 and $\sim$ 70 kilometres. As χ increases the height of maximum energy loss rises. The rise is at first very gradual, (for $\chi = 70^\circ$ the maximum is still below 80 kilometres), but rapidly becomes more sensitive to χ. At $\chi = 77^\circ$ it has risen to $\sim$ 87 kilometres, and for $\chi = 78^\circ$ the particle mirrors near 100 kilometres and escapes from the atmosphere, leaving less than 20% of its initial energy between 100 and 110 kilometres. Electrons with χ greater than 78° are mirrored with

negligible energy loss. The fact that the height of maximum energy loss rises with increasing χ is of course due to the increase of path length in each lamination with increasing χ.

In figure 22 (Case II) the energy loss is smaller, and occurs at higher levels, due to the smaller initial energy for this case (E_o = 20 keV). Otherwise the behaviour is very similar to that for Case I. Particles with χ greater than 80^o mirror above 120 kilometres, and lose a negligible amount of their energy to the atmosphere. Those penetrating to relatively low levels in the atmosphere lose most of their energy just below the 90 kilometre level.

Figure 23 (Case III) shows the results for 100 keV electrons incident at 1000 kilometres over Iowa. The fact that we have chosen to fix the values of E_o and χ at a height of 1000 kilometres results in the lowering of the critical value of χ, so that only electrons with χ less than 56^o contribute any energy to the atmosphere. The main contribution is seen to occur between 65 and 80 kilometres.

4-6 Electron Flux and Energy Input to the Atmosphere.

In order to estimate the total energy input to the atmosphere we need to know the electron flux, energy spectrum, and pitch-angle distribution. Now we have pointed out in Chapter 3, that electrons drifting over our location for Case I, will in fact have drifted over our location for Case III on the northern part of their trajectory. Extensive observation of electrons have been made at an altitude of 1000 kilometres over Iowa with the U.S. satellite Injun I, and this

Figure 21 Graphs of energy lost by an electron, versus height, for selected values of χ, for Case I.

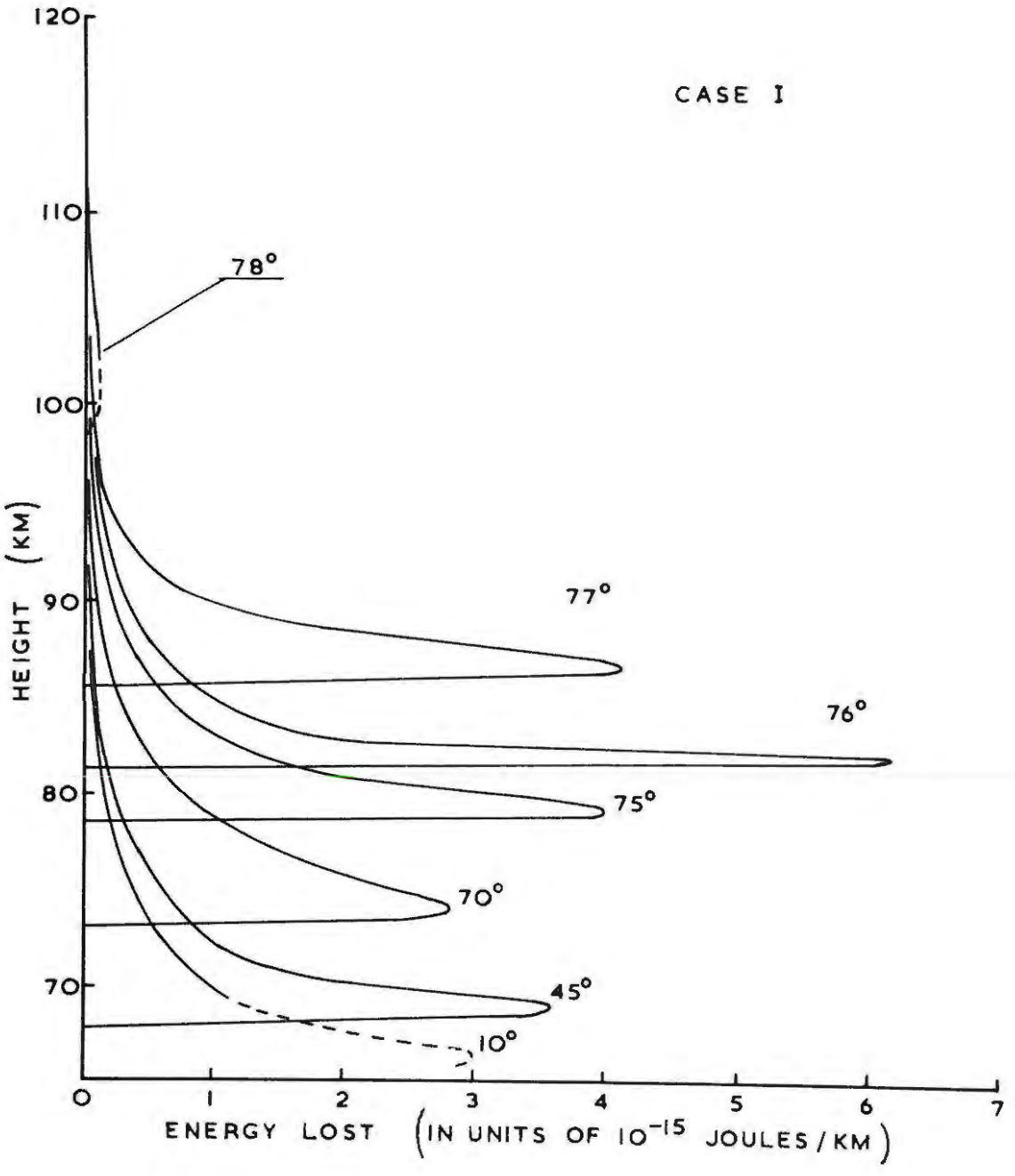
CASE I
120
110
100
90
80
70
HEIGHT (KM)
78°
77°
76°
75°
70°
45°
10°
0
1
2
3
4
5
6
7
ENERGY LOST (IN UNITS OF 10^{-15} JOULES/KM)

Figure 22 Graphs of energy lost by an electron, versus height for selected values of χ, Case II.

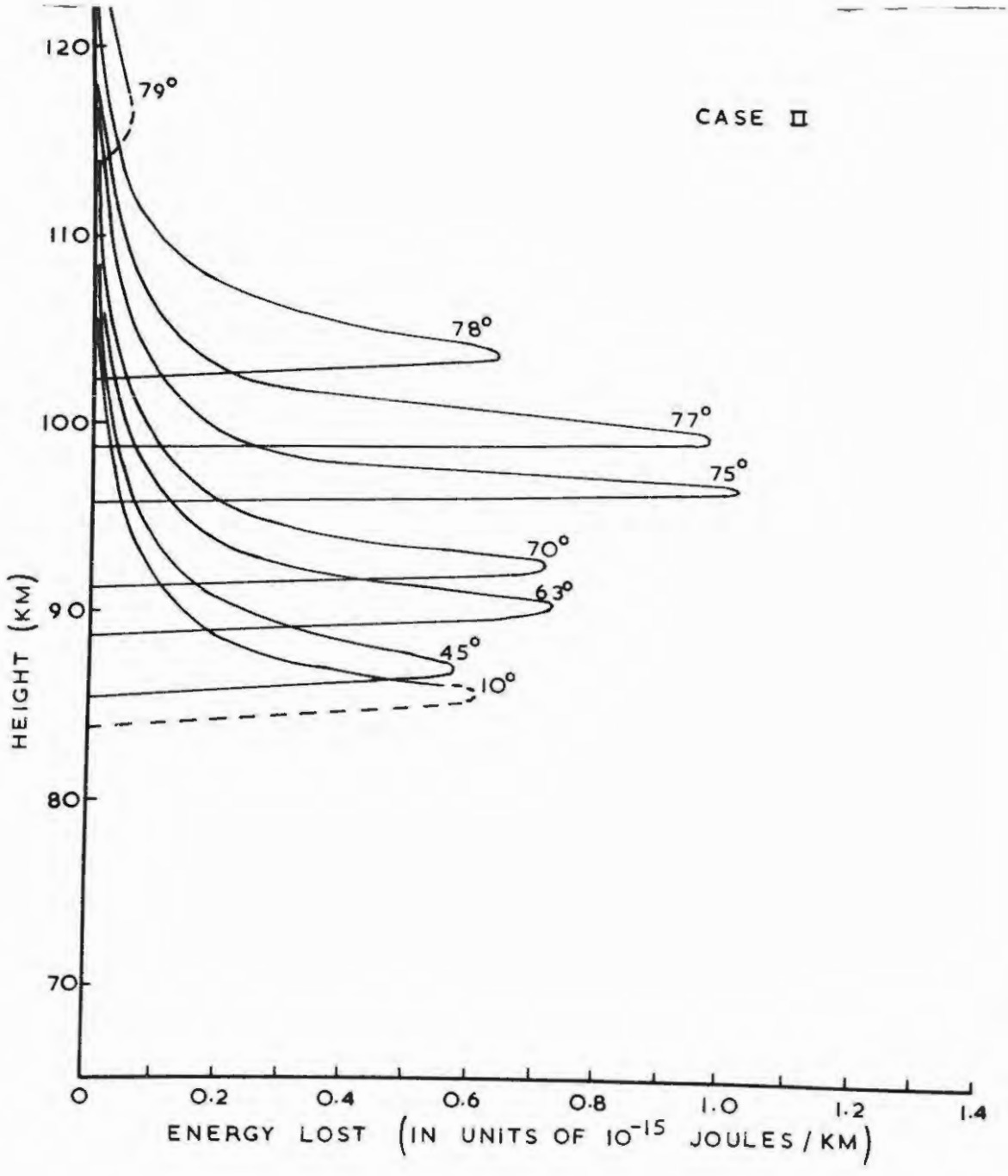
CASE II
120
110
100
90
80
70
79°
78°
77°
75°
70°
63°
45°
10°
HEIGHT (KM)
0
0.2
0.4
0.6
0.8
1.0
1.2
1.4
ENERGY LOST (IN UNITS OF 10^{-15} JOULES / KM)

Figure 23 Graphs of energy lost by an electron, versus height, for selected values of χ, for Case III.

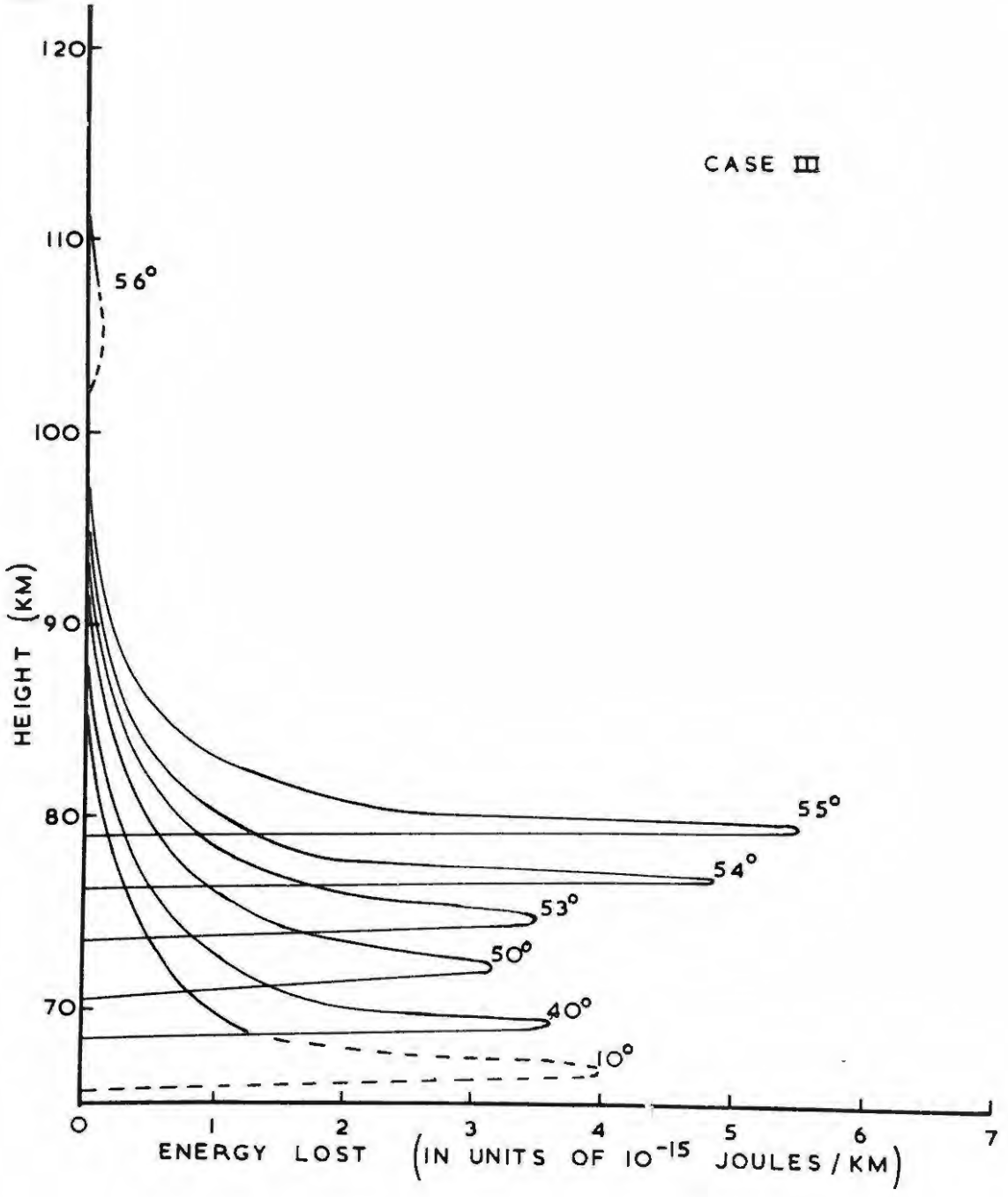
CASE III
120
110
100
90
80
70
HEIGHT (KM)
56°
55°
54°
53°
50°
40°
10°
0
1
2
3
4
5
6
7
ENERGY LOST (IN UNITS OF 10^{-15} JOULES / KM)

is the reason why we chose to fix the values of E_o and χ at 1,000 kilometres for Case III. We now argue as follows. Satellite data are available for the region over Iowa for electrons with L values between 2.5 and 3.5 at 1000 kilometres. The L values of electrons entering the South Atlantic radiation anomaly at 200 kilometres lie in approximately this range, and therefore these electrons are those monitored at 1000 kilometres over Iowa a short time, before, as indicated by the two traces of figure 15. Further, electrons mirroring at approximately 1000 kilometres over Iowa mirror at 200 kilometres over the South Atlantic radiation anomaly, since the magnetic intensity is about the same for these two positions (see figure 18). On the basis of these points, and our estimated traces shown in figure 15, we intend to assume that data, for the Iowa region, from the satellite Injun I represent fairly well, the electrons entering the South Atlantic radiation anomaly. We are therefore in a position to combine this data with our results for Case I, and estimate from it, the energy input to the atmosphere in the region of the South Atlantic radiation anomaly. Unfortunately no data on the pitch-angle distributions of electrons at the location of Case II are available at present.

4-6-1 Relevant Satellite Data.

Satellite data from Injun I for the Iowa regions have been reported in references (44), (62) and (120). Figure 24, reproduced from reference (120), shows some typical types of pitch-angle distribution observed over this region. The upper half of the figure shows a narrow distribution for which no appreciable "dumping" or precipitation of electrons into the lower atmosphere occurs. The distributions in the lower half of the figure are wider, and all electrons with pitch angles less than about 56° will be "dumped" into the lower atmosphere (ie. they will mirror below about 110 kilometres and therefore have all or most of their energy absorved in the atmosphere). The "back scattered" component consists of those electrons which have escaped dumping due to large increases in their pitch angles caused mainly by scattering processes somewhere in the region between 100 and 1000 kilometres. Under conditions of no dumping we see that the distribution cuts off rather sharply at $\chi = 60^{\circ}$, thus we expect from our results in Case III that no energy is absorbed in the atmosphere over Iowa under these conditions. On the other hand, we may easily estimate from figure 24 that over 20% of these electrons have χ less than 77° and will therefore give up all their energy to the atmosphere in the South Atlantic radiation anomaly (see figure 21). Referring to the lower half of figure 24 we see from our results for Case III that most of electrons labelled as "dumped" will lose energy in the atmosphere over Iowa (see figure 23).

Figure 24 Typical types of pitch-angle distribution observed over Iowa U.S. satellite Injun I. Those in the lower half of the figure show backscatter and dumping. Values of B are in gauss, and altitudes are given in kilometres. (Note that the pitch-angle, $\alpha \equiv \chi$). Reproduced from reference (120).

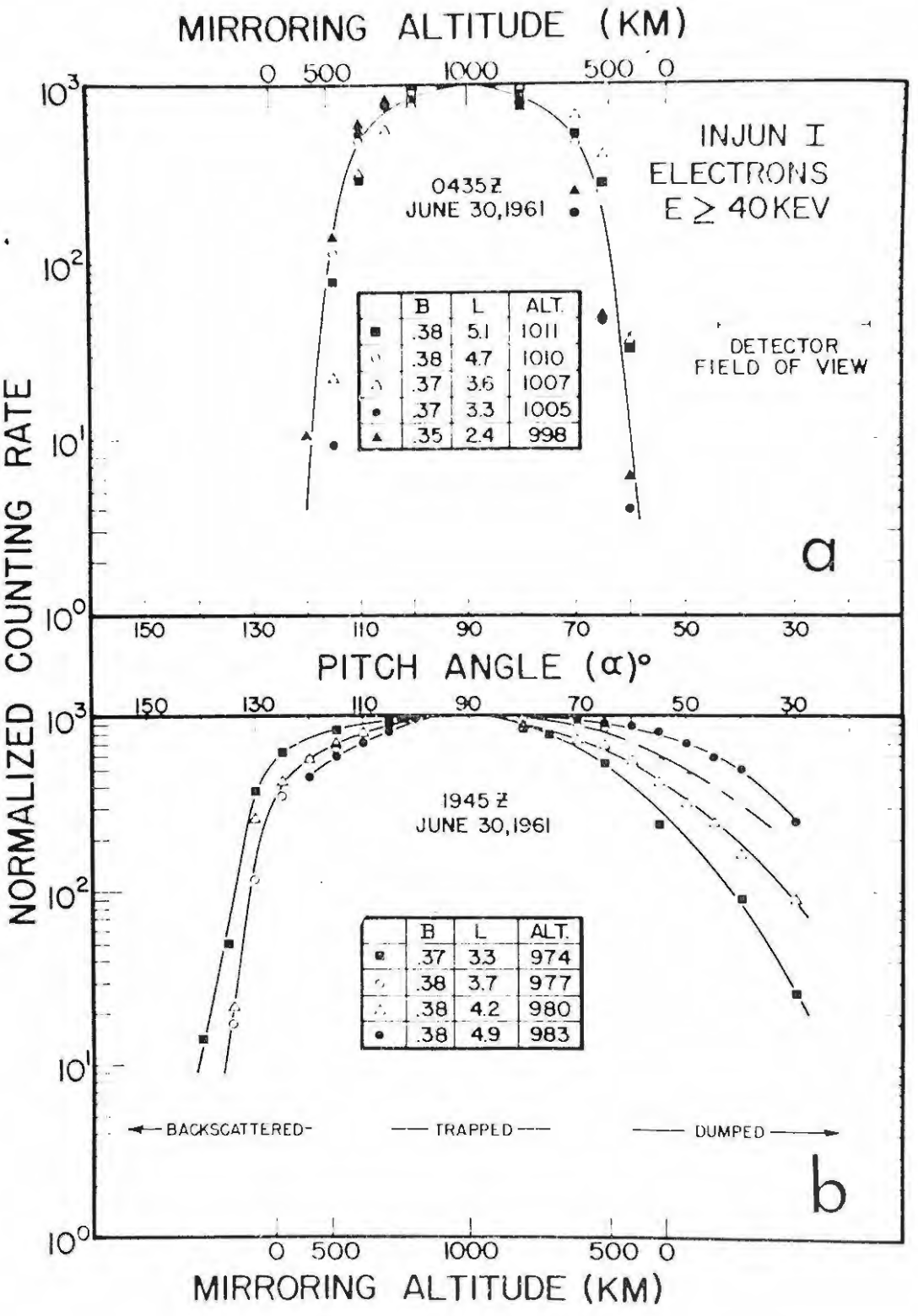
MIRRORING ALTITUDE (KM)
0 500 1000 500 0
INJUN I
ELECTRONS
E ≥ 40 KEV
0435 Z
JUNE 30, 1961
DETECTOR
FIELD OF VIEW
B L ALT.
.38 5.1 1011
.38 4.7 1010
.37 3.6 1007
.37 3.3 1005
.35 2.4 998
a
NORMALIZED COUNTING RATE
150 130 110 90 70 50 30
PITCH ANGLE (α)°
1945 Z
JUNE 30, 1961
B L ALT.
.37 3.3 974
.38 3.7 977
.38 4.2 980
.38 4.9 983
BACKSCATTERED
TRAPPED
DUMPED
b
MIRRORING ALTITUDE (KM)

O'Brien (68) has published an article on the precipitation of electrons over the Iowa regions in which he combines the Injun I data with measurements of the intensity of electrons in the equatorial plane taken with Explorer 12. Figure 25, reproduced from his paper, shows the spatial parameters used (upper half) and a summary of the data used by O'Brien projected on a map of North America (lower half). He has used the parameters Λ, the "invariant latitude", defined by

$$L \cos^2 \Lambda = 1 ,$$

and the L values at an altitude of 100 kilometres. Note that since the dipole approximation has been used in the upper half of figure 25 the values of L are identically equal to the radii of the shells (in E_R units).

We are interested in the region lying between invariant latitudes 50° and 55°. Early Injun I data (62) indicated that the unidirectional flux of electrons with $E_e \geq 40$ keV was typically of the order 10^6 /cm^2 sec ster at 1000 kilometres over Iowa, of which less than 10% is due to protons. Assuming an isotropic distribution, this implies an omnidirectional flux of approximately 10^7 electrons /cm^2 sec. We assume this figure for the omnidirectional intensity in our calculations. [A better estimate of the omnidirectional flux can be found from figure 25 by adding the values for the trapped and dumped (undirectional) fluxes, and multiplying by 10. This gives the omnideractional flux as 2.08×10^6, ie. one fifth of the figure we ...

Figure 25 Upper half. Special parametres (L and Λ) used by O'Brien (68). Reproduced from figure 2 of his paper.
Lower half. Data from U.S. satellite Explorer 12 and Injun I, together with auroral data, projected on a map of North America. Reproduced from figure 10 of O'Brien's paper (68).

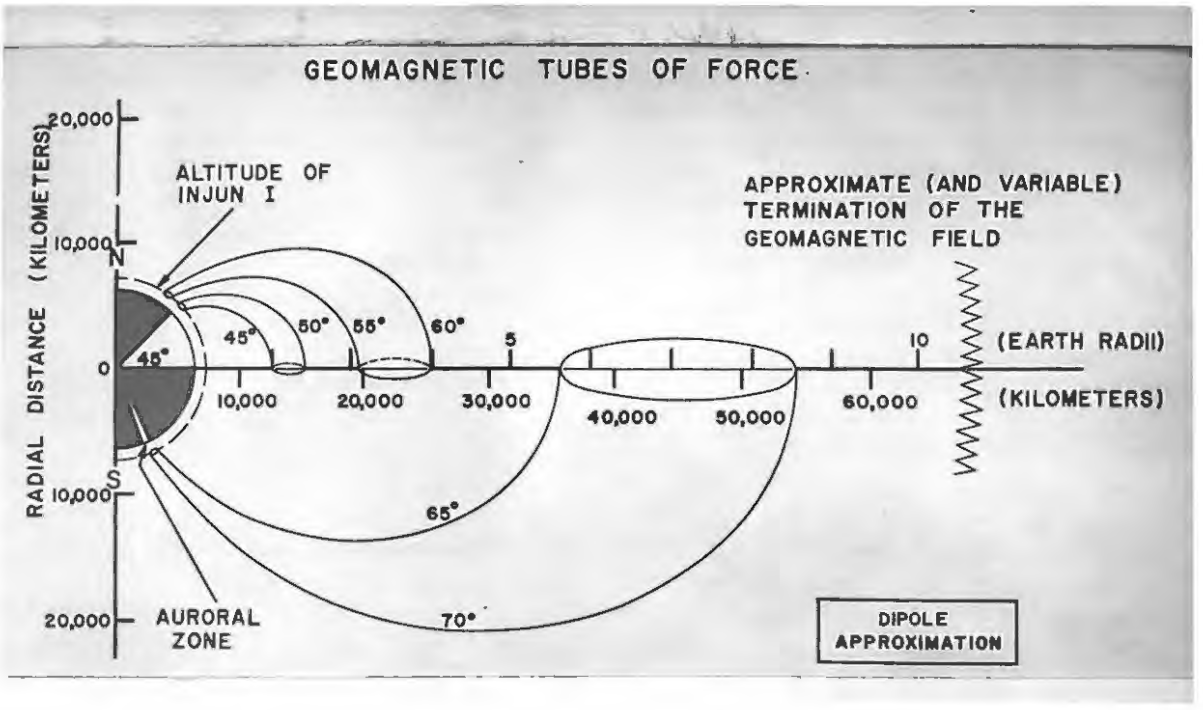
GEOMAGNETIC TUBES OF FORCE
RADIAL DISTANCE (KILOMETERS)
20,000
10,000
N
0
S
10,000
20,000
ALTITUDE OF INJUN I
APPROXIMATE (AND VARIABLE) TERMINATION OF THE GEOMAGNETIC FIELD
45°
50°
55°
60°
65°
70°
5
10
(EARTH RADII)
(KILOMETERS)
10,000
20,000
30,000
40,000
50,000
60,000
AURORAL ZONE
DIPOLE APPROXIMATION

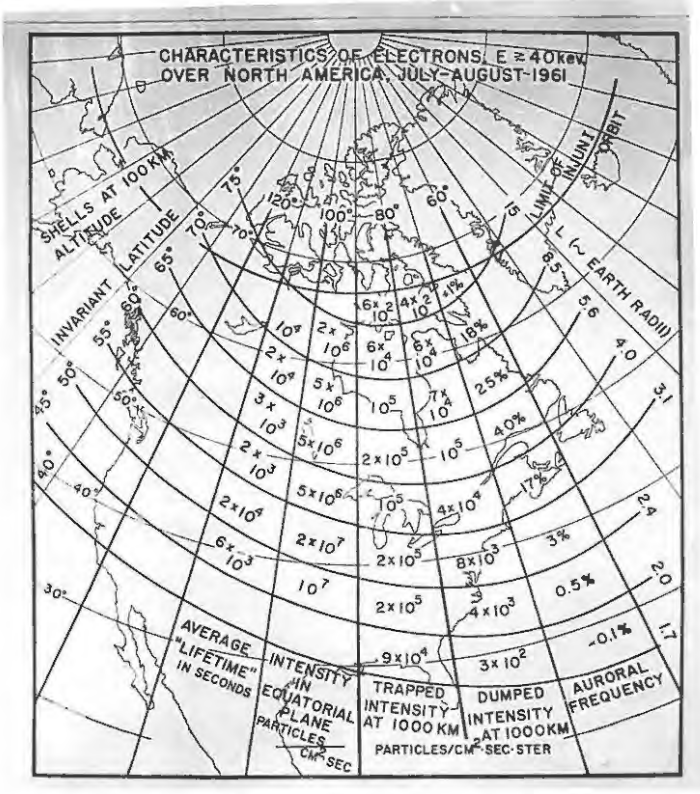
CHARACTERISTICS OF ELECTRONS, E ≥ 40keV OVER NORTH AMERICA, JULY-AUGUST 1961
SHELLS AT 100 KM ALTITUDE
INVARIANT LATITUDE
L (EARTH RADII)
TIME OF INJUN ORBIT
AVERAGE "LIFETIME" IN SECONDS
INTENSITY IN EQUATORIAL PLANE PARTICLES/CM² SEC
TRAPPED INTENSITY AT 1000 KM
DUMPED INTENSITY AT 1000 KM
PARTICLES/CM² SEC STER
AURORAL FREQUENCY

have assumed. This will not radically effect our results however, these being in any case intended only as order of magnitude estimates. (See also section 5-1).] We now have estimates of the omnidirectional flux and pitch angle distribution of electrons at 200 kilometres over the South Atlantic radiation anomaly.

Now it must be pointed out that all the data referred to in this sub-section have been for electrons with energies greater than 40 keV. The time and/or special variations of the energy spectrum of these electrons make it difficult to arrive at a reasonable figure for their average energy, if indeed the terms"average energy"is meaningful in this context. From figure 5 (for L = 2.4), a value of 100 keV seems a reasonable, though fairly arbitrary choice. Thus we decide finally on an omnidirectional flux of 10^7 electrons /cm^2 sec of energy 100 keV, with a pitch-angle distribution similar to that shown in the upper half of figure 24.

4-6-2. Energy Input to the atmosphere.

By estimating the fraction of our assumed omnidirectional flux of 100 keV electrons which lies in successive 2^o ranges of α for the assumed pitch-angle distribution, and then adding the energy contributions in each lamination using figure 21, we may plot a graph of the energy input as a function of height in the South Atlantic radiation anomaly. The result of such an estimate is shown in figure 26 where we

Figure 26 Graph of the estimated energy input to the atmosphere versus height.

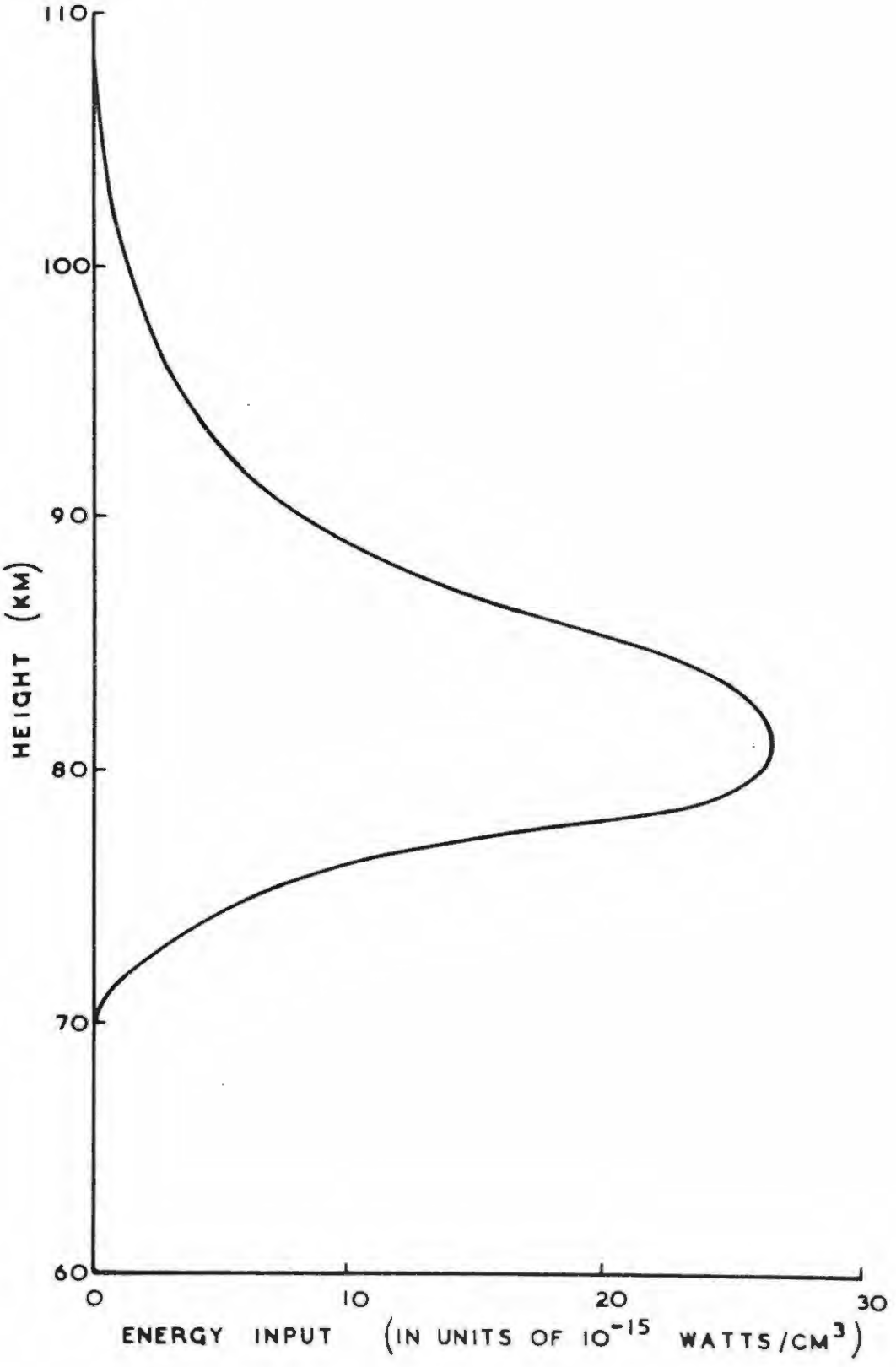
110
100
90
80
70
60
HEIGHT (KM)
0
10
20
30
ENERGY INPUT (IN UNITS OF 10^{-15} WATTS/CM^3)

have drawn a smoothed curve through the values of the energy input for each lamination. Note that we know, from figure 21, the energy absorbed from one electron with given pitch angle in a given lamination in units of Joules/cm. From the assumed data on pitch-angle distribution and omni-directional flux we find the flux /cm^2 sec of this type of electron. Thus it is convenient for us to express the energy input in the lamination in units of Joules/cm^3 sec, i.e. in Watts/cm^3, as we have done in figure 26. We see that nearly all the energy is lost between the 70 and 100 kilometre levels. From figure 26 and our assumed flux of 100 keV electrons we may easily estimate the corresponding total energy input to the atmosphere between these levels. The result is approximately 3.6×10^{-8} Watts/cm^2, which if spread over 40 kilometres in height gives an average energy dissipation of 9×10^{-15} Watts/cm^3.

In addition to the above there is some evidence of large fluxes of electrons with energies of approximately 10 keV just above the atmosphere [(44), (68), (120)]. Krasovskii et al (44) have estimated that these may carry an energy flux of about 10^{-7} Watts/cm^2 down into the atmosphere between heights of 200 and 300 kilometres. Our results seem to indicate that very little of this energy will be absorbed by the atmosphere at these levels. We estimate from figures 7 and 9 of their paper (44) that about 10% of this energy flux will be absorbed in the atmosphere, i.e.

about 10^{-8} Watts/cm^2. O'Brien [(68), (120)] has reported energy fluxes between 1 and 7 x 10^{-6} Watts/cm^2 due to electrons with energies in the range 1 to 40 keV at 1000 kilometres over Iowa. Again assuming a pitch angle distribution similar to that of the more energetic component, we may estimate that about 20% of this energy flux, i.e. about 2 x 10^{-7} Watts/cm^2, will be absorbed in the atmosphere over the South Atlantic radiation anomaly. Our results for Case 2 lead us to believe that this energy will be deposited mainly around the 120 kilometer level. (See, however, Rees (125) and section 5-6).

4-7. Discussion of Simplifying Assumptions.

Before going on to discuss the geophysical effects of the influx of energy into the atmosphere over the South Atlantic radiation anomaly in Chapter 5, we will discuss briefly the two main simplifying assumptions made in this chapter. These are in connection with (1), the use of the range-energy relation, and (2), the fact that we have ignored the effects of scattering in the atmosphere on the mirror heights of the electrons.

4-7-1. The use of the Range-Energy relation.

Though there is some doubt about the validity of the way in which we have found the energy at the bottom of each lamination, i.e. by considering the residual range (119), the way we have used the range energy relation is, in general,

justifiable. One point which should be cleared up is the following. The range-energy relation we have used was derived for the absorption of β - particles in aluminium. Now it is well known that the ability of an element to stop β - particles depends on the ratio of the atomic number to the atomic mass, i.e. on Z/A. When the range in aluminium is expressed in terms of the thickness of the absorber multiplied by its density, we may apply the resulting figure without too much loss of accuracy to absorbing materials for which the ratio Z/A is approximately the same as that for aluminium. For example, in the case of aluminium (Z/A = 0.48) the range of a 1 MeV β-particle is about 400 mg/cm^2 while in the case of gold (Z/A = 0.40) the range is about 500 mg/cm^2, which is not very different from the range in aluminium. We may guess that at heights of about 100 kilometres in the atmosphere the effective value of Z/A is about 0.5 (i.e. the value for oxygen and nitrogen), so that it is permissible to use the range-energy relation as given.

We must point out that the term "path length" has been loosely used in this chapter. What we have in fact done is to assume that the element of range of an electron passing through a given lamination may be found by multiplying the density of the lamination by its "thickness", measured along the path that the electron would follow in free space in a monopole field.

4-7-2-. The Effects of Scattering on the Mirror Heights.

It is clear that scattering perpendicular to the magnetic field line (i.e. the axis of the cone) will not materially affect our results. It has been shown, however, that the effect of scattering parallel to the magnetic field line will disperse the heights of the mirror points. That is, if we consider a group of electrons with the same initial pitch angle, their mirror points will be spread through a fairly wide range of altitude (14). The electrons which contribute significantly to the energy input shown in figure 26 have initial pitch angles in the range 60° to 78°. The downward spread of the mirror heights of these electrons will not affect our results radically since the electrons are stopped just below 70 kilometres even for $\chi = 1^{\circ}$. Also we expect that the upward spread of the mirror heights of these electrons will be more than made up by the downward spread of the mirror heights of electrons with initial pitch angles between 78° and 90°, since the great majority of the incident electrons will have initial pitch angles in this range.

In conclusion we may point out that it seems that the only factors which can radically alter the height range in which the energy input to the atmosphere is significant are the initial energy and the initial pitch-angle distribution. We expect from our experience with figure 22 that decrease of the initial energy will increase the heights at which the

energy is deposited. Satellite readings indicate that there is an increase of flux towards low energies. Thus our assumed mean energy of 100 keV is probably too large, and as a result it is likely that the maximum energy liberation will be between 95 and 105 kilometres rather than at about 80 kilometres as shown in figure 26. The effect of broadening our assumed initial pitch-angle distribution would be to introduce a greater part of the total electron flux into the lower atmosphere, thus increasing the energy influx. In addition we may expect that the curve shown in figure 26 would have a flatter peak, and that considerably more energy would be absorbed between heights of 70 and 75 kilometres because of the larger flux of electrons with small initial pitch angles.

As a result of the considerations in this section we conclude that the energy influx due to 100 keV electrons is probably spread between about 70 kilometres and about 110 kilometres, and that our estimate of the total energy influx is probably a fair one on the average, though too high for quiet time since we have assumed a high value for the omnidirectional electron flux (see section 4-3-1)

CHAPTER 5.

Geophysical Effects.

5-1 Introduction.

A preliminary report on the work described in the previous chapter was presented recently by Gledhill and van Rooyen (121). In this paper the geophysical effects which may be expected from the predicted energy influx to the lower atmosphere were briefly discussed. It must be pointed out that (a) the value of the total magnetic intensity on which we based our calculations for Case I is in doubt (122), and (b), that the major geophysical effects may be expected from the very low energy component of the precipitated electron flux, which we have not investigated directly in Chapter 4. In connection with point (a) it should be mentioned that new data indicate that the value of B_e at our location for Case I should be revised from 0.40 gauss to 0.37 gauss (122), which would mean that all the electrons monitored by Injun I at 1000 kilometres over the Iowa region would have mirror points at or below sea level in the South Atlantic radiation anomaly. Now we have assumed an omnidirection flux of 10^7 electrons/cm^2 sec, of which about 20%, i.e. 2×10^6 /cm^2 sec, are absorbed in the atmosphere over the anomaly. As pointed out in section 4-6-1, a more correct estimate of the omnidirectional flux is 2.08×10^6 electrons/cm^2 sec. If B_e is in fact 0.37 gauss in the anomaly, the entire flux of 2.08×10^6 /cm^2 sec will be absorbed there, which means that our value of the absorbed flux (2×10^6/cm^2 sec) would be correct. Also, the height at which the main energy

flux would be absorbed would not be very different, since if B_s is 0.37 gauss, all electrons arriving at the 200 kilometre level in the anomaly would have pitch angles less than 78°.

It is clear that we cannot base a completely reliable discussion of the geophysical effects associated with the South Atlantic radiation anomaly on our present estimates. This research is continuing, however, and it is hoped that we will, at a later date, be able to present a thorough examination of the subject, based on more extensive computations of the type described in Chapter 4. (Some suggestions for such extensions are put forward briefly in Chapter 5 of this thesis). The discussion given in the present chapter is intended to give an indication of what effects may be detectable, both as a guide to future research, and as an aid in the planning of observations in this region. [Experimental investigation of the region is already underway, see (121)]

5-2. General Considerations.

It is generally accepted that precipitation of large fluxes of charged particles into the atmosphere causes the auroras and the high latitude X-ray bursts associated with them. In addition there is a considerable amount of evidence that such precipitation is responsible for certain ionospheric anomalies. [It must be pointed out that precipitation of electrons into the atmosphere is a common

phenomenon, even though it is only in the South Atlantic that high fluxes are a permanent feature of low altitude (i.e. ~ 250 kilometres) observations] Observations of the geophysical effects accompanying the precipitation of particles immediately after high altitude atomic explosions has helped to clarify the position. It is certain that such precipitation causes auroral emission and ionospheric perturbations commonly observed both in the vicinity of these explosions, and at the conjugate points.

Mc Ilwain (123) investigated the nature and energies of the charged particles which produced visible aurorae over Fort Churchill in Canada, and found that, in the two cases investigated, a major fraction of the auroral light was produced by electrons with energies of 10 keV and less.

Observations of electrons with $E_e \geqslant 40$ keV carried out with Explorer 12 indicate that their intensity in the equatorial plane is essentially constant between equatorial radial distances of ~ 2 and ~ 10 E_R (68). Soviet measurements with Lunik 2, (60), gave essentially the same results for the intensity of electrons with $E_e > \sim 200$ eV, though there was evidence of a slight increase in intensity near I ~ 10. Now the lines of force from the auroral zone cross the equatorial plane at radial distances between ~ 6 and 8 E_R. Thus there is a potential source of auroral electrons in the appropriate region of the geomagnetic field. O'Brien (60) has found that the similarity of the auroral latitude

profile and the precipitation profile is remarkably close between invariant latitudes of $\sim 55^{o}$ and $\sim 75^{o}$, and reasonably close in other regions (see lower half of figure 25). Since this similarity is for electrons with $E_e \geq 40$ keV, and the auroras are caused primarily by electrons with $E_e \sim 10$ keV, this agreement may be purely coincidental. It seems reasonable however, to regard the dumped electrons observed by Injun I as the high-energy tail of the spectrum of the electrons causing the auroras (68).

As mentioned in Chapter 2, there are two qualitative models of the outer zone. The original model was the so called "leaky bucket" model. In this model, the electrons of the solar wind are accelerated, by an unknown primary acceleration mechanism, and injected into the trapping region, where they remain for the time being. When a magnetic (or other) disturbance occurs, some of these electrons have their orbits perturbed and are accelerated into the atmosphere, causing the auroras. O'Brien (68) has recently proposed the "splash catcher" model, which is very much simplified in that it only requires one acceleration mechanism, which simultaneously produces both auroral and outer-zone electrons. When electrons are accelerated and injected into the magnetosphere, those which have small pitch angles are 'dumped", probably producing auroras, while those with large pitch angles are trapped. Thus all precipitated electrons are regarded as freshly accelerated

ones. (Note that O'Brien has not suggested that there is only one type of acceleration mechanism operating, but merely that each acceleration produces electrons which will be dumped). The essential difference between these two mechanisms is, then, that in the latter, the dumped fluxes are to be regarded as more fundamental than the trapped fluxes, which are merely the "splash" from the acceleration mechanism. This attitude, namely that the outer zone is not so much a source, but a sink of energetic electrons (i.e. $E > \sim 40$ keV), is justified by the high loss rate from the outer zone by precipitation. O'Brien (68) has shown that, if unreplenished, the outer zone would empty on the average in a period of some hours, and occasionally in a few seconds. [See also (124) and (82)]. Although, as he points out, his splash catcher model is undoubtedly an oversimplified one, its strong point lies in the fact that it makes allowance for this high loss rate.

If the loss rate over North America is high, it is obvious that the loss rate in the South Atlantic radiation anomaly is even higher, so that we may expect any geophysical effects correlated with the precipitation of electrons between invariant latitudes of 50° and 55° over North America to be more pronounced in the South Atlantic radiation anomaly. In particular we would expect the auroral frequency to be significantly greater than 3% (of figure 25).

Though particle loss must be very great indeed in this anomaly, we cannot however regard the comparatively low value of total magnetic intensity in this region as the dominant cause of particle loss from the outer zone. This is obvious from the following considerations. (1) If it was a locality of dominant particle loss, we would expect it to cause an observable slot in the outer zone. (2) Explorer 12 measurements indicate that no such slot exists in the equatorial plane in the outer belt. (3) It appears, from the fact that there is no fall off of counting rate towards the east at low altitude in the South Atlantic radiation anomaly, that no "low altitude" slot is created by it. That is, the loss rate of electrons with pitch angles less $\sim 78^{\circ}$ at 200 kilometres in the anomaly is not so large, compared with the replenishment rate, as to cause a noticeable fall off of the intensity of this type of electron across the anomaly. One must however be cautious about this point since the pitch angle distributions of the particles entering the eastern sector of the anomaly have not yet been measured, and it may be that most of the electrons with small pitch angles are in fact removed in the anomaly, but that they do not constitute a large enough component of the omnidirectional flux for this effect to show up in the available data. If such measurements were to prove otherwise, it would imply a very high rate of replenishment of electrons with small pitch angles, which would be explainable only with O'Brien's

splash catcher model. In any case, these electrons are replaced by the time the radiation has drifted round the earth since electrons with pitch angles $< 78^{\circ}$ constitute at least 20% of the flux over Iowa at all times.

One point we must mention here is that the loss rate in the anomaly may become comparatively more important under certain conditions, in which case it is possible that it can produce the bifurcation of the outer zone which is occasionally observed with detectors which respond only to more energetic electrons. (See remarks on bifurcation 2-3-2 B). Unfortunately lack of time has prevented a detailed investigation of this point, though the anomaly does lie in approximately the right range of I to cause the observed bifurcation.

Having discussed briefly some general points in connection with the precipitation of electrons from the outer zone, we now proceed to examine effects of precipitation in the South Atlantic anomaly more specifically.

5-3 Auroral Emission.

For a bright aurora the total energy of ionization is typically in the region of 4×10^{-5} Watts/cm^2 or more. We have estimated a quiet time input of $\sim 2 \times 10^{-7}$ Watts/cm^2 for the low energy ($E_e \sim 10$ keV) component of the flux entering the South Atlantic radiation anomaly, and $\sim 3.6 \times 10^{-8}$ Watts/cm^2 for the component with $E_e \geq 40$ keV.

Further, it is generally accepted that electrons with $E_e \sim 10$ keV are the principal cause of auroral luminosity (123). Rees (125) has recently computed the ionization rates as a function of height for 51 values of E_e in the range of $0.40 \leqslant E_e \leqslant 300$ keV for various angular distributions of the primary (monoenergetic) electron stream. He finds, for a model atmosphere similar to that adopted in Chapter 4, that although 300 keV electrons deposit most of their energy below 90 kilometres, they still contribute to the ionization in the height range of auroral luminosity (i.e. above ~100 kilometres). Figure 27, reproduced from his paper, shows the effect of adopting different angular distributions for the primary stream for E_e = 1.0, 10, and 300 keV. Notice that the energy loss profile in figure 26 is in general agreement with the profile for 300 keV electrons in figure 27. Rees has proceeded to compute the luminosity curves for 3914 Å emission for isotropic streams of electrons obeying energy distributions given by various rocket measurements, applied over the energy range mentioned above. [Note that Rees has not taken account of the effect of the geomagnetic field on the electrons, as we have.] In general these luminosity curves extend deeper into the atmosphere (below 90 kilometres) than the observed luminosity. This is apparently due to the comparatively large fluxes of high energy particles assumed. [The average heights of the lower borders of auroral arcs and

Figure 27 Figure 3 from Rees's paper (125), showing the effect of adopting various angular distributions for the primary electron stream, for selected values of energy in the range 0.4 keV to 300 keV.

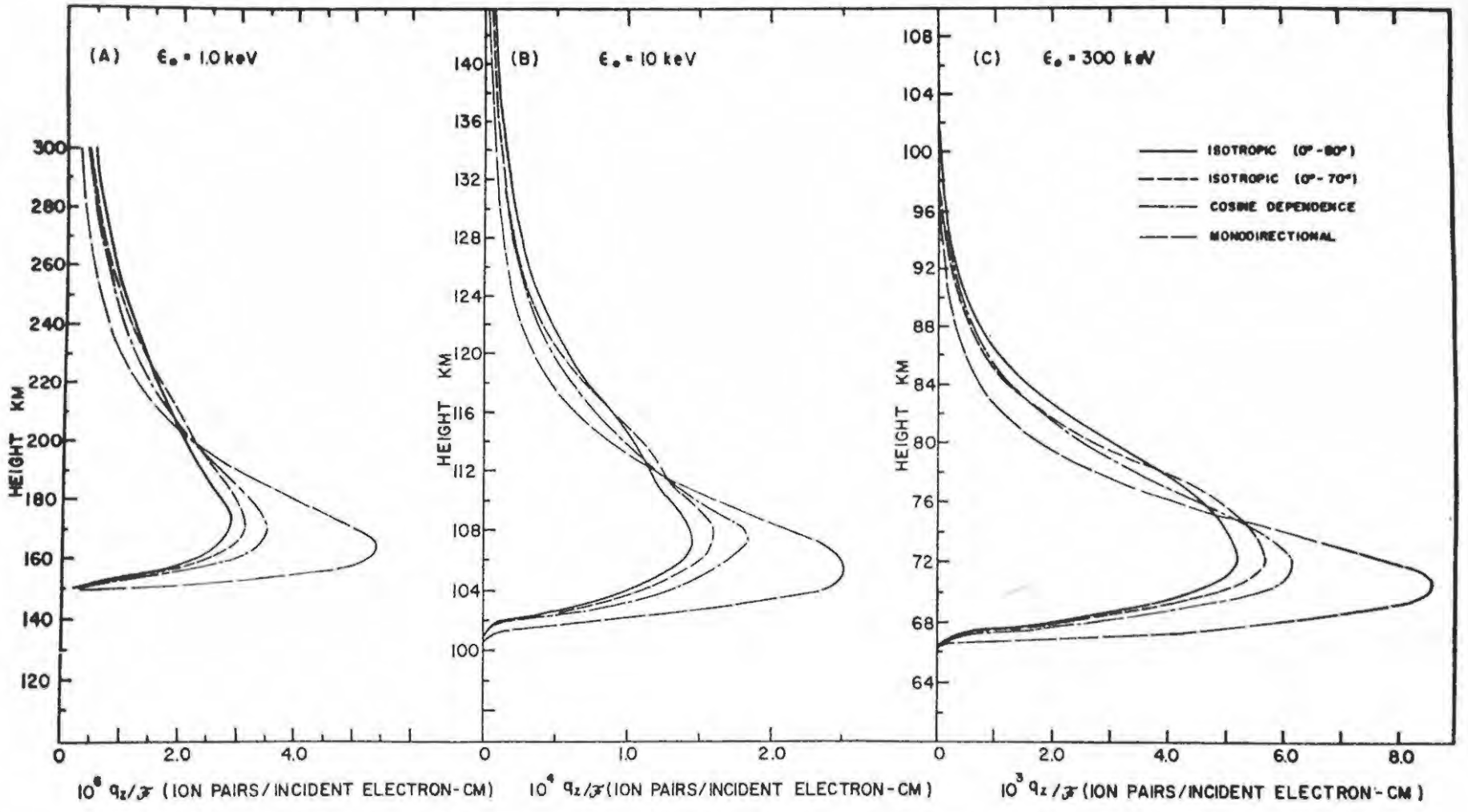

FIG. 3. IONIZATION PRODUCTION BY MONO-ENERGETIC ELECTRON STREAMS HAVING VARIOUS ANGULAR DISTRIBUTIONS: (a) $\varepsilon_0 = 1{\cdot}0$ keV; (b) $\varepsilon_0 = 10$ keV; (c) $\varepsilon_0 = 300$ keV.

bands range from 114.3 kilometres for a weak aurora, to 94.7 kilometres for a strong aurora, the overall average being at about 106 kilometres (126)].

From the above considerations, and those in section F-2, we may draw the following tentative conclusions in connection with the South Atlantic radiation anomaly. (1) The auroral frequency is probably significantly greater than 3%. (2) Mc Ilwain (123) has found than an incident energy flux of 2×10^{-6} Watts/cm^2 carried by electrons in the range 3 to 30 keV can cause "a faint, quiescent auroral glow". This is only one order of magnitude greater than our estimate of the energy influx in the anomaly due to low energy electrons. Thus, assuming the pitch-angle distribution of electrons with $E_e < 40$ keV to be at least as broad as that for electrons with $E_e > 40$ keV at all times, we would expect an apparently colourless (126) amorphous glow, probably without distinct boundaries, to be permanently present over the anomaly. This may be difficult to observe since it could well be so uniform over the visible sky that the absence of a background for comparison prevents its immediate visual detection. (3) During times when the pitch-angle distribution is as broad as those shown in the lower half of figure 24, we may expect a reasonably bright auroral glow with a lower boundary at about 85 kilometres. [See also (112)].

Recent efforts to detect these effects were inconclusive (127), although some evidence of anomalous emission was found in the region between Cape Town and Gough Island.

One further set of phenomena which we must mention here, are the newly discovered mid-latitude 6300 Å auroral arcs. A review of their properties has been published recently by Roach and Roach (128). Figure 28 shows the regions, labelled "M", in which these arcs have been detected. The zones labelled "E" and "A" are characteristic of the equatorial and auroral zone 6300 Å arcs respectively. Comparison with figure 15 shows that the regions in which the M arcs are observed correspond remarkably closely to the mirror point traces of particles drifting through the anomaly. In fact their orientation shows remarkable parallelism with the invariant latitude (128). Some of the prominent features of these arcs are the following (128). (1) They are classified as auroral since they are controlled by the geomagnetic field. (2) Their principal radiation is at 6300 Å, which means that they are generally invisible. (3) They cover some hundreds of kilometres in latitude and in height, and have been directly observed to extend over some 3000 kilometres in longitude. (It is possible that they extend right round the earth). (4) It appears that these M arcs may follow the solar cycle. During the 1957 - 1958 solar activity maximum they were present during approximately 20% of the

Figure 28 Zones of 6300 Å activity after Roach and Roach (127). The zones labelled "A" correspond to the centre of the auroal zones; "M" to the regions within which M arcs have been observed; "E" to the regions in which the equatorial 6300 Å arcs are observed.

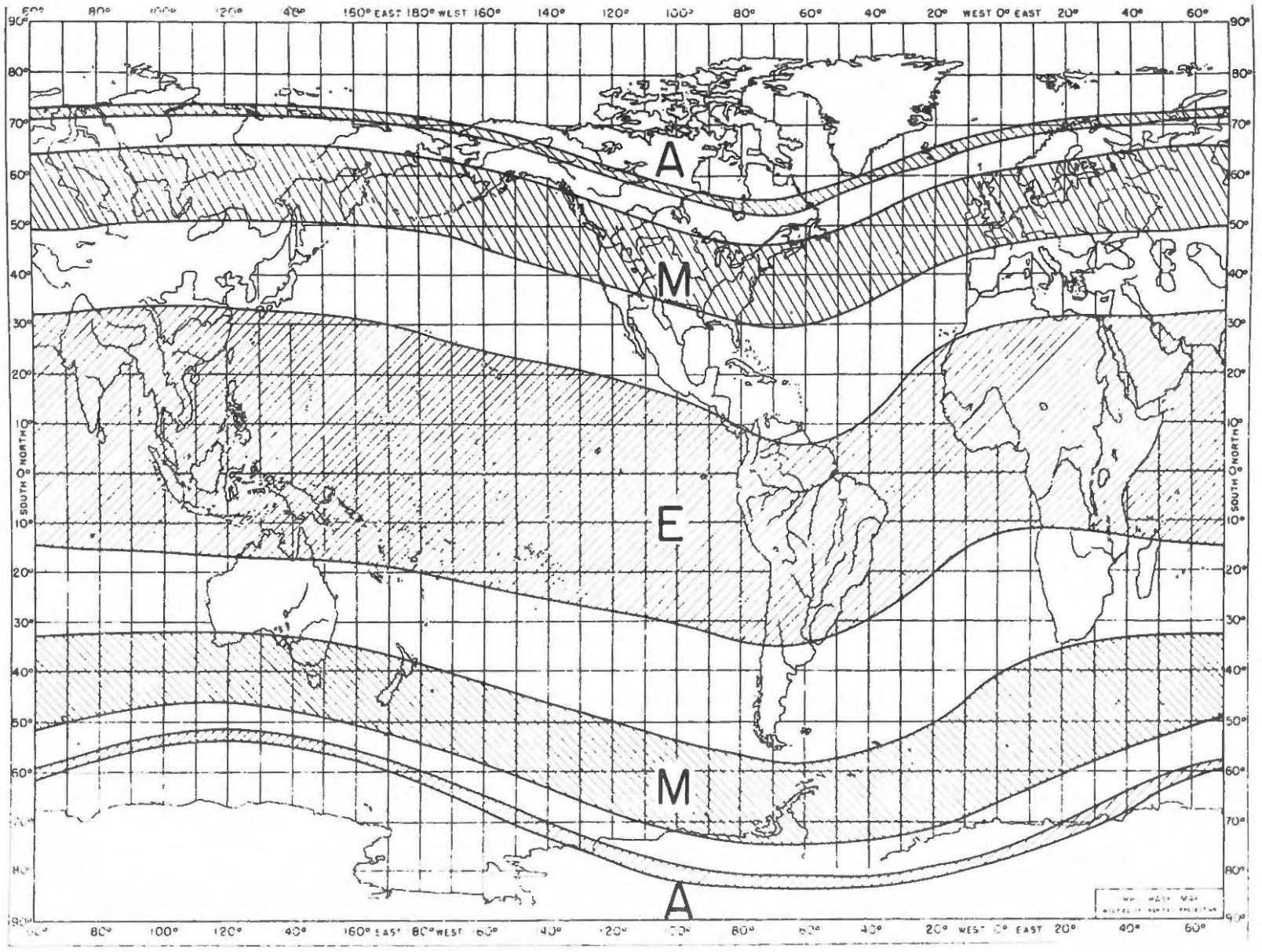
A
M
E
M
A
150° EAST 180° WEST 160°
140°
120°
100°
80°
60°
40°
20° WEST 0° EAST 20°
40°
60°
90°
80°
70°
60°
50°
40°
30°
20°
10°
SOUTH 0° NORTH

observing time, but the frequency has decreased as solar minimum has approached. (5) They are observed during periods of increased magnetic activity, and their intensity increases with the magnetic activity index. (6) They are tubes of emission with maximum intensity near the centre of the tube at a height of about 400 kilometres. The suggested excitation mechanisms for the M arcs have been discussed by Roach & Roach (128). Precipitation of large fluxes of low energy electrons (below 1 keV, see figure 27) seems to be a highly attractive answer to the problem when the characteristics mentioned above are considered. There are, however, considerable problems connected with such an explanation [See (128)]. In view of the importance of the M arcs in general auroral theory, the following point is of interest. If observations of these arcs in the anomaly prove that they are more pronounced and frequent there than anywhere else in the M zones, we may conclude that they are definitely correlated with precipitation of electrons, and that not all of the low energy electrons have small pitch angles. (It is not known at present whether any electrons with energies $\leqslant$ 10 keV are trapped in the magnetosphere. If all such electrons were injected into the magnetosphere with small pitch angles, we would not expect preferential dumping in the anomaly. If, on the other hand, large trapped fluxes of such electrons exist, we may expect continuous loss of part of the trapped

fluxes in the anomaly, and also more pronounced 6300 Å arcs there during magnetically disturbed times. See also Chapter 6).

5-4. X-rays at balloon heights.

X-ray bursts detected at balloon heights are a regular feature associated with electron bombardment of the upper atmosphere [see, for examples, references (129), (130), (131)] and are the result of bremsstrahlung from the more energetic electrons. These bursts are not necessarily always associated with visible auroras, although this is frequently the case. Most of the bursts have been recorded during magnetic storms. Winckler estimates that strong bursts are the result of electron fluxes of the order of 10^8 electrons/cm^2 sec with energies of $\sim$ 100 keV, which are stopped at about the 100 kilometre level. This implies that our assumed (absorbed) flux of 2×10^6 electrons/cm^2 sec (with E_e = 100 keV), should cause an X-ray flux of easily detectable magnitude in the South Atlantic radiation anomaly. In fact this should be a reasonable permanent feature there.

Though we will not undertake to present a detailed analysis to support this conclusion, (such analyses are very complicated), we may draw on the results on one such analysis to justify the statements above. Cladis and Dessler (132) estimated the X-ray flux likely to be found

in the neighbourhood of Cape Town. Though they estimated the absorbed flux of electrons in the energy range 60 to 800 keV to be only 720/cm^2 sec, they concluded, on valid grounds, that this would cause an X-ray flux which is just detectable. [Their estimate of the absorbed electron flux was far too low because it was based on the assumption that small-angle atmospheric scattering is dominant loss mechanism for these electrons, and that the electrons therefore have a lifetime of the order of several hundred years, in accordance with the neutron decay theory of the origin of the outer belt, now discarded.] We therefore conclude that an absorbed flux of 2×10^6 electrons/cm^2 sec with E_c = 100 keV should produce an easily measurable X-ray flux.

4-5. Ionospheric Ionization.

There seems little doubt that the precipitation of energetic electrons produces some heating and ionization in the atmosphere at mid- and high latitudes, though the extent of this effect has not yet been gauged with certainty. [See, for example, (133), (134), (135)]. We have estimated an energy input of the order of 9×10^{-15} Watts/cm^3 or 56 keV/cm^3 sec for the South Atlantic radiation anomaly, which may be expected to produce some ionization in the D and E regions of the ionosphere. Since the electrons will lose approximately 35 eV per ion pair produced in the atmosphere (125), the corresponding

rate of production of electrons is about 1.6×10^3 /cm^3 sec. Assuming equilibrium conditions,

$$\frac{dN}{dt} = q - \gamma N^2 = 0 \qquad 5.1$$

where q is the production rate, γ is the recombination coefficient, and N is the equilibrium density. From equation 5.1,

$$N = \sqrt{\frac{q}{\gamma}}$$

$$= \left[\frac{1.6 \times 10^3}{10^{-7}}\right]^{\frac{1}{2}}$$

$$\doteq 1.2 \times 10^5$$

where we have assumed a recombination coefficient of 10^{-7}/cm^3 sec, which is the largest that has been seriously suggested for the E region. The corresponding plasma frequency is about 3.1 Mc/sec. This makes the layer readily detectable with an ordinary ionosonde. Such a layer would be particulary noticeable at night, when the normal E layer electron density goes below the lower limit on ionosondes (about 1 Mc/sec). Unfortunately efforts to observe this layer have been unsuccessful up to now (121).

E-6. Atmospheric Heating.

As indicated previously there is evidence that corpuscular heating of the atmosphere is significant,

particularly at higher latitudes. Energy lost by electrons in the region above 70 kilometres will, in the long run, end up as heat, even if an intermediate step such as ionization or excitation takes place. If we use the ideal gas approximation, the heat capacity C at various heights in our model atmosphere can easily be found from the equation,

$$C = \frac{5}{2} \frac{\rho R}{M} \quad \text{Joules/cm}^3 \ ^\circ\text{K} \qquad 5.2.$$

where ρ is the density of the atmosphere at the particular height (in gms/cm^3), R is the universal gas constant, and M is the molecular weight of the air in grams. We take the values of R and M as:

$$R = 8.3 \text{ Joules/Mole } ^\circ\text{K}$$

$$M = 28 \text{ gms.}$$

in the following estimates.

At 80 kilometres the result is $C = 1.9 \times 10^{-8}$ Joules/cm^3 $^\circ$K, and the temperature rise produced by our estimated energy input of 9×10^{-15} Watts/cm^3 would thus be 5×10^{-7} $^\circ$K/sec. It is evident from this that there will be very little resultant heating of the atmosphere by 100 keV electrons in the region round 80 kilometres.

The effect of the soft component of the electron flux may well be appreciable however, since this will deposit its

energy at greater heights, where the heat capacity is very much less than at the 80 kilometres level because of the rapid decrease of density with increasing height in the atmosphere. If we assume that the low energy component consists predominantly of 10 keV electrons, the energy carried by it would be deposited round the 110 kilometre level (see figure 27) where the heat capacity $C = 1.3 \times 10^{-10}$ Joules/cm^3 ^{o}K. If the energy input of 2×10^{-7} Watts/cm^2 is spread over say 20 kilometres (see figure 27), this corresponds to an average power dissipation of 10^{-13} Watts/cm^3, which would produce a temperature rise of 6.7×10^{-4} ^{o}K/sec, i.e. about 2^{o}K per hour. This may be enough to cause slight turbulence of the ionosphere, and a a small increase of the scale height at these levels.

The most interesting possibility is that, judging from such measurements of the spectrum as are available, about 40% of the energy flux carried by electrons with 1 keV $\leq E_e \leq$ 40 keV may be due to electrons with $E_e \sim 1$ keV. [(66),(123)]. This would amount to 4×10^{-8} Watts/cm^2, and would be absorbed at the 180 kilometre level (see figure 27), where the heat capacity $C = 5.1 \times 10^{-13}$ Joules/cm^3^{o}K. If spread over 60 kilometres (see figure 27), this energy input of 4×10^{-8} Watts/cm^2 corresponds to an average power dissipation of 5×10^{-15} Watts/cm^3. Thus the resulting temperature rise is approximately 10^{-2}^{o}K/sec, i.e. about 36^{o}K/hour.

Prolonged heating of the type discusses in the previous two paragraphs can have many consequences. The easiest of these to look for would be the following. (1) Increased densities at great heights may cause increased satellite drag. (2) Increased temperatures at great heights. (3) Increased electron temperatures and a "topside" bulge in the ionosphere which could be detected by topside ionosphere sounders [see also (135)]. (4) Spread echoes and oblique reflections from turbulent ionospheric layers.

5-7. Discussion

Obviously, more complete elucidation of the effects discussed in the last four sections must await a fuller investigation of the energy input from the soft electron component, and geophysical investigation in the South Atlantic radiation anomaly. We may, however, conclude from our examination of the possible geophysical effects in the anomaly, that a thorough investigation of the area is desirable. Ship-borne riometers, airglow photometers, and ionosondes, probably represent the simplest means of carrying out such an investigation. Finally, it is of interest to point out that one would also expect to find increased VLF activity in the region of the anomaly. Such activity is often correlated with auroral and ionospheric phenomena [see (136) and (137) for interesting cases].

CHAPTER 6.

A GENERAL DISCUSSION.

6-1 Our Approach to the Problem.

It must be emphasized that our approach to the problem of the precipitation of charged particles into the atmosphere, presented in Chapter 4 of this thesis, is significantly different from previous work in this connection. [See, for comparison with some previous work (125), (138), and Chapter 18 of "The Polar Aurora".] The approach presented in this thesis is, as far as the author knows, the first to use a range-energy relation in conjunction with a method which takes account of the effect of the magnetic field on the motion of electrons which have a given pitch-angle distribution.

Using the techniques developed in Chapter 4, we have been able to show directly that the ionospheric ionization and X-ray bursts caused by the precipitation of electrons (with E_e = 100 keV) into the South Atlantic radiation anomaly should be of detectable magnitude. The usefulness of these techniques in making such estimates has therefore been tested, and we are justified in claiming that, with suitable extensions, they could be employed in a rigorous theoretical investigation of the anomalous region provided that adequate data on the flux, pitch-angle distribution, and energy spectrum of the electrons entering the anomaly were available.

6-2 The Low Energy Component of the Electron Flux.

Any thorough treatment of the problem we have tackled in

this thesis obviously requires more complete knowledge of the characteristics of the low energy ($E_e \leq$ 40 keV) component of the electrons flux. A detailed investigation of these soft electrons is not only of interest in connection with the work presented in Part II of this thesis, but is also important in other respects. For example, it would be invaluable in the study of auroras (125). In addition, such an investigation may provide the answers to the theoretical problems pertaining to the injection of charged particles into the magnetosphere, and their subsequent (and/or prior) acceleration.

The drift times of electrons with $E_e \leq$ 10 keV are of the order of a few days. Thus, if intense trapped fluxes of such electrons are present in the trapping region, we may expect geophysical events connected with their precipitation into the anomaly to persist for at least a few days after the end of large scale precipitation events such as may cause the mid-latitude auroral arcs.

6-3 Suggestions for Further Research.

The form of the range-energy relation employed in the computations described in Chapter 4 is such that it limits the sensitivity of the calculations. It is recommended therefore, that a more suitable range-energy relation be found. [See for example the range-energy relation (for air) used by Rees (125)].

A possible extension of the computations can be based on the following steps. (We assume that mathematical forms have been found for the pitch-angle distribution and the energy spectrum).

(i) Consider electrons with energy E_o and pitch angle χ at the reference level. Assume that the pitch-angle distribution has the same form for each value of E_o. From the assumed pitch angle distribution, find the fraction of the total number of electrons which have pitch angle χ, i.e. find

$$P = \frac{N(\chi)}{N}$$

where $N(\chi) = f(\chi)$ is the number of electrons with pitch angle χ, and N is the total number of electrons. (Note that the fraction P has a unique value for each χ, even though $N(\chi)$ and N have different values for each value of E_o considered.)

(ii) Find, as in Chapter 4, the energy absorbed, in the n'th lamination, from an electron having initial energy E_o, and initial pitch angle χ. Let this be $\equiv Q$

(iii) Find the number of electrons with energy E_o. Let this be $N(E_o) = f'(E_o)$. The number of electrons with initial energy E_o and initial pitch angle χ is then

$$P\ N(E_o) = S$$

(iv) The total energy absorbed in the n th lamination (from electrons with initial energy E_o and pitch angle χ) is then given by

$$Q\ P\ N(E_o) = Q\ S = T$$

(v) Finally, evaluate the double integral

$$\int_{\chi=0^\circ}^{90^\circ} \int_{E_o = 0.4\ keV}^{600\ keV} T\ d\chi\ dE_o = E_n$$

where E_n is the total energy absorbed in the n^{th} lamination.

The range of energy chosen above is not entirely arbitary. The lower limit is that used by Rees (125). Also, Rees (125) finds that electrons with E_c = 300 keV contribute significantly to the ionization at auroral heights, so we want the upper limit to be at least 300 keV. On the other hand, there are very few trapped electrons with energies greater than 600 keV in the outer zone, so that 600 keV is probably a good choice for the upper limit.

Finally, we must point out that with some small modifications the method we have used in Chapter 4 can be applied to the Brazil radiation anomaly.

6-4 Note on the Variation of α.

We have put the factor $\cos\alpha$ equal to unity in equation 4.9 i.e. in the equation

$$Y_{n,\chi} = \frac{\rho_h}{\cos\alpha}\left[(Z_n^2 - Z_\chi^2)^{\frac{1}{2}} - (Z_{n+1}^2 - Z_\chi^2)^{\frac{1}{2}} \right]$$

In doing so we have fixed α, i.e. we have not taken account of the decrease in α with decreasing electron energy. This is justified by the following considerations.

(1) Let the value of $\cos\alpha$, calculated from Z, and the gyroradius of the electron at the reference level, be $1 - \delta$, where $0 < \delta < 1$. As pointed out in section 4-4-F, δ is so small that we may, for our purposes, put $\delta = 0$, i.e. $\cos\alpha = 1$

(2) The values of δ which apply to the cases we consider are in fact so small that if we are computing the values of χ_m, χ correct to 5 figures we get the same answer whether we use $\cos \alpha = 1 - \delta$ or $\cos \alpha = 1$. In other words our calculation is not sensitive enough to show the variation of α in the cases considered.

For very high energy electrons, the magnitude of $\cos \alpha$ could be fixed for each lamination using the value of the electron energy at the top of the lamination. This would provide a satisfactory solution to the problem for any electron energy likely to be encountered in this type of work.

It is interesting to note that putting $\cos \alpha = 1$ implies that we have collapsed the cone. The electron may be thought of as moving along the line traced out by its guiding centre. Let us imagine that the electron has energy E, of which an amount E_p is associated with its movement along the line, while the remaining energy $E_s = E - E_p$, is stored in a "sink". If it moves in free space, E is of course a constant. As it moves down the line towards the monopole E_s increases at the expense of E_p until, at the mirror point, $E_s = E$ and $E_p = 0$. [This division of the energy corresponds to resolving the velocity of an electron spiraling round the lines of force into components perpendicular to, and parallel to, the magnetic field vector. $E_p = 0$ corresponds to the case where the pitch angle is 90°, while $E_p = E$ corresponds to the case where the pitch angle is zero.] The electron then moves up the line, E_p now increasing

at the expense of E_s. If, on the other hand, the electron is moving in the atmosphere, there is a continuous decrease of E in addition to the above processes. We have in effect assumed that this decrease of E takes place in such a way that the ratio of E_s to E_a is, at each stage the same when the electron is moving in the atmosphere as when it is moving in free space.

S U M M A R Y.

Part I.

(1) An elementary treatment of the motion of charged particles in a magnetic field is presented. The concept of guiding centre motion is introduced, and is used in outlining the theory of particle drifts.

(2) The motion of charged particles in the geomagnetic field is discussed, and the comcept of adiabatic invariance introduced.

(3) Mc Iliwains coordinates for mapping the distribution of charged particles trapped in the geomagnetic field are defined and briefly discussed.

(4) A survey of present knowledge of the Van Allen radiation zones is made. Particular attention is given to the distribution, characteristics, and variability of the trapped radiation.

(5) The Cape Town magnetic anomaly, the Brazil radiation anomaly and the South Atlantic radiation anomaly are discussed. The electrons entering the South Atlantic radiation anomaly are shown to be those monitored over Iowa by U.S. satellite Injun I.

PART II.

(1) It is shown how the geomagnetic field can, at high altitudes and over relatively short distances, be approximated by the field of a monopole. A new method

is developed which enables one to plot the energy absorbed from an electron (which moves in a monopole field in the atmosphere) against altitude, given the initial energy and pitch angle of the electron. Some numerical computations using this method are described, and the results discussed. These results are used, in conjunction with data from U.S. satellite Injun I for the Iowa region, to estimate the energy input to the atmosphere in the South Atlantic radiation anomaly. The main approximations and simplifying assumptions made in this treatment are discussed.

(2) Geophysical effects generally recognized to be connected with the precipitation of charged particles are discussed. In the course of this discussion the two main theories of the connection between the radiation zones and the auroras are examined.

(3) A preliminary discussion, based on the work summarized in point (1), of detectable geophysical events associated with the precipitation of electrons into the South Atlantic radiation anomaly is given. It is concluded that auroral emission, X-ray bursts, and ionospheric ionization in the E region, should be more frequent and pronounced in the South Atlantic radiation anomaly than in any other region at comparable invariant latitudes, and that the effects of atmospheric heating by precipitated electrons should be detectable over the anomaly.

(4) An assessment is made of the value of the method referred to in point (1). Suggestions for its modification and extension are put forward. It is suggested that if more extensive rocket and satellite data on the low energy component of the electron flux become available, this method can be employed in a rigorous theoretical investigation of the South Atlantic radiation anomaly.

TABLE I

(M.K.S. UNITS)

n	h_n ($\times 10^{-3}$)	Case I. $Z_n - Z_s$ ($\times 10^{-3}$)	Case II. $Z_n - Z_s$ ($\times 10^{-3}$)	Case III. $Z_n - Z_s$ ($\times 10^{-3}$)	n	ρ_n (kgm/m^3)
1	200	220.68	261.08	212.84	1	4.3×10^{-10}
2	190	209.64	248.03	202.19	2	5.1×10^{-10}
3	185	204.12	241.50	196.87	3	5.9×10^{-10}
4	180	198.61	234.97	191.55	4	6.9×10^{-10}
5	175	193.09	228.45	186.23	5	8.0×10^{-10}
6	170	187.57	221.92	180.91	6	9.1×10^{-10}
7	165	182.06	215.39	175.59	7	1.0×10^{-9}
8	160	176.54	208.87	170.27	8	1.2×10^{-9}
9	155	171.02	202.34	164.95	9	1.4×10^{-9}
10	150	165.51	195.81	159.63	10	1.7×10^{-9}
11	145	159.99	189.29	154.31	11	2.3×10^{-9}
12	140	154.47	182.76	148.99	12	3.6×10^{-9}
13	135	148.96	176.23	143.66	13	5.7×10^{-9}
14	130	143.44	169.70	138.34	14	9.7×10^{-9}
15	125	137.92	163.18	133.02	15	2.2×10^{-8}
16	120	132.41	156.65	127.70	16	5.2×10^{-8}
17	115	126.89	150.12	122.38	17	1.1×10^{-7}
18	110	121.37	143.60	117.06	18	2.0×10^{-7}
19	105	115.85	137.07	111.74	19	4.3×10^{-7}
20	100	110.34	130.54	106.42	20	8.2×10^{-7}
21	97.5	107.58	127.28	103.76	21	1.2×10^{-6}
22	95.0	104.82	124.01	101.10	22	1.9×10^{-6}
23	92.5	102.06	120.75	98.437	23	3.0×10^{-6}
24	90.0	99.304	117.49	95.776	24	4.6×10^{-6}
25	87.5	96.545	114.22	93.116	25	7.3×10^{-6}
26	85.0	93.787	110.96	90.455	26	1.1×10^{-5}
27	82.5	91.028	107.70	87.795	27	1.8×10^{-5}
28	80.0	88.270	104.43	85.134	28	2.6×10^{-5}
29	77.5	85.512	101.17	82.474	29	3.8×10^{-5}
30	75.0	82.753	97.906	79.814	30	5.6×10^{-5}

Table I continued.

n	h_n ($\times 10^{-3}$)	Case I. $Z_n - Z_s$ ($\times 10^{-3}$)	Case II. $Z_n - Z_s$ ($\times 10^{-3}$)	Case III. $Z_n - Z_s$ ($\times 10^{-3}$)	n	ρ_n (kgm/m^3)
31	72.5	79.995	94.643	77.153	31	8.2×10^{-5}
32	70.0	77.236	91.379	74.493	32	1.2×10^{-4}
33	67.5	74.478	88.115	71.832	33	1.6×10^{-4}
34	65.0	71.719	84.852	69.172	34	2.3×10^{-4}
35	62.5	68.961	81.588	66.511	35	3.0×10^{-4}
36	60.0	66.203	78.325	63.851	36	4.1×10^{-4}
37	57.5	63.444	75.061	61.190	37	5.4×10^{-4}
38	55.0	60.686	71.798	58.530	38	7.1×10^{-4}
39	52.5	57.927	68.534	55.869	39	1.1×10^{-3}
40	50.0	55.169	65.271	53.209	40	-

TABLE II
(M.K.S. UNITS)

n	Case I. Z^2_n ($\times 10^{-13}$)	n	Case II. Z^2_n ($\times 10^{-13}$)	n	Case III. Z^2_n ($\times 10^{-13}$)	n
1	2.37547	1	3.34244	1	2.22146	1
2	2.36472	2	3.32736	2	2.21144	2
3	2.35936	3	3.31983	3	2.20643	3
4	2.35401	4	3.31231	4	2.20144	4
5	2.34865	5	3.30481	5	2.19645	5
6	2.34331	6	3.29731	6	2.19147	6
7	2.33797	7	3.28981	7	2.18649	7
8	2.33264	8	3.28234	8	2.18152	8
9	2.32731	9	3.27486	9	2.17655	9
10	2.32200	10	3.26739	10	2.17159	10
11	2.31668	11	3.25994	11	2.16663	11
12	2.31137	12	3.25249	12	2.16168	12
13	2.30607	13	3.24505	13	2.15673	13
14	2.30078	14	3.23761	14	2.15179	14
15	2.29548	15	3.23019	15	2.14686	15
16	2.29021	16	3.22278	16	2.14193	16
17	2.28493	17	3.21537	17	2.13701	17
18	2.27965	18	3.20798	18	2.13209	18
19	2.27438	19	3.20058	19	2.12718	19
20	2.26913	20	3.19320	20	2.12228	20
21	2.26650	21	3.18952	21	2.11983	21
22	2.26388	22	3.18582	22	2.11738	22
23	2.26125	23	3.18214	23	2.11493	23
24	2.25863	24	3.17847	24	2.11249	24
25	2.25601	25	3.17478	25	2.11004	25
26	2.25339	26	3.17111	26	2.10760	26
27	2.25077	27	3.16744	27	2.10516	27
28	2.24815	28	3.16376	28	2.10271	28
29	2.24554	29	3.16009	29	2.10027	29
30	2.24292	30	3.15643	30	2.09783	30
31	2.24032	31	3.15276	31	2.09540	31
32	2.23771	32	3.14910	32	2.09296	32
33	2.23510	33	3.14544	33	2.09053	33
34	2.23249	34	3.14177	34	2.08810	34
35	2.22988	35	3.13812	35	2.08567	35
36	2.22727	36	3.13447	36	2.08324	36
37	2.22467	37	3.13081	37	2.08081	37
38	2.22208	38	3.12716	38	2.07838	38
39	2.21947	39	3.12350	39	2.07596	39
40	2.21687	40	3.11986	40	2.07354	40

TABLE III
(M.K.S. UNITS)

	Case I		Case II		Case III	
χ	$Z^2\chi$ ($\times 10^{-13}$)	χ	$Z^2\chi$ ($\times 10^{-13}$)	χ	$Z^2\chi$ ($\times 10^{-13}$)	χ
1	0.00072	1	0.00100	1	0.00094	1
2	0.00289	2	0.00407	2	0.00377	2
3	0.00651	3	0.00917	3	0.00848	3
4	0.01156	4	0.01627	4	0.01507	4
5	0.01805	5	0.02539	5	0.02352	5
6	0.02596	6	0.03652	6	0.03383	6
7	0.03528	7	0.04964	7	0.04599	7
8	0.04601	8	0.06474	8	0.05997	8
9	0.05813	9	0.08179	9	0.07577	9
10	0.07163	10	0.10078	10	0.09337	10
11	0.08649	11	0.12168	11	0.11274	11
12	0.10268	12	0.14448	12	0.13384	12
13	0.12021	13	0.16913	13	0.15670	13
14	0.13903	14	0.19561	14	0.18123	14
15	0.15914	15	0.22389	15	0.20742	15
16	0.18047	16	0.25396	16	0.23525	16
17	0.20306	17	0.28571	17	0.26468	17
18	0.22683	18	0.31919	18	0.29570	18
19	0.25179	19	0.35431	19	0.32823	19
20	0.37789	20	0.39101	20	0.36222	20
21	0.30510	21	0.42928	21	0.39768	21
22	0.33335	22	0.46907	22	0.43456	22
23	0.36267	23	0.51031	23	0.47276	23
24	0.39299	24	0.55296	24	0.51225	24
25	0.42428	25	0.59697	25	0.55305	25
26	0.45651	26	0.64232	26	0.59507	26
27	0.48960	27	0.68891	27	0.63822	27
28	0.52354	28	0.73669	28	0.68246	28
29	0.55833	29	0.78562	29	0.72781	29
30	0.59390	30	0.83561	30	0.77412	30
31	0.63016	31	0.88667	31	0.82140	31
32	0.66709	32	0.93863	32	0.86954	32
33	0.70464	33	0.99156	33	0.91851	33
34	0.74278	34	1.04516	34	0.96827	34
35	0.78154	35	1.09965	35	1.01869	35
36	0.82071	36	1.15478	36	1.06981	36
37	0.86037	37	1.21062	37	1.12151	37
38	0.90042	38	1.26693	38	1.17368	38
39	0.94077	39	1.32380	39	1.22633	39
40	0.98151	40	1.38101	40	1.27942	40

TableIII continued.

χ	Case I. Z^2_χ ($\times 10^{-13}$)	χ	Case II. Z^2_χ ($\times 10^{-13}$)	χ	Case III. Z^2_χ ($\times 10^{-13}$)	χ
41	1.02246	41	1.43861	41	1.33276	41
42	1.06361	42	1.49653	42	1.38637	42
43	1.10490	43	1.55465	43	1.44028	43
44	1.14630	44	1.61291	44	1.49421	44
45	1.18777	45	1.67126	45	1.54827	45
46	1.22920	46	1.72956	46	1.60224	46
47	1.27057	47	1.78777	47	1.65625	47
48	1.31189	48	1.84591	48	1.71007	48
49	1.35306	49	1.90384	49	1.76375	49
50	1.39398	50	1.96143	50	1.81706	50
51	1.43474	51	2.01870	51	1.87013	51
52	1.47510	52	2.07553	52	1.92282	52
53	1.51516	53	2.13195	53	1.97500	53
54	1.55480	54	2.18771	54	2.02671	54
55	1.59401	55	2.24278	55	2.07772	55
56	1.63273	56	2.29728	56	2.12825	56
57	1.67085	57	2.35099	57	2.17800	57
58	1.70842	58	2.40384	58	2.22699	58
59	1.74540	59	2.45580	59	2.27510	59
60	1.78160	60	2.50690	60	2.32237	60
61	1.81715	61	2.55682	61	2.36867	61
62	1.85193	62	2.60580	62	2.41405	62
63	1.88590	63	2.65359	63	2.45828	63
64	1.91897	64	2.70015	64	2.50140	64
65	1.95125	65	2.74545	65	2.54349	65
66	1.98256	66	2.78953	66	2.58420	66
67	2.01278	67	2.83216	67	2.62369	67
68	2.04214	68	2.87339	68	2.66194	68
69	2.07043	69	2.91319	69	2.69880	69
70	2.08940	70	2.95142	70	2.73424	70
71	2.12374	71	2.98815	71	2.76823	71
72	2.14869	72	3.02335	72	2.80084	72
73	2.17240	73	3.05676	73	2.83173	73
74	2.19502	74	3.08847	74	2.86118	74
75	2.21634	75	3.11855	75	2.88906	75
76	2.23644	76	3.14687	76	2.91524	76
77	2.25530	77	3.17329	77	2.93981	77
78	2.27281	78	3.19802	78	2.96262	78
79	2.28905	79	3.22079	79	2.98378	79
80	2.30390	80	3.24171	80	3.00315	80

Table III continued.

χ	Case I. z^2_χ ($\times 10^{-13}$)	χ	Case II. z^2_χ ($\times 10^{-13}$)	χ	Case III. z^2_χ ($\times 10^{-13}$)	χ
81	2.31736	81	3.26064	81	3.02071	81
82	2.32951	82	3.27768	82	3.03656	82
83	2.34024	83	3.29281	83	3.05046	83
84	2.34953	84	3.30591	84	3.06263	84
85	2.35739	85	3.31707	85	3.07293	85
86	2.36390	86	3.32617	86	3.08136	86
87	2.36896	87	3.33333	87	3.08802	87
88	2.37257	88	3.33841	88	3.09269	88
89	2.37481	89	3.34142	89	3.09559	89
90	2.37549	90	3.34246	90	3.09648	90

REFERENCES.

(Papers marked with an asterisk are English translations of Russian papers.)

(1)	STØRMER, C.	"The Polar Aurora"	(Clarendon Press, Oxford) (1955)
(2)	SPITZER, LYMAN JR.	"Physics of Fully Ionized Gases"	(Interscience Publishers, Inc. New York) (1956)
(3)	CHAMBERLAIN, J.W.	"Theories of the Aurora"	Advances in Geophysics, 4, 110. (1958)
(4)	POINCARE, H.	"Remarques sur une experience de M. Birkeland"	Comptes. rend. 123,669. (1896)
(5)	AFVEN, H.	"Cosmical Electrodynamics"	(Oxford University Press) (1950)
(6)	NORTHROP, T.G. and TELLER, E.	"Stability of Adiabatic Motion of Charged Particles in the Earth's Magnetic Field"	Phys. Rev., 117, 215. (1960)
(7)	WENTZEL, D. G.	"Hydromagnetic Waves and the Trapped Radiation. Part I. Breakdown of Adiabatic Invariance"	J. G. R., 66, 359 (1961)
(8)	WENTZEL, D.G.	"Hydromagnetic Waves and the Trapped Radiation. Part II. Displacement of the Mirror Points"	J. G. R., 66, 363. (1961)
(9)	PARKER, E. N.	"Effect of Hydromagnetic Waves in a Dipole Field on the Longitudinal Invariant"	J. G. R., 66, 693. (1961)

(10)	DAVIS, L. Jr. and CHANG, D. B.	"On the Effect of Geomagnetic Fluctuations on Trapped Particles"	J. G. R., 67, 2169. (1962)
(11)	PENNINGTON, R.H.	"The Equation of a Charged Particle Shell in a Perturbed Dipole Field"	J. G. R., 66, 709. (1961)
(12)	HONES, E. W. Jr.	"Motions of Charged Particles Trapped in the Earth's Magnetosphere"	J. G. R., 68, 1209. (1963)
(13)	WALT, M. and MC DONALD, W. M.	"Diffusion of Electrons in the Van Allen Radiation Belt. 1. Treatment of Particles with Mirroring Points at High Altitudes"	J. G. R., 67, 5013. (1962)
(14)	WALT, M. and MC DONALD, W. M.	"Diffusion of Electrons in the Van Allen Radiation Belt. 2. Particles with Mirroring Points at Low Altitude"	J. G. R., 67, 5023. (1962)
(15)	MC ILWAIN, C. E.	"Coordinates for Mapping the Distribution of Magnetically Trapped Particles"	J. G. R., 66, 3681. (1961)
(16)	STONE, E. C.	"The Physical Significance and Application of L, B_o and R_o to Geomagnetically Trapped Particles"	J.G.R., 68, 4157. (1963)
(17)	GOLD, T.	"Motions in the Magnetosphere of the Earth"	J.G.R., 64, 1219. (1959)
(18)	SMITH, E. J.	"A Comparison of Explorer VI and Explorer X Magnetometer Data"	J.G.R., 67, 2045. (1962)
(19)	BADER, M.	"Preliminary Explorer 12 Data on Protons below 20 keV"	J.G.R., 67, 5007. (1962)

(20) HEPPNER, J.P., HESS, N.F., SCEARCE, S.C. and SKILLMAN, T.L. "Explorer 10 Magnetic Field Measurements" J.G.R., 68, 1. (1963)

(21) CAHILL, L.J. and AMAZEEN, P.G. "The Boundary of the Geomagnetic Field" J.G.R., 68, 1835 (1963)

(22) FREEMAN, J.W., VAN ALLEN, J. A. and CAHILL, L. J. "Explorer 12 Observations of the Magnetospheric Boundary and Associated Solar Plasma on September 13, 1961" J.G.R., 68, 2121. (1963)

(23) BONETTI, A., BRIDGE, H.S., LAZARUS, A.J., ROSSI, B. and SCHERB, F. "Explorer 10 Plasma Measurements" J.G.R., 68, 4017. (1963)

(24) MALVILLE, J.M. "The Effect of the Initial Phase of a Magnetic Storm upon the Outer Van Allen Belt" J.G.R., 65, 3008. (1960)

(25) PARKER, E. N. "Geomagnetic Fluctuations and the Form of the Outer Zone of the Van Allen Radiation Belt" J.G.R., 65, 3117. (1960)

(26) JOHNSON, F.S. "The Gross Character of the Geomagnetic Field in the Solar Wind" J.G.R., 65, 3049. (1960)

(27) SPREITER J.R. and BRIGGS, B.R. "Theoretical Determination of the Form of the Boundary of the Solar Corpuscular Stream produced by Interaction with the Magnetic Dipole Field of the Earth" J.G.R., 67, 37. (1962)

(28) AXFORD, W.I. "The Interaction between the Solar Wind and the Earth's Magnetosphere" J.G.R., 67, 3791. (1962)

(29) KELLOGG, P.J. "Flow of Plasma around the Earth. J.G.R., 67, 3805. (1962)

(30)	SPREITER, J.R. and HYETT, B.J.	"The Effect of a Uniform External Pressure on the Boundary of the Geomagnetic Field in a Steady Solar Wind"	J.G.R., 68, 1631. (1963)
(31)	AXFORD, W.I.	"Rotation of the Magnetosphere"	J.G.R., 68, 5883. (1963)
(32)	O'BRIEN, B.J.	"Radiation Belts"	Sci.Am., 208, 84. (May 1963)
(33)	VAN ALLEN, J.A. and FRANK, L.A.	"Radiation Around the Earth to a Radial Distance of 107,400 kilometers"	Nature, 183, 430. (1959)
(34)	VAN ALLEN, J.A., MC ILWAIN, C.E. and LUDWIG, G.H.	"Radiation Observations with Satellite 1958 €"	J.G.R., 64, 271. (1959)
(35)	VAN ALLEN, J.A.	"Radiation Belts Around the Earth"	Sci. Am., 204, (March 1959)
(36)	ROSEN, A., SONETT, C.P., COLEMAN, P.J. Jr., and MC ILWAIN, C.E.	"Ionizing Radiation at Altitudes of 3,500 to 36,000 kilometers, Pioneer I"	J.G.R., 64, 709. (1959)
(37)	ROSEN, A., COLEMAN, C.P. Jr., and SONETT, C.P.	"Ionizing Radiation Detected by Pioneer II"	Planet. and Space Sci., 1, 343. (1959)
(38)	VAN ALLEN, J.A.	"The Geomagnetically Trapped Corpuscular Radiation"	J.G.R., 64, 1683. (1959)
(39)	VAN ALLEN, J.A. and FRANK, L.A.	"Radiation Measurements to 658,000 kilometers with Pioneer IV"	Nature, 184, 219. (1959)
(40)	ROTHWELL, PAMELA and MC ILWAIN, C.E.	"Magnetic Storms and the Van Allen Radiation Belts - Observations from Satellite 1958 € (Explorer IV)"	J.G.R., 65, 799. (1960)
(41)	YOSHIDA, SEKIKO, LUDWIG, G.H., and VAN ALLEN, J.A.	"Distribution of Trapped Radiation in the Geomagnetic Field"	J.G.R., 65, 807. (1960)

*(42)	VERNOV, S.N., CHUDAKOV, A.E., GORCHAKOV, E.V., LOGACHEV, J.L. and VAKULOV, P.V.	"Study of Cosmic-ray Soft Component by the Third Soviet Earth Satellite"	Planet. and Space Sci., 1, 86. (1959)
(43)	VERNOV, S.N., CHUDAKOV, A.E., VAKULOV, P.V., and LOGACHEV, Yu I.	"Study of Terrestrial Corpuscular Radiation and Cosmic Rays during Flight of the Cosmic Rocket"	Dorklady.Akad. Nauk. S.S.S.R., 125, 304, (1959)
*(44)	KRASOVSKII, V.I., SCKLOVSKI, I.S., GAL'PERIN, Yu I., SVETLITSKII, E.M., KUSHNIR, Yu M. and BORDOVSKII, G.A.	"The Detection of Electrons with Energies of Approximately 10 keV in the Upper Atmosphere"	Planet. and Space Sci., 9, 27. (1962)
(45)	FREDEN, S.C. and WHITE, R.S.	"Protons in the Earth's Magnetic Field"	Phys. Rev. Letters, 3, 9. (1959)
(46)	HOLLY, F.E. and JOHNSON, R.G.	"Measurement of Radiation in the Lower Van Allen Belt"	J.G.R., 65, 771. (1960)
(47)	FREDEN, S.C. and WHITE, R.S.	"Particle Fluxes in the Inner Radiation Belt"	J.G.R., 65, 1377. (1960)
(48)	ARNOLDY, R.L., HOFFMAN, R.A. and WINCKLER, J.R.	"Observations of the Van Allen Radiation Regions during August and September, 1959. Part I"	J.G.R., 65, 1361. (1960)
(49)	O'BRIEN, B.J. and LUDWIG, G.H.	"Development of Multiple Radiation Zones on October 18, 1959"	J.G.R., 65, 2695. (1960)
(50)	VAN ALLEN, J.A. and CHING LIN, WEI.	"Outer Radiation Belt and Solar Proton Observations with Explorer VII during March-April 1960"	J.G.R., 65, 2998. (1960)
(51)	FARLEY, T.A. and ROSEN, A.	"Charged-particle Variations in the Outer Van Allen Zone during a Geomagnetic Storm"	J.G.R., 65, 3494. (1960)
(52)	ARMSTRONG, A.H., HARRISON, F.B., HECKMAN, H.H. and ROSEN, L.	"Charged Particles in the Inner Van Allen Radiation Belt"	J.G.R., 66, 351. (1961)

(53)	ROSEN, A. and FARLEY, J.A.	"Characteristics of the Van Allen Radiation Zones as measured by the Scintillation Counter on Explorer VI"	J.G.R., 66, 2013. (1961)
(54)	NAUGLE, J.E. and KNIFFEN, D.A.	"Flux and Energy Spectra of Protons in the Inner Van Allen Belt"	Phys. Rev. Letters, 7, 3. (1961)
(55)	CLADIS, J.B., CHASE L.F. Jr., IMHOF, W.L. and KNECHT, D.J.	"Energy Spectrum and Angular Distributions of Electrons Trapped in the Geomagnetic Field"	J.G.R., 66, 2297. (1961)
(56)	FORBUSH, S.E., VENKATESAN, D. and MC ILWAIN, C.E.	"Intensity Variations in Outer Van Allen Radiation Belt"	J.G.R., 66, 2275. (1961)
(57)	FAN, C.Y., MEYER, P. and SIMPSON, J.A.	"Dynamics and Structure of the Outer Radiation"	J.G.R., 66, 2607. (1961)
(58)	O'BRIEN, B.J., VAN ALLEN, J.A., LAUGHLIN, C.D. and FRANK, L.A.	"Absolute Electron Intensities in the Heart of the Earth's Outer Radiation Zone"	J.G.R., 67, 397. (1962)
(59)	HOFFMAN, R.A., ARNOLDY, R.L. and WINCKLER, J.R.	"Observations of the Van Allen Radiation Regions during August and September 1959. 3. The Inner Belt"	J.G.R., 67, 1. (1962)
*(60)	GRINGAUZ, K.I., KURT, V.G., MOROZ, V.I. and SHKLOVSKII, I.S.	"Ionized Gas and Fast Electrons in the Vicinity of the Earth and in Interplanetary Space"	Planet. and Space Sci., 9, 21. (1962)
*(61)	GINZBURG, V.I., KURNOSOVA, L.V., RAZARENOV, L.A. and FRADKIN, M.I.	"Some Investigations of the Nuclear Component of Cosmic Rays and the Earth's Radiation Belts carried out on Soviet Artificial Satellites and Rockets : A Review"	Geomag. and Aer., 2, 165. (1962)
(62)	O'BRIEN, B.J., LAUGHLIN, C.D., VAN ALLEN, J.A. and FRANK, L.A.	"Measurements of the Intensity and Spectrum of Electrons at 1000 kilometres Altitude and High Latitude"	J.G.R., 67, 1209. (1962)

(63)	PIZZELLA, G., MC ILWAIN, C.E. and VAN ALLEN, J.A.	"The Time Variations of Intensity in the Earth's Inner Radiation Zone, October 1959 through December 1960"	J.G.R., 67, 1235. (1962)
(64)	HECKMAN, H.H. and ARMSTRONG, A.H.	"Energy Spectrum of Geomagnetically Trapped Protons"	J.G.R., 67, 1255. (1962)
(65)	ARNODLY, R.L., HOFFMAN, R.A. and WINCKLER, J.R.	"Observations of the Van Allen Radiation Regions during August and September, 1959. Part 4. The Outer Zone Electrons"	J.G.R., 67, 2595. (1962)
(66)	PIZZELLA, G., LAUGHLIN, C.D. and O'BRIEN, B.J.	"Note on the Electron Energy Spectrum in the Inner Van Allen Belt"	J.G.R., 67, 3281. (1962)
(67)	FORBUSH, S.E., PIZELLA, G. and VENKATESAN, D.	"The Morphology and Temporal Variations of the Van Allen Radiation Belt, October 1959 to December 1960"	J.G.R., 67, 3651. (1962)
(68)	O'BRIEN, B.J.	"Lifetimes of Outer-zone Electrons and their Precipitation into the Atmosphere"	J.G.R., 67, 3687. (1962)
(69)	LUNDQUIST, C.A., NAUMANN, R.J. and WEBER, A.A.	"Directional Flux Densities and Mirror-point Distributions of Trapped Particles from Satellite 1958 ϵ Measurements"	J.G.R., 67, 4125. (1962)
(70)	ROSSER, W.G.V., O'BRIEN, B.J., VAN ALLEN, J.A., FRANK, L.A. and LAUGHLIN, C.D.	"Electrons in the Earth's Outer Radiation Zone"	J.G.R., 67, 4533. (1962)
(71)	HOFFMAN, R.A., ARNOLDY, R.L. and WINCKLER, J.R.	"Observations of the Van Allen Radiation Regions during August and September, 1959. 6. Properties of the Outer Region"	J.G.R., 67, 4543. (1962)
*(72)	GORCHAKOV, Ye. V.	"The Outer Radiation Belt and the Aurora Borealis"	Planet. and Space Sci., 9, 829. (1962)

*(73)	GORCHAKOV, Ye. V.	"The Position of the Inner Radiation Belt and the Earth's Magnetic Field"	Planet. and Space Sci., 9, 841. (1962)
(74)	PIEPER, G.F., ZMUDA, A.J., BOSTROM, C.O. and O'BRIEN, B.J.	"Solar Protons and Magnetic Storms in July, 1961"	J.G.R., 67, 4959. (1962)
(75)	BRYANT, D.A., CLINE, T.L., DESAI, U.D. and MC DONALD, F.B.	"Explorer XII Observations of Solar Cosmic Rays and Energetic Storm Particles after the Solar Flare of September 28, 1961"	J.G.R., 67, 4983. (1962)
(76)	HOFFMAN, R.A., DAVIS, L.R. and WILLIAMSON, J.M.	"Protons of 0.1 to 5 MeV and Electrons of 20 keV at 12 Earth Radii during Sudden Commencement on September 30, 1961"	J.G.R., 67, 5001. (1962)
(77)	BAME, S.J., CONNER, J.P., HILL, H.H. and HALLY, F.E.	"Protons in the Outer Zone of the Radiation Belt"	J.G.R., 68, 55. (1963)
(78)	FRANK, L.A., VAN ALLEN, J.A., WHELPLEY, W.A. and CRAVEN, I.D.	"Absolute Intensities of Geomagnetically Trapped Particles with Explorer 14"	J.G.R., 68, 1573. (1963)
(79)	FRANK, L.A. and VAN ALLEN, J.A.	"Intensity of Electrons in the Earth's Inner Radiation Zone"	J.G.R., 68, 1203. (1963)
(80)	MC ILWAIN, C.E. and PIZZELLA, G.	"On the Energy Spectrum of Protons Trapped in the Earth's Inner Van Allen Zone"	J.G.R., 68, 1811. (1963)
(81)	NAUGLE, J.E. and KNIFFEN, D.A.	"Variations of the Proton Energy Spectrum with Position in the Inner Van Allen Belt"	J.G.R., 68, 4065. (1963)
*(82)	IVANOV-KHOLODNY, G.S.	"The Part Played by, and Source of, Particles Observed in the Ionosphere and Aurorae"	Planet. and Space Sci., 10, 219. (1963)

(83)	SINGER, S.F.	"Radiation Belt" and Trapped Cosmic-ray Albedo	Phys. Rev. Letters 1, 171. (1958)
(84)	SINGER, S.F.	"Trapped Albedo Theory of the Radiation Belt"	Phys.Rev.Letters., 1, 181. (1958)
(85)	KELLOGG, P.J.	"Electrons of the Van Allen Radiation"	J.G.R., 65, 2705. (1960)
(86)	HESS, W.N.	"The Radiation Belt Produced by Neutrons Leaking out of the Atmosphere of the Earth"	J.G.R., 65, 3107. (1960)
(87)	HESS, W.N., CANFIELD, E.H. and LINGENFELTER, R.E.	"Cosmic-ray Neutron Demography"	J.G.R., 66, 665. (1961)
(88)	LENCHEK, A.M., SINGER, S.F. and WENTWORTH, R.C.	"Geomagnetically Trapped Electrons from Cosmic-ray Albedo Neutrons"	J.G.R., 66, 4027. (1961)
(89)	FREDEN, S.C. and WHITE, R.S.	"Trapped Proton and Cosmic Ray Albedo Neutron Fluxes"	J.G.R., 67, 25. (1962)
(90)	LENCHEK, A.M. and SINGER, S.F.	"Geomagnetically Trapped Protons from Cosmic-ray Albedo Neutrons"	J.G.R., 67, 1263. (1962)
(91)	LENCHEK, A.M.	"On the Anamalous Component of Low Energy Geomagnetically Trapped Protons"	J.G.R., 67, 2145. (1962)
(92)	NAKADA, M.P.	"High Energy Electrons in the Radiation Belt"	J.G.R., 68, 47. (1963)
(93)	LIWSHITZ, M. and LENCHEK, A.M.	"Impulsive Injection of Electrons into the Earth's Inner Trapping Region from Solar Cosmic-ray Events"	J.G.R., 68, 4091. (1963)
(94)	LENCHEK, A.M. and SINGER, S.F.	"The Albedo Neutron Theory of Geomagnetically Trapped Protons"	Planet. and Space Sci., 11, 1151. (1963)
(95)	BAME, S.J., CONNER, J.P., BRUMLEY, F.B., HOSTETLER, R.L. and GREEN, A.C.	"Neutron Flux and Energy Spectrum above the Atmosphere"	J.G.R., 68, 1221. (1963)

(96)	CHRISTOFILOS, N.C.	"The Argus Experiment"	J.G.R., 64, 869. (1959)
(97)	CHAPMAN, S. and BARTELS, J.	"Geomagnetism"	(Clarendon Press, Oxford) p.648-658. (1951)
(98)	DESSLER, A.J.	Private communication.	(1963)
(99)	DESSLER, A.J.	"Effect of Magnetic Anomaly on Particle Radiation Trapped in the Geomagnetic Field"	J.G.R., 64, 713. (1959)
(100)	DESSLER, A.J. and KARPLUS, R.	"Some Properties of the Van Allen Radiation"	Phys.Rev.Letters, 4, 271. (1960)
(101)	HOFFMAN, R.A.	"Observations of the Van Allen Radiation Regions during August and September 1959. 2. The Cape Town Anomaly and the Shape of the Outer Belt"	J.G.R., 66, 4003. (1961)
*(102)	SAVENKO, I.A., SHAVRIN, P.I. and PISARENKO, N.F.	"Detection of Soft Corpuscular Radiation at a Height of 320 km. in Near-equatorial Latitudes"	Geomag. and Aeron., 1, 762. (1961)
*(103)	VERNOV, S.N., SAVENKO, I.A., SHAVRIN, P.I., NESTEROV, V. Ye. and PISARENKO, N.F.	"The Earth's Radiation Belts at Heights of 180-250 km."	Geomag. and Aeron., 2, 31. (1962)
*(104)	KUROSOVA, L.V., KOLOBYANINA, T.N., LOGACHEV, V.I., RAZORENOV, L.A., SIROTKIN, I.A. and FRADKIN, M.I.	"Discovery of Radiation Anomalies above the South Atlantic at Heights of 310-340 km."	Planet. and Space Sci., 9, 513. (1962)
*(105)	GINSBURG, V.L., KURNOSOVA, L.V., LOGACHEV, V.I., RAZORENOV, L.A., SIROTKIN, I.A. and FRADKIN, M.I.	"Investigation of Charged Particle Intensity during the Flights of the Second and Third Space-ships"	Planet. and Space Sci., 9, 845. (1962)

*(106)	VERNOV, S.N., SAVENKO, I.A., SHAVRIN, P.I. and PISARENKO, N.F.	"The Outer Radiation Belt of the Earth at the Altitude of 320 km."	Planet. and Space Sci., 9, 855. (1962)
*(107)	VERNOV, S.N., SAVENKO, I.A., SHAVRIN, P.I. and PISARENKO, N.F.	"Detection of an Inner Radiation Belt at the Altitude of 320 km. in the Region of the South Atlantic Magnetic Anomaly"	Planet. and Space Sci., 9, 861. (1962)
*(108)	SAVENKO, I.A., SHAVRIN, P.I.,and PISARENKO, N.F.	"Soft Particle Radiation at an Altitude of 320 km. in the Latitude near the Equator"	Planet. and Space Sci., 11, 431. (1963)
*(109)	VERNOV, S.N., SAVENKO, I.A., SHAVRIN, P.I., NESTEROV, V. Ye. and PISARENKO,N.F.	"The Earth's Radiation Belts at Altitudes of 180-250 km."	Planet. and Space Sci., 11, 567. (1963)
(110)	SEVARD, S.F.	Private Communication.	(1962)
(111)	LIN, W.C., VENKATESAN, D. and VAN ALLEN, J.A.	"Latitude Survey of Cosmic-Ray Intensity by Explorer 7, October 1959 to February 1961"	J.G.R., 68, 4885. (1963)
(112)	GLEDHILL, J.A. and VAN ROOYEN, H.O.	"Cape Town Anomaly and Auroral Emission"	Nature, 196, 973. (1962)
(113)	VESTINE, E.H. and SIBLEY, W.L.	"The Geomagnetic Field in Space, Ring Currents and Auroral Isochasms"	J.G.R., 65, 1967. (1960)
(114)	WELCH, J.A. Jr., and WHITAKER,W.A.	"Theory of Geomagnetically Trapped Electrons from an Artificial Source"	J.G.R., 64, 909. (1959)
(115)	HESS, W.N.	Private Communication.	(1963)
(116)	CHAPMAN, S. and BARTELS, J.	"Geomagnetism"	(Clarendon Press, Oxford) p.100 (1951)

(117)	COOK, G.E.	Geophysical Results obtained from Satellite orbits.	Rep. Prog. Phys. 25,64. (1962)
(118)	NICOLET, M.	Constitution of the Atmosphere at Ionospheric Levels.	JGR, 64, 2092. (1959)
(119)	KATZ, L and PENFOLD, S.	Range-Energy Relations for Electrons and the Determination of Beta-Ray End-Point Energies by Absorption.	Rev. Mod. Phys., 24, 28. (1952)
(120)	O'BRIEN, B.J.	Direct Observations of Dumping of Electrons at 1000 km. Altitude and High Latitudes.	JGR, 67, 1227. (1962)
(121)	GLEDHILL, J.A. and VAN ROOYEN, H.O.	The South Atlantic Geomagnetic Anomaly and the Radiation Belts.	Read by Prof. Gledhill at the Fifth International Conference on Space Technology and Science, Tokyo. (1963)
(122)	SHLYAKHTINA, A.P.	A Map of the distribution of the strength of the T Geomagnetic Field in Antarctica.	Geomag, and Aeron. 2, 635. (1962)
(123)	MC ILWAIN, C.E.	Direct measurement of Particles Producing Visible Auroras.	JGR, 65, 2727. (1960)
(124)	KELLOGG, P.J.	Auroral X-Rays, Electron Bombardment and Trapped Radiation.	Planet and Space Sci., 10, 165. (1963)
(125)	REES, M.I.	Auroral Ionization and Excitation by incident Energetic Electrons.	Planet and Space Sci., 11, 1209. (1963)

(126)	CHAMBERLAIN, J.W.	Physics of the Aurora and Airglow.	(Academic Press Inc., New York) (1961)
(127)	GREENSPAN, J.A. and STONE, C.A.	The Longitudinal Variation of Night Air glow intensity in the region of the South Atlantic Magnetic Anomaly.	JGR, (in press) (1963)
(128)	ROACH, F.E.	Stable 6300 Å Auroral Arcs in Mid-Latitudes.	Planet and Space Sci., 11, 523. (1962)
(129)	ARNOLDY, R.L. WINCKLER, J.R., AKASOFU, S.L.	Observations of the Van Allen Radiation Regions during August and September, 1959. 5. Visual Auroras, High-Altitude X-Ray bursts, and simultaneous Satellite Observations.	JGR, 67, 3673. (1962)
(130)	WINCKLER, J.R., BHAVSAR, P.D. ANDERSON, K.A.	A Study of the Precipitation of Energetic Electrons from the Geomagnetic Field during Magnetic storms.	JGR, 67, 371/. (1962)
(131)	WINCKLER, J.R.	Balloon Study of High-Altitude Radiations during the International Geophysical Year.	JGR, 65, 1331 (1960)
(132)	CLADIS, J.B., DESSLER, A.J.	X-Rays from Van Allen Belt Electrons.	JGR, 66, 343. (1961)

(133) PEDERSEN, A.	Time, Height and Latitude Distribution of D-Layers in the Subauroral Zone and their relation to Geomagnetic Activity and Aurora.	JGR, 67, 2685. (1962)
(134) LAL, C.	Corpuscular Radiation and the Ionospheric Anomalies.	J. Instn. Telecomm. Engrs (India) 9, 95. (1963)
(135) KING, J.W., SMITH, P.A., ECCLES, D., HELM, H.	The Structure of the Upper Ionosphere as observed by the Topside Sounder Satellite, Alouette.	RRS Report. Document Number RRS/I.M. 94. (1963)
(136) ELLIS, G.R.A.	Low Frequency Electromagnetic Radiation Associated with Magnetic Disturbances.	Planet and Space Sci., 1, 253. (1959)
(137) REAR ADMIRAL J.R. REEDY.	Year in Review. A Report on United States Antarctic Activities.	Bul. U.S. Antarctic Projects Officer 4, 119. (1963)
(138) VEGARD, L.	Recent Result of Northlight Investigations and the Nature of the Cosmic Electric Rays.	Phil. Mag., 42, 47. (1921)